Titre: Title:	Analysis of bolted flanged gasketed joints
Auteur: Author:	Abdel-Hakim Bouzid
Date:	1994
Type:	Mémoire ou thèse / Dissertation or Thesis
Référence: Citation:	Bouzid, A.-H. (1994). Analysis of bolted flanged gasketed joints [Thèse de doctorat, École Polytechnique de Montréal]. PolyPublie. https://publications.polymtl.ca/33490/

UNIVERSITÉ DE MONTRÉAL

ANALYSIS OF BOLTED FLANGED GASKETED JOINTS

ABDEL-HAKIM BOUZID
DÉPARTEMENT DE GÉNIE MÉCANIQUE
ÉCOLE POLYTECHNIQUE DE MONTRÉAL

THÈSE PRÉSENTÉE EN VUE DE L'OBTENTION
DU DIPLÔME DE PHILOSOPHIAE DOCTOR (Ph.D.)
(GÉNIE MÉCANIQUE)
DÉCEMBRE 1994

ISBN 0-315-99724-9

UNIVERSITÉ DE MONTRÉAL

ÉCOLE POLYTECHNIQUE DE MONTRÉAL

Cette thèse intitulée:

ANALYSIS OF BOLTED FLANGED GASKETED JOINTS

présentée par: BOUZID Abdel-hakim
en vue de l'obtention du diplôme de: Philosophiae Doctor
a été dûment acceptée par le jury d'examen constitué de:

M. MARCHAND Luc, Ph.D., Président
M. CHAABAN Ahmad, Ph.D., Directeur de recherche
M. BAZERGUI André, Ph.D., membre et co-directeur de recherche
M. MASSICOTTE Bruno, Ph.D, membre
M. PICK Roy, Ph.D., membre

To my parents for teaching me the thirst for knowledge.

ABSTRACT

Structurally sound bolted joints often fail due to loss of tightness. This is because the clamping load is affected not only by the application of the internal fluid pressure but also by the amount of creep relaxation, thermal degradation and difference in expansion of the joint members. Most significant contributions over the years were put towards better structural integrity performance of the joint while no particular attention was paid to the complex behavior of the gasket. With working conditions becoming more and more severe due to the required increasing performance and efficiency demands, it is evident that bolted flanged joints require rigorous analysis for both structural integrity and leakage tightness.

This thesis presents a study of a new and accurate approach to the modeling and design of bolted flanged gasketed joints. The new proposed design model that our program "POLYFLG" is based on, encompasses most aspects of joint behavior in order to produce both structural integrity and efficient sealing performance within the defined limits of the method used. The method is based on the elastic interactions of all the flanged joint elements taking into account their flexibility and considers the change in joint element dimensions during operation produced by temperature induced effects.

The work includes a detailed review of the literature on the design and analysis of bolted flanged joints. Also included is the development of a simple analytical model

which is based on an extension of the Taylor-Forge approach to which flange rotation, flexibility of both the gasket and the bolts, friction between the gasket and flange and, when applicable, the stiffness of the end closure are incorporated. These parameters have a strong influence on the gasket and bolt stresses and have partly enabled us to resolve some ambiguities and to better understand the complex mechanical behavior of bolted flanged joints.

In addition, the proposed model accounts for the short and the long term behavior by simulating the relaxation of the remaining load on the gasket after the application of the internal fluid pressure and temperature. The influence of the bolted joint stiffness on the relaxation of the gasket is clearly demonstrated. In general, the results obtained by the proposed model compare well with those obtained experimentally, at room temperature, on real bolted flanged joints. In some cases comparisons are made using finite element analyses.

Finally, an improved model capable of taking into account most of the parameters involved and guiding the designer towards a long term safe leak design have been developed. The proposed model has potential for becoming a design tool for leakage prediction.

SOMMAIRE

La perte d'étanchéité est la défaillance la plus répandue dans les assemblages à brides boulonnées munies de joint d'étanchéité. La raison principale de cette défaillance est la diminution de la charge sur le joint due à l'application de la pression interne du fluide ainsi que le fluage, la relaxation, la dégradation et la différence de dilatation thermique. Pendant plusieurs années, le soucis majeur a été la performance des assemblages à brides du point de vue intégrité mécanique sans attacher d'intérêt particulier au comportement complexe du joint. Avec la sévérité accrue des conditions de fonctionnement pour des raisons de performance et de rendement, il est évident que les assemblages à brides nécessitent une analyse rigoureuse et doivent satisfaire les deux critères: la tenue mécanique et l'étanchéité.

Cette thèse présente une méthode d'analyse du comportement d'un assemblage à brides circulaires boulonnées soumis à différentes sollicitations. Une nouvelle approche d'analyse et de conception des brides boulonnées, incluant la plupart des aspects relatifs au comportement des éléments de l'assemblage et conduisant à une meilleure performance à l'étanchéité dans les limites clairement définies par la méthode utilisée, a été développée. Cette méthode sur laquelle est fondé le programme d'analyse "POLYFLG", est basée sur l'interaction élastique des différents composants de l'assemblage brides-joint-boulons, en considérant la rigidité ainsi que la variation des

dimensions de chaque élément produit par les effets pré-cités induits thermiquement pendant opération.

On trouvera également dans cette thèse, une revue bibliographique détaillée sur les différentes approches utilisés dans la conception des brides boulonnées. L'analyse complète ainsi que le développement du modèle analytique basé sur une extension de la méthode de Taylor-Forge en considérant la rotation de la bride, la flexibilité du joint et des boulons, le frottement entre le joint et la bride, seront présentés. L'introduction de ces paramètres, qui ont une grande influence sur les contraintes dans le joint et dans les boulons, nous a permis de clarifier certaines ambiguïtés et de mieux comprendre le comportement mécanique complexe d'un assemblage à brides.

De plus, on présente un modèle qui considère le comportement d'un assemblage à brides, aussi bien à court terme qu'à long terme, en simulant l'effet de la relaxation dans le temps de la charge résiduelle sur le joint, après application de la pression du fluide et, plus particulièrement, à haute température. L'influence de la rigidité de l'assemblage à brides boulonnées sur la relaxation du joint est démontrée. En général, à la température ambiante une très bonne corrélation existe entre les résultats obtenus par le modèle proposé et ceux obtenus expérimentalement sur des assemblages à brides boulonnées réels. Dans certains cas, lorsque les tests expérimentaux ne le permettent pas, on a eu recourt aux analyses numériques par la méthode éléments finis pour confirmer la validité des résultats.

Finalement, l'évaluation précise des contraintes résiduelles sur le joint s'avère nécessaire pour la prédiction des fuites. Un modèle capable de prendre en compte la plupart des paramètres impliqués et visant à garantir à long terme un degré d'étanchéité acceptable, a été développé. Le modèle proposé a la capacité d'être un outil de conception pour la prédiction des fuites.

ACKNOWLEDGEMENT

I would like to express my sincere gratitude to my advisors, Dr Ahmad Chaaban, professor at the mechanical engineering department and Dr André Bazergui, professor and dean of the Ecole Polytechnique for their wise guidance, encouragement and continuous support from the inception to the present form of this project. I am very grateful to them for their valuable comments and suggestions, for the financial support they have granted me and for the finishing touches they have brought to this thesis.

I would also acknowledge the help I received from many friends and members of staff of the applied mechanics section and in particular Mr Michel Derenne, Dr Luc Marchand, Mr François Deshaies and Mr Umberto Muzzo for the frequent and useful discussions in relation to this work.

Finally, I wish to thank my wife for her encouragement, support, understanding and patience during the course of this project.

RÉSUMÉ

Les assemblages à brides sont les moyens les plus répandus qui servent de connexion entre les équipements et les différents systèmes où un fluide sous pression y est contenu ou y circule. Pour ne citer que quelques exemples, ces assemblages sont utilisés dans les échangeurs de chaleur, les générateurs de vapeur, les systèmes de tuyauterie, les turbines, les compresseurs et les colonnes de distillation. Les principales industries qui les utilisent, sont les usines chimiques et pétrochimiques, raffineries, les centrales thermiques et nucléaires ainsi que les industries de transport et de transformation. Même si d'autres types de joints tels que les joints soudés garantissent une étanchéité presque parfaite par rapport aux joints boulonnés, ceux-ci sont nécessaires parce que démontables. Ils permettent ainsi l'entretien et l'inspection des installations.

Généralement, un assemblage boulonné est constitué de deux brides entre lesquelles est comprimé, à l'aide de boulons, un joint d'étanchéité. La déformation plastique du matériau du joint nécessite un serrage adéquat des boulons, afin que le matériau épouse les aspérités des brides et empêche ainsi les fuites. L'intégrité mécanique et l'étanchéité sont les deux critères fondamentaux pour assurer le bon fonctionnement du joint. Du point de vue tenue mécanique, les méthodes de calcul des assemblages à brides donnent de bons résultats et sont fiables. C'est donc l'étanchéité qui constitue la principale préoccupation des utilisateurs des assemblages boulonnés et qui apparait pour le moment comme étant le problème le moins maîtrisable. Une fuite même minime peut,

dans certaines circonstances, avoir des conséquences couteuses. Une fuite peut provoquer un arrêt de fonctionnement d'une installation; elle peut aussi déclencher un feu, une explosion ou pis encore, être la cause de désastres graves incluant la contamination. C'est dans ce sens que l'Agence Américaine de Protection de l'Environnement EPA a adopté, par le biais du Congrès, une réglementation très stricte concernant les émissions fugitives dans les installations industrielles.

Avec l'utilisation ubiquiste des assemblages à brides munis de joints d'étanchéité alors que les contraintes environnementales deviennent de plus en plus sévères , il est impératif afin de réduire la fuite au minimum d'en comprendre le phénomène et d'en étudier son évolution en cours d'opération. L'introduction d'une méthode améliorée de conception des assemblages à brides s'avère donc plus que nécessaire.

Le choix et l'installation des assemblages à brides nécessitent une attention particulière. En effet, maintenir un niveau adéquat d'étanchéité dans les conditions de fonctionnement souvent très sévères telles que les hautes pressions et températures, les milieux corrosifs, toxiques, inflammables et en présence des vibrations, est un dilemme de taille pour les fabricants d'assemblage boulonnés sans compter les nombreux paramètres qui doivent être pris en considération: la géométrie et la configuration de l'assemblage, les propriétés des matériaux, la sélection du joint, le serrage initial requis, la rotation de la bride et sa relaxation due au fluage.

La revue bibliographique démontre que les assemblages à brides ont fait l'objet de nombreuses études depuis l'adoption de la méthode de Taylor-Forge par l'ASME au début des années 40. Depuis une vingtaine d'années, on a remis en cause la méthode de calcul des brides boulonnées du code ASME et on a questionné, en particulier, la validité des coefficients de joints "m" et "y" qui semble-t-il n'ont jamais été vérifiés expérimentalement. C'est pourquoi plusieurs organismes internationaux tels que le PVRC entreprennent des travaux de recherche approfondies afin de bien cerner le problème des fuites. A l'Ecole Polytechnique de Montréal, le laboratoire d'étanchéité (TTRL) de la section mécanique appliquée est activement impliqué dans ce domaine. Ces activités sont principalement axées sur la compréhension du comportement des joints aussi bien à température ambiante qu'à haute température avec une attention particulière au développement de nouvelles normes pour la caractérisation mécanique des joints.

Dans ce sens, suite aux nombreux tests dirigés par Bazergui, Payne, Marchand et Derenne, une nouvelle procédure de conception des assemblages à brides basée sur le critère d'étanchéité, a été développée avec succès. En effet, de nouvelles constantes de joints, G_b, a et G_s, ont été définies à partir des courbes de la contrainte d'écrasement en fonction d'un paramètre d'étanchéité T_p. Ces courbes sont obtenues à partir de tests d'étanchéité effectués à température ambiante.

La compréhension de l'influence de la température et du temps sur le comportement à l'étanchéité est un élément clef à la réussite et à la maîtrise de

conception d'assemblages à brides sans fuite. Le fluage, la dégradation thermique et la différence de dilatation thermique sont des éléments qui contribuent à la variation de la charge dans le joint. La diminution de la contrainte sur le joint due, surtout aux deux premiers phénomènes et communément appelée relaxation, est un processus physique rattaché à la perte d'épaisseur du joint. Aucune des méthodes présentement disponibles pour la conception des brides ne présente un modèle suffisamment sophistiqué pour tenir compte des paramètres pouvant guider l'ingénieur à des assemblages étanches à long terme. C'est l'objet de notre travail.

Dans cette thèse, nous présentons une méthode d'analyse des forces et des déplacements existant dans les assemblages à brides boulonnées munis de joints d'étanchéité à l'intérieur du cercle des boulons. Deux configurations d'assemblage sont considérées; les brides simples et les brides avec collerettes , toutes deux à faces surélevées. Ces deux types de bride peuvent être montés en paire ou munies d'un couvert plat. En développant un modèle analytique basé sur l'interaction élastique entre les différents éléments de l'assemblage, on est capable de tenir compte des effets de la température notamment le fluage, la différence de dilatation thermique et la dégradation du joint. Le modèle a été validé en effectuant des comparaisons avec des résultats expérimentaux ou numériques tels qu'obtenus par la méthode des éléments finis.

Ayant identifié, en premier lieu, la dépendance des conditions de fonctionnement aux conditions de serrage initial, nous avons élaboré un modèle mettant en relation la

force résiduelle sur le joint lors du fonctionnement, et la force appliquée lors du serrage initial. Ceci est une amélioration par rapport au code ASME ou une telle interdépendance n'est pas prise en compte dans le calcul des forces de l'assemblage, ce qui pourrait expliquer en partie la faible performance à l'étanchéité de certains assemblages conçus suivant le code. Cependant, la philosophie générale ainsi que la méthodologie adoptées dans notre modèle reste de près semblable à celle dite de Taylor-Forge utilisée dans le code de l'ASME.

L'assemblage est divisé en trois éléments distincts, à savoir: le joint, les boulons et la bride. Ces trois éléments sont représentés par des ressorts élastiques distincts montés en série. En réalité, le joint offre un comportement généralement non-linéaire. Cependant, puisque notre souci est le contrôle de la fuite, nous avons pu exploiter les caractéristiques du joint dans les conditions de fonctionnement. Ainsi, le fait que le joint se comporte linéairement lors du déchargement est un avantage important puisqu'il permet la simplification du modèle. Cette quasi-linéarité se maintient d'ailleurs, lors des chargements et déchargements subséquents. En effet, lors de l'écrasement initial, suite à la séquence de serrage initial, le joint subit des alternances de chargements, déchargements et rechargements qui démontrent toutes un comportement quasi-linéaire.

La bride est l'élément de l'assemblage qui exige une analyse plus complexe. Les différentes parties qui la constituent, à savoir: le plateau, la collerette et l'enveloppe cylindrique, doivent être analysées séparément. Le plateau est traité par la théorie des

anneaux ou la théorie des plaques dépendant du rapport des diamètres extérieur et intérieur. La théorie des coques cylindriques d'épaisseur constante est appliquée à l'enveloppe cylindrique et la théorie des coques cylindriques d'épaisseur linéairement variable à la collerette. Ainsi, ces éléments sont traités en tant qu'entités indépendantes avec des conditions aux frontières communes: aux jonctions entre le cylindre, la collerette et le plateau, les conditions d'équilibre et de compatibilité des déplacements et des rotations sont établies. En particulier, la compatibilité géométrique axiale impliquant le déplacement du boulon est nécessaire pour mettre en relation la condition de fonctionnement et de pré-serrage. Il est à noter que l'effet de résistance au frottement entre les surfaces des brides et le joint, a été introduit en option. Cet effet pourrait être très important pour la prédiction des contraintes limites des "blow-out" au niveau des joints.

Nous avons ainsi développé un programme, "POLYFLG", fonctionnant sur micro-ordinateur. Le programme résout le système d'équation à 5 inconnues M_0, P_0, V_g, θ_f et F_b, pour les brides sans collerette et à 11 inconnues M_1, P_1, M_2, P_2, C_1, C_2, C_3, C_4, V_g, θ_f et F_b, pour les brides avec collerette. Ces variables permettent le calcul des déformations et des contraintes dans les différents éléments de l'assemblage servant à examiner le degré d'étanchéité. Les exemples d'assemblages considérés ont montré que le modèle peut prédire la variation de la charge dans les boulons avec une erreur de moins de 4 % . Ainsi, comme dans les tests expérimentaux entrepris par Kohmura (1985) et Sawa et al. (1991), notre modèle a pu également prédire le maintient et même la

diminution de la charge dans les boulons avec augmentation de la pression et cela suivant les caractéristiques de l'assemblage.

L'évaluation de la distribution de la contrainte radiale dans le joint a pu être faite à partir du modèle élaboré incluant une représentation simplifiée du joint. Il va sans dire qu'une bonne estimation de la rotation de la bride est un paramètre essentiel dans cette évaluation. La modélisation du joint par un ressort élastique dont la position est réajustée suivant le point d'application de la charge du joint s'avère une méthode efficace. Elle permet, en outre, d'éviter une modélisation plus complexe impliquant plusieurs petits éléments de joints concentriques dont la réaction totale, résultante de ces derniers, aurait le même module et la même position. Toutefois, cette méthode est limitée aux joints dont la rigidité est relativement faible qui subissent des déformations plus importantes que les surfaces de contact des brides. D'autre part, la bride est supposée suffisamment rigide pour négliger les déformations due à la flexion. Néanmoins, les rotations de brides calculées à partir de ces suppositions sont en bonne comparaison avec celles mesurées sur des brides réelles. La répartition radiale de la contrainte sur le joint n'a fait l'objet que d'une étude par éléments finis. L'étude expérimentale que nous avons entreprise à l'aide du système "DynaForce" de mesure de pression de contact s'est avérée très peu fiable à cause du comportement fortement non-linéaire du capteur avec un hystérésis prononcé. Cependant, des observations qualitatives sur des joints en feuille ont confirmé la tendance linéaire de la distribution de la contrainte avec une mise en évidence nette de la contrainte maximale du côté du diamètre extérieure du joint.

Notre modèle inclut, en outre, les effets thermiques qui, en général, ont tendance à causer une relaxation du joint et des boulons dans le temps. Dans notre modèle, la perte de la charge sur le joint est traduite par une diminution de l'épaisseur due au fluage et/ou à la dégradation thermique. Par ailleurs, la différence de dilatation thermique entre les différents éléments de l'assemblage est, le plus souvent, la cause d'une augmentation de la charge dans les boulons et sur le joint. En effet, étant à une température inférieure à celle de la bride et du joint, les boulons subissent une dilatation inférieure ce qui engendre, par conséquent une augmentation de la charge. La diminution de la charge sur le joint due au fluage à température ambiante a été le sujet d'une étude expérimentale détaillée. Celle-ci a permis de valider le modèle de relaxation proposé. En effet, la comparaison avec les résultats de relaxation effectués sur des assemblages à bride réels a révélé que l'approche analytique entreprise donne de bon résultats.

Tous les tests de relaxation ont été effectués avec un assemblage à brides de 4 po. (102 mm) de diamètre de classe 600. Deux type de joints à base de PTFE avec deux épaisseurs différentes, 1/8 et 1/16 po. (3.2 et 1.6 mm), ont été laissés relaxer sur cet assemblage pendant une période de quelque 5 heures. Les mesures coïncident aux valeurs calculées à l'aide du modèle à quelque 2% près. A titre d'exemple, un joint en PTFE de 1/8 po. subit une perte de charge de 30% due à sa relaxation durant la durée du test. De plus, plus le joint est épais, plus sa relaxation est importante. La rigidité de l'assemblage a une influence directe sur la relaxation; plus la rigidité est grande plus la relaxation est

importante. Ainsi, l'extension des boulons ou l'introduction de rondelles "Belleville" diminuent la rigidité et améliorent la situation.

Il est bien établi que le comportement à l'étanchéité des assemblages à brides est relié directement à la pression de contact sur le joint. La répartition radiale de la contrainte sur le joint doit donc faire l'objet d'une étude expérimentale plus approfondie. C'est pourquoi, le capteur "DynaForce" et l'amélioration de la procédure d'étalonnage sont plus que nécessaires pour la validation de nos résultats et la compréhension de l'étanchéité des assemblages boulonnés munis de joint. Même si notre modèle de fluage relaxation n'a été validé que pour les températures ambiantes, il pourrait être utilisé pour inclure la relaxation due au fluage à hautes températures. Par ailleurs, il serait souhaitable d'inclure éventuellement dans le modèle les charges externes, les effets transitoires et les chocs thermiques qui peuvent compromettre l'étanchéité des assemblages boulonnés.

TABLE OF CONTENT

LIST OF SYMBOLS AND ABBREVIATIONS

α,rd	tapper hub angle
β_c,in^{-1}	cylinder constant
γ	flange constant
Δ_n,in	nut axial displacement
θ_c,rad	cylinder rotation
θ_f,rad	flange rotation
θ_h,rad	hub rotation
κ	reference exposure
ε	dimensionless position on hub
η	degradation constant
λ	degradation constant
ρ,in^{½}	hub flexural rigidity
ν_c	cylinder Poisson's ratio
ν_f	flange Poisson's ratio
ν_g	gasket Poisson's ratio
ν_h	hub Poisson's ratio
ψ_1 to ψ_4	Schleicher functions proportional to Kelvin functions
a	slope of tightness loading curve
a_h,in	hub mean radius
a_g,in	gasket outside diameter

A,in	flange outside diameter
A_b,in^2	bolt area
A_p,in^2	pressure area
A_g,in^2	full gasket contact area
A_e	equivalent aged exposure parameter
A_p	aging parameter based on weight loss correlation
b,in	effective gasket seating width
b_g,in	gasket inside diameter
B,in	flange inside diameter
c	time exponent for A_e
C,in	bolt circle diameter
C_1 to C_4	hub constant of integration
d	time exponent for A_p
D,lb.in	plate flexural rigidity
D_0,in	diameter location of flange centroid
D_c,in	cylinder flexural rigidity
D_g,in	gasket deflection
D_{gmax},in	maximum gasket deflection
D_p,in	blind cover flexural rigidity
e	joint assembly efficiency
e_c,in	gasket relaxed deflection
E_b,psi	bolt modulus of elasticity

E_c,psi	cylinder modulus of elasticity
E_e,psi	joint element modulus of elasticity
E_f,psi	flange modulus of elasticity
E_g,psi	gasket modulus of decompression
E_p,psi	blind cover modulus of elasticity
F_b,lb	bolt force
F_e,lb	joint element force
F_g,lb	gasket force
F_D,lb	hydrostatic end force on area inside of flange
F_G,lb	gasket load
F_T,lb	hydrostatic end force on annular area outside of flange
g_1,in	radial thickness of hub at junction with flange
G,in	effective gasket diameter
G_b,psi	loading intercept on a tightness curve
G_s,psi	unloading intercept on a tightness curve
h_D,in	radial distance from bolt circle to F_D
h_G,in	radial distance from bolt circle to F_G
h_T,in	radial distance from bolt circle to F_T
K	ratio of outside diameter to inside diameter of flange
K_b,lb/in	bolt uniaxial stiffness
K_e,lb/in	joint element uniaxial stiffness
K_f,lb/in	flange uniaxial stiffness

K_g,lb/in	gasket uniaxial stiffness
K_p,lb/in	blind closure uniaxial stiffness
K_j,lb/in	joint uniaxial stiffness
l_b,in	initial bolt length
l_g,in	gasket width
l_h,in	tapered hub length
L_{RM},mg/s	mass leak rate
L^*_{RM},mg/s	unit mass leak rate
m	gasket factor
m_w,°K	slope of curve w_{48} versus 1/T
M,in.lb/in	discontinuity moment
M_0,in.lb/in	flange to cylinder discontinuity moment
M_1,in.lb/in	hub to cylinder discontinuity moment
M_2,in.lb/in	flange to hub discontinuity moment
M_f,in.lb/in	total equivalent flange moment
n	number of bolts
N,in	effective gasket width
N_l,lb/in	longitudinal force in cylinder
p,psi	internal pressure
p^*,psi	reference pressure
P,lb/in	discontinuity force
P_0,lb/in	flange to cylinder discontinuity force

P_1,lb/in	hub to cylinder discontinuity force
P_2,lb/in	flange to hub discontinuity force
S_1 to S_8	functions depending on ψ and ψ'
S_a,psi	allowable bolt stress at ambient temperature
S_A,psi	gasket assembly stress
S_{Amin},psi	minimum gasket assembly stress
S_b,psi	allowable bolt stress at design temperature
S_g,psi	gasket stress
S_{gmin},psi	minimum operating gasket stress
S_{m1},psi	gasket operating stress
S_{m2},psi	gasket seating stress
S_y,psi	flange yield stress
S_{ya},psi	theoretical gasket seating stress
t,hr	exposure time
t_c,in	cylinder thickness
t_e,in	equivalent cylinder thickness
t_f,in	flange thickness
t_g,in	initial gasket thickness
t_p,in	blind cover thickness
T,°K	exposure absolute temperature
T_p	tightness parameter or factor
T_{pmin}	minimum tightness

T_r	tightness ratio
T_t, °K	reference threshold temperature
u,in	axial displacement
$u_{1,2,g}$,in	gasket axial displacement
u_b,in	bolt axial displacement
u_e,in	joint element axial displacement
u_f,in	flange axial displacement
u_p,in	blind cover axial displacement
V_g,lb	frictional force
w,in	radial displacement
w′	fraction of gasket weight loss
w_{48},	fraction of gasket weight loss after 48-hr exposure
w_f,in	flange radial displacement
w_g,in	gasket radial displacement
w_h,in	tapered hub radial displacement
W_m,lb	design bolt load
W_{m1},lb	operating design bolt load
W_{m2},lb	seating design bolt load
y,psi	gasket design seating stress
Y	ASME Code factor involving K

LIST OF ACRONYMS

AHOT	Aged Hot Operational Tightness Test
ANSI	American National Standard Institute
ARLA	Aged Relaxation Leakage Adhesion Screen Test
ASCII	American Standard Code for Information Interchange
ASME	American Society of Mechanical Engineers
ASTM	American Society of Testing and Materials
ATRS	Aged Tensile Relaxation Screen Test
BHRG	British Hydrodynamics Research Group (UK)
BS	British Standard (UK)
CETIM	Centre Technique des Industries Mécaniques (France)
DIN	Deutshes Institut fuer Normung (Germany)
EPA	Environmental Protection Agency
FEM	Finite Element Method (sometimes just FE)
FIRS	Fire Simulation Screen Test
FITT	Fire Tightness Test
HATR	High Temperature Aged Tensile Relaxation Screen Test
HOTT	Hot Operating Tightness Test
MPA	Materialprüfungsanstalt Studgart (Germany)
MTI	Materials Technology Institute of the Chemical Process Industries (USA)
MTS	Material Testing Specification

NBR	Acrylonitrile Butadiene Rubber
NCR	Nitrile-Chloroprene Rubber
NPS	Normal Pipe Size
NTC	Neotetrazolium Chloride
PTFE	Polytetrafluoroethylene
PVRC	Pressure Vessel Research Council
ROTT	Room Temperature Tightness Test
SAE	Society of Automotive Engineers
SS	Stainless Steel
TTRL	Tightness Testing and Research Laboratory
UGR	Universal Gasket Test Rig

LIST OF FIGURES

LIST OF TABLES

LIST OF APPENDICES

CHAPITER 1

INTRODUCTION

1.1 GENERAL SCOPE

Bolted flanged joints are extensively used to connect shell elements containing a fluid under pressure (Fig. 1.1). Bolted joints offer the possibility of disassembly for maintenance and inspection. In comparison with other types of joints, like welded joints, they are often seen as a source of potential leakage during operation. Bolted flanged joints are used in virtually all pressure vessels such as heat exchangers, steam generators, piping systems, turbines, compressors and process columns. They have a wide range of applications in chemical and petrochemical plants, oil refineries, thermal and nuclear power plants and transportation and transformation industries.

Flanged joints come in different design configurations. During assembly, the bolts are tightened in a way that the gasket located between the flanges, as shown in Fig. 1.2, provides tightness when the system is under internal pressure. It is obvious that the bolt load that holds the flanges together must be equal to the sum of the force developed by the internal pressure that tends to separate the flanges, and the contact pressure force on the gasket needed to prevent leakage.

At the heart of the bolted flanged joint is the gasket. The function of the flanges and the bolts is to maintain on the gasket such deformation, surface constraint and normal compressive force as may be needed to prevent leakage of the contained pressurised fluid. This cannot be achieved unless there exists a sufficient load and hence deformation on the gasket so as to cause intimate contact with the irregularities of the flange surfaces, but not so great as to crush the gasket. The gasket must exhibit a good resilience in order to recover when the fluid pressure is released. It must also have good creep and relaxation resistance under often demanding operating conditions. In order to respond to user demands for reliability and improved gasket performance, gasket manufacturers rely on a variety of tests for evaluating gasket behavior.

At this point, it is perhaps necessary to give some descriptive details on different joints and gaskets. According to the available methods for the design of bolted gasketed joints, flanges can be classified under several categories. The most popular ones, often referred to as the raised face flanges, are fitted with a ring-type gasket located inside the bolt circle and with no contact outside this circle. Less popular types of flanges include the flat face flanges in metal-to-metal contact and the full-face gasketed flanges (Fig. 1.3). For the purpose of the present study, only two types of raised face flanges will be considered. They are namely the welding neck type and the ring type flanges.

As to the gaskets used, not only do they come in different types, shapes and sizes but they are selected according to specific applications. The material of which they are

made may be metallic (steel, stainless steel, copper), non-metallic (Elastomer, fibres, graphite, PTFE) or a combination of both. Figure 1.4 shows schematically some of the most commonly used types of gaskets.

1.2 HISTORICAL BACKGROUND

Flanges are classified according to their dimensions and pressure-temperature ratings. The history of the development of flange dimensions and ratings can be traced back to their prototype cast iron flanges and flange fittings in the late 1880's. It was at that time that the first step towards standardization began when the ASME appointed a committee to obtain the views of manufacturers of pumps, steam engines and valves on the matter. The continuous requirement and need to develop better joints has led to the establishment of the present ASME/ANSI B16.5 and B16.34 Standards. Within the framework of established dimensions, the B16.5 Standard has shown remarkable progress in the diversity of types of flanges, sizes, and materials; and in self-consistency in ratings and consistency with the ASME Boiler Code design concepts.

Flange design has been extensively researched and written about for many decades and has possibly attracted more investigations than almost any other pressure vessel component. The most significant contribution over the years was the paper published by Waters et al. (1937) in which they presented a flange design system which has led to the

well known "Taylor-Forge" method (G&W Taylor,1978). The wide acceptance and the relative simplicity in its application have meant that this method has become the most extensively used technique in modern flange design and it forms the basis of the ASME Boiler and Pressure Vessel Code procedure (ASME,1992) for the design of flanges with gaskets.

However, the present flange design procedure is far from being sophisticated enough to meet today's technological and environmental requirements so that many joint problems still remain unsolved. The reliability of the m and y gasket factors in terms of tightness and the relative difficulty in sealing 3 inch class 150 lb flanges are a few examples that are presently of major concern (Short II,1992).

1.3 FUNCTIONAL BEHAVIOR AND ASSOCIATED PROBLEMS

One of the major issue of today's increasing environmental consciousness is the need to reduce fugitive emissions which refers to leakage in joints. In this respect, preventing leakage produced via bolted joints is perhaps one of the most challenging tasks for joint designers and gasket manufacturers. The problem is made more difficult to overcome due to the relatively poor performance of many asbestos gaskets substitutes such gaskets made of elastomer binders mixed with organic fibres.

Fluids to be sealed can be toxic, explosive and/or flammable having potential for considerable health and environmental damages. In other cases, replacement of leaky gaskets will cause an interruption in service which often means a considerable revenue loss and possibly a complete shutdown due to government sanctions. Indeed, with the new strict environmental regulations known as the Clean Air Act, recently adopted by the American Congress and to be imposed by the EPA (Environmental Protection Agency) in the future to already existing plants, manufacturers have to place more emphasis on the leakage performance and long term behavior of their gasketed joints. Most countries plan or are already implementing clean air regulations. The US is a bell-weather of things to come.

With the increasing ubiquitous use of the previous mentioned bolted joints and with the more restrictive environmental protection laws, attention has focused upon ways not only to reduce the problem of leakage but also to improve the general performance of joints by introducing an efficient design method. By far the largest majority of flanges are selected from standards such as ASME/ANSI B16.5 (1988), and the designer is required to give only small consideration to gaskets, bolts and stresses. Likewise, he often relies on joint designs which have been derived from a combination of past experience, tests and calculations, and with usually provide adequate performance in service.

With higher pressures and temperatures becoming evident due to the required increasing performance and efficiency requirements in power and chemical plants, bolted joint connections require rigorous analysis for both structural integrity and leakage tightness. In most joint analyses, little attention is focused on leakage performance of the joint with the emphasis being put towards structural integrity by keeping all joint component stresses below specified levels.

Leakage is, however, not just related to the gasket. It is dependent on the whole flanged joint which is composed of three separate and independent, although interrelated components: the flanges, the gasket, and the bolts, and which are assembled by yet another influence, the assembly procedure. Proper controls must be exercised in the selection and application of all of these elements to attain a joint with an acceptable leak tightness.

Primarily all types of joints are required to seal without leakage. To achieve this, the correct combination of some parameters such as geometry, material, gasket, bolts and surface finish must be specified. The problem is made more difficult by the practical variability of some of these parameters. A good design technique should encompass most aspects of joint behavior and produce efficient sealing performance within the clearly defined limits of the method used.

A number of questions have been raised for the past 10 years with regards to the precision of the methods used for the design of bolted flanged connections. In the field, investigators has shown that leakage in gasketed joints is still a major problem yet to be overcome. In 1985, an important survey on flange joints led by Payne (1985) confirmed that leakage is indeed the big issue in bolted flanged joints and is primarily due to both increased temperature and gasket failure. Since the early definition of the gasket "m" and "y" factors in a paper by Rossheim and Markl (1943), little has been done to revise or confirm their validity. The result of numerous inquiries to ASME concerning the adequacy of these factors, led to a request for their evaluation by the PVRC Subcommittee on Bolted Flanged Connections (PVRC,1975, Raut and Leon,1977).

An investigation by Kraus (1980a) established that, effectively, one of the major discrepancies in the design of flanges was related to the use of factors "m" and "y" for which no experimental verification was ever undertaken. As a result, the PVRC launched a comprehensive research program to investigate the behavior of commonly used gaskets in order to predict the tightness performance of actual flanged assemblies. Some parameters such as the gasket width, gasket thickness, contained fluid, initial assembly stress, residual gasket stress and fluid pressure were shown to have a major impact on the performance of various common types of gaskets. As a direct result, the concept of gasket leak rate started to be evoked as a design criteria. Indeed, it was not until 1985 that the concept of leakage, once completely ignored by the ASME code, was successfully introduced in the design of flanges by Payne et al., and is presently in the

process of being adopted by the ASME code as an alternative procedure for the design of bolted flanged connections that are based on tightness.

Important research entities throughout the world and mainly in USA (PVRC, MTI), France (CETIM), England (BHRG) and Germany (MPA) are fully active trying to understand the complex phenomenon involved in the leakage of gasketed joints. At the Ecole Polytechnique of Montreal, the Tightness Testing and Research Laboratory (TTRL) of the applied mechanics section has been intensively working in this field since the early 1980's: Problems associated with both room temperature and elevated temperature behavior of bolted flanged joints are tackled with particular focus on the development of new standardized gasket test methods.

1.4 OBJECTIVE OF THE RESEARCH WORK

No bolted joint design method has been developed which is capable of taking into account most of the parameters involved in the operation of a flanged joint and which guide the design engineer towards a long term leak proof design. As an example, little has been done with regard to the influence of creep relaxation of the bolted joint especially at high temperature. It would also be desirable to have a precise evaluation of the remaining compression stress on the gasket at all times, so as to predict leakage. Initial joint assembly conditions, on the other hand, are known to have a direct influence

on the operating conditions and there exists a relationship for both the deformations and the loads of the different joint elements between the two states. But yet, the present ASME code design procedure fail to comply with this relationship.

This work presents a method to analyze the actual force relationships in a joint assembly, and therefore provides accurate values for use in predicting the joint tightness obtained from a ROTT gasket test. One of our prime objectives is to expand our knowledge of the behavior of bolted flanged joints through the development of an analytical model based on elastic interaction of all joint members and capable of taking into account temperature induced effects, namely thermal expansion, gasket creep and degradation. In concentrating on the two types of joints already mentioned, the model will be tested and validated by comparison with experimental and finite element results.

A first basic development is to find a relationship between the bolt initial seating and final operating loads taking into account flange rotation, flexibility of both the gasket and the bolts and friction between gasket and flange and, when applicable, the stiffness of the end closure. However, the general philosophy adopted is similar to the one used in the Taylor-Forge method. In addition, effects such as creep relaxation of the bolts and the gasket and thermal expansion of the different joint elements will eventually be incorporated. A simple analytical method for evaluating the joint stiffness which has a strong influence on the relaxation of the clamping load will also be included. Provided that enough data of a pure creep test of any gasket material exists, the model is capable

of simulating, with reasonable accuracy, its true creep relaxation behavior when installed in a flanged joint. Finally, a study of the influence of flange rotation on the radial distribution of gasket contact stress and the load on the bolts will also be investigated using the DynaForce sensing system described in Chapter 3 and strain gages. The objectives of the proposed research are summarised as follows;

1. Identify all important flange parameters and develop an analytical model based on the elastic interaction of all joint members capable of a more accurate prediction of the gasket compression and bolt loads at all times.
2. Develop a gasket model including an adjustment of the gasket reaction and study the effect of flange rotation on the gasket stress distribution.
3. Study the redistribution of the normal stresses on the gasket and the final forces in a flanged joint, due to small displacements in both the gasket and the bolts so as to simulate relaxation due to gasket creep and thermal degradation as well as the difference in expansion of all joint components.
4. Study the effect of joint rigidity on the creep relaxation and the leakage performance of a typical bolted gasketed joint.
5. Contribute to the improvement and extension of the ASME Code flange design procedure by providing a more accurate and complete analytical tool to be used for maintenance purposes, design modifications and the development of new gaskets and joints, and capable of incorporating future development especially the effects of elevated temperatures and external loads.

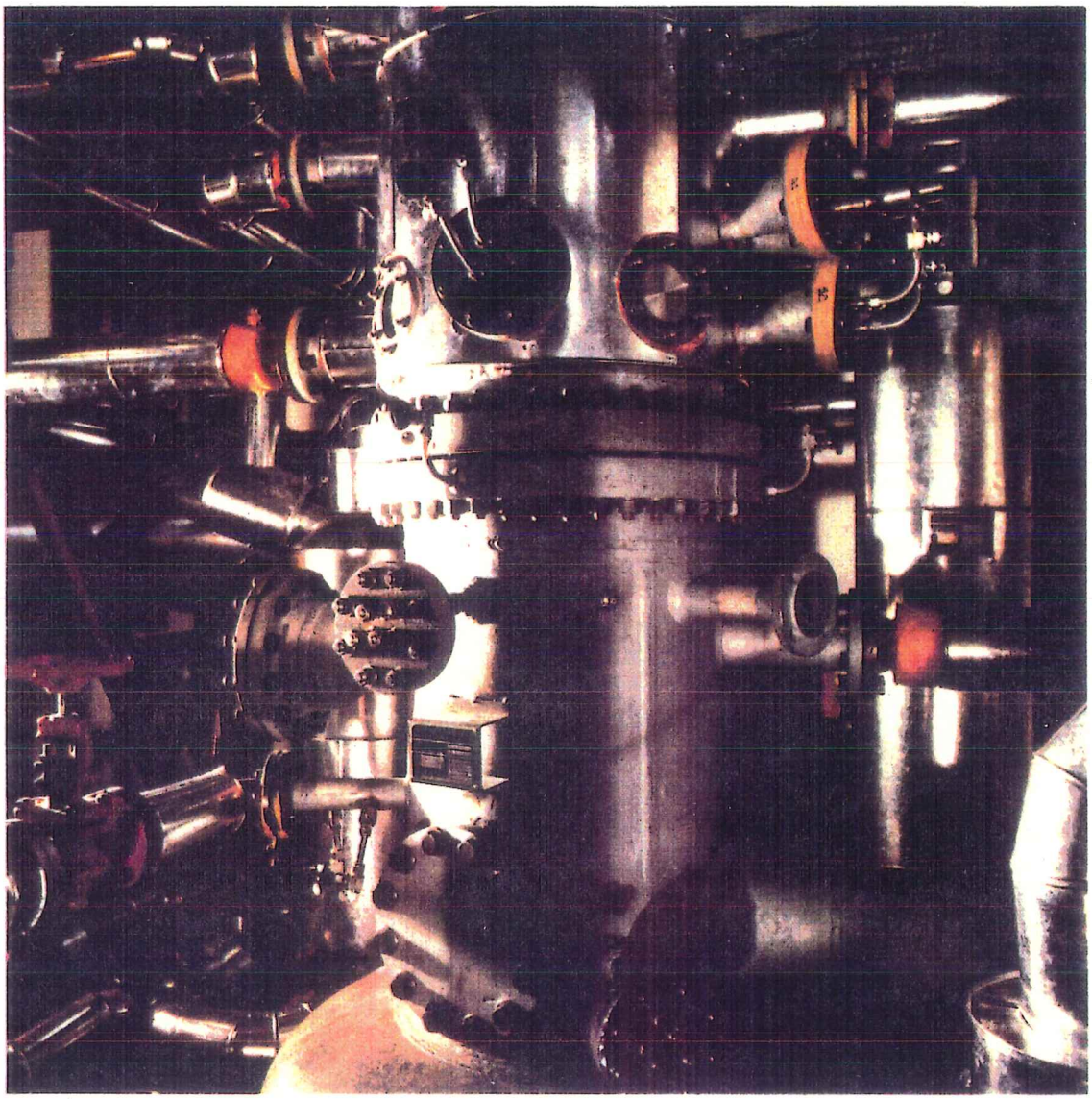

Figure 1.1 Use of bolted flanged joints

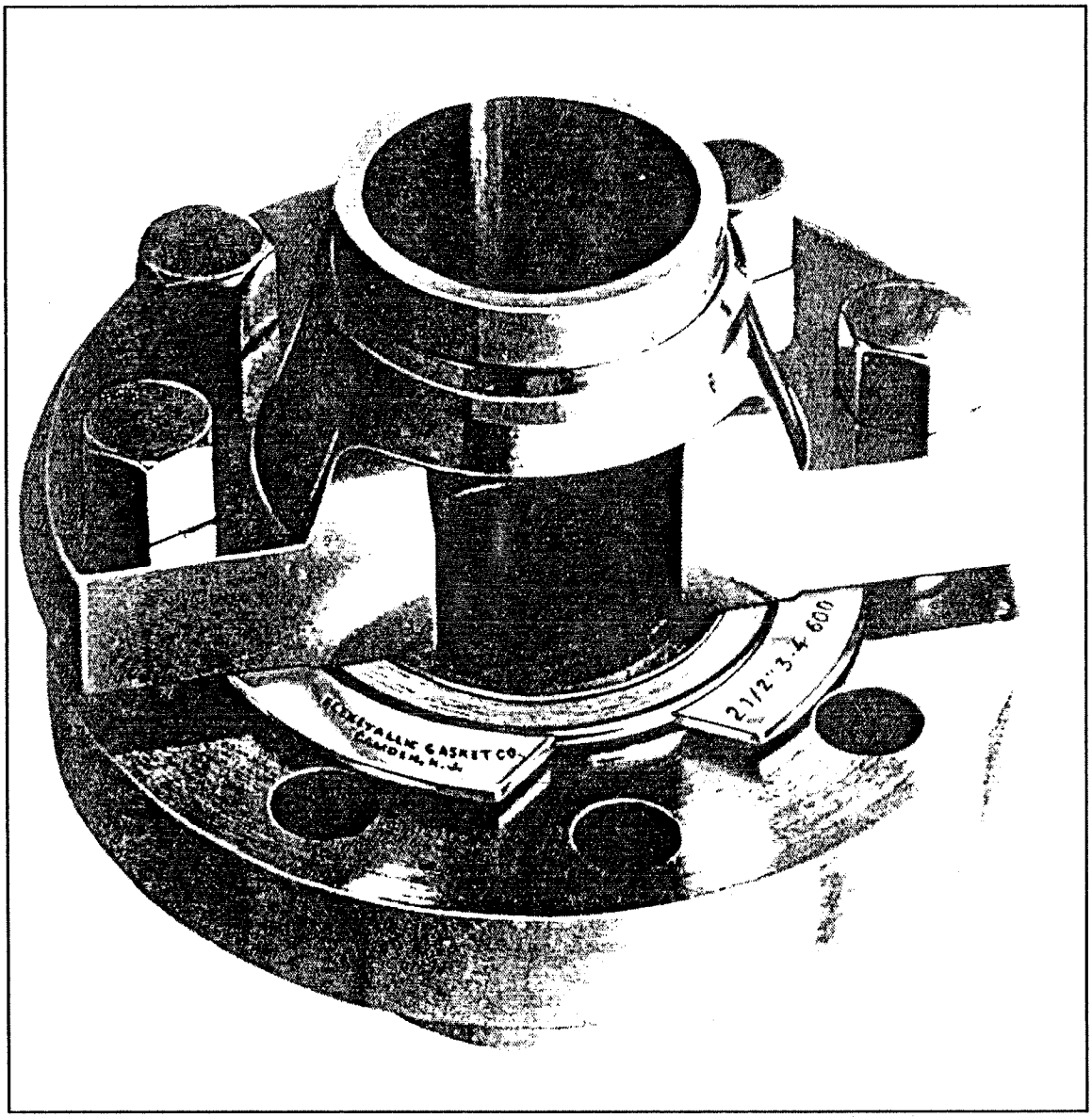

Figure 1.2 Section of a typical bolted flanged joint

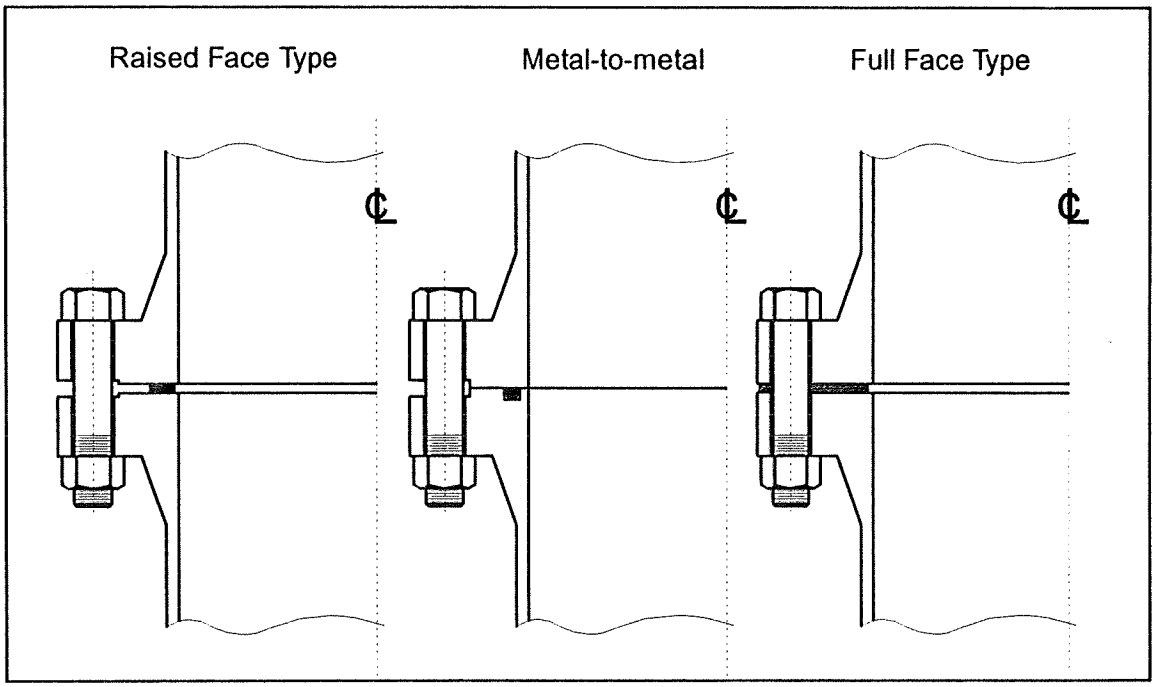

Figure 1.3 Gasket used in bolted flanged joints

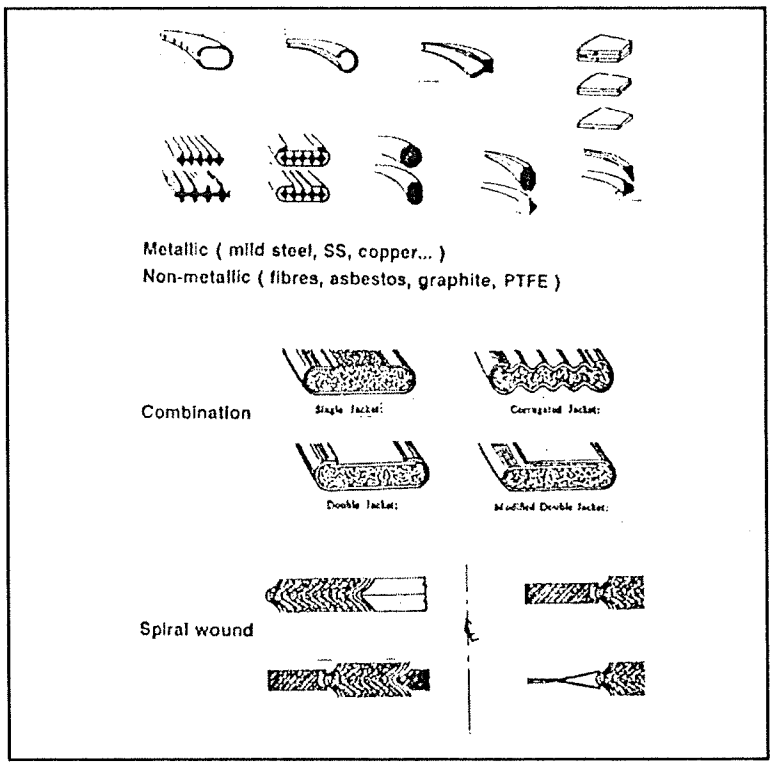

Figure 1.4 Gasket used in bolted flanged joints

CHAPTER 2

LITERATURE SEARCH

2.1 INTRODUCTION

The technology of gasketed flanged joints has drawn considerable attention since the early use of boilers and pressure vessels. With the increasing use of fluids under pressure in general and steam in particular in some industries, it appeared necessary to find simple methods to design flanges. Before the end of the 19th century, there was no known design method in use for flanged joints and people relied on their own experience. Begining in 1891, attempts were made by several researchers (Bach,1891,1896 and Westphal,1897) in Germany and later in the USA (Anonymous,1905), to develop simple methods for flange design based on the theory of elasticity and some empirical formulations. These methods proved to be inaccurate and it was not until 1927 that the technology of flange analysis began to emerge with a new approach by Waters and Taylor. They later introduced some sophistication in their analysis to include the effect of integral and loose tapered hubs (Waters et al.,1937). This was a major contribution to flange technology and forms the basis of the present ASME Boiler and Pressure Vessel Code flange design procedure.

Ever since, the original work of Water and Taylor, a number of publications have appeared offering alternative methods and improvements and a few of these are worth reviewing. Three of the most interesting bibliographical reviews on the subject of bolted flanged joints are worth mentioning. The first one is by Schneider and Rodabaugh (1982) which deals with relevant background material of several existing flange designs, most of which were allowed by the code at one time. The paper by Blach and Bazergui (1981) reviewed methods of analysis of bolted flanged connections including an extensive list of 262 references with short comments for quick review. Finally, Kraus (1980) reviewed qualitatively and quantitatively the gasket leakage testing literature and concluded that the gasket factors "m" and "y", still recommended in the ASME Code, were not verified experimentally. He added that these factors depend not only on the gasket type and material but also on gasket width, surface finish of the flanges, gasket stress, assembly stress, internal pressure, contained fluid and permissible leakage rate, and concluded that further gasket testing was required.

There are as many designs as different available flange types. Since the appearance of the Taylor Forge method applicable to flanges with gaskets located inside the bolt circle and with no contact outside this circle, people considered the design of flat face flanges in metal-to-metal contact (Schneider,1968 and Waters,1971). Following extensive work (Schneider and Waters,1969,1978,1979) on flat face flanges in metal-to-metal contact with a blind cover, the code added this case to its Summer 1977 Addenda. In the same year, rules for the design of reverse flanges also appeared after an adaptation

of the conventional approach. Derivation formulas are given in a paper by Waters and Schneider (1980). The case of flat flanges with full face gaskets was investigated by Blach et al. (1986) who proposed a formulation consistent with the ASME Code philosophy. Full details of the plate flange case is given by Blach (1983).

2.2 ROOM TEMPERATURE BEHAVIOR OF BOLTED JOINTS

From the leakage tightness considerations, the design of gasketed joints relies very much on the "m" and "y" gasket factors that have been in use in the ASME Code since the early 1940's (Rosshein and Markl,1943). However it is surprising not to find, in a literature survey on flange design, a single paper which gives either an analytical or an experimental background to these two factors although people were concerned about their validity since they were first presented (Roberts,1950, Thorn,1955 and Donald and Salomon,1957). The "m" and "y" factors which are considered constant by the ASME code for a class of gasket material, were found to vary with fluid pressure gasket stress, gasket geometry and flange surface finish.

In an effort to clarify this situation, the PVRC Committee on Bolted Flanged Connections as requested by the ASME Boiler and Pressure Vessel Committee (DDP N°.XIII,1984), formed a task group on gasket testing. Extensive experimental tests, part of the Exploratory Gasket Program, conducted by Raut and Leon (1977) on some

gaskets, pointed out that some parameters have a major impact on the performance of various common types of gaskets. These parameters include gasket width and thickness, contained fluid, initial or assembly gasket stress, residual gasket stress under pressure and the fluid pressure itself. Ever since, many research programs have been launched to try and explain the different phenomena involved with gasket leakage and how to introduce these parameters in the design of bolted joints.

Quantitative leakage tests were performed for the first time in 1942 by Siebel and Wellinger who measured leak rate of a gasket compressed between rigid platens and pressurized with air, but no discussion was given of the method used for . Ever since, many researchers (Schwaigerer and Seufert,1951, Boon and Lok,1958, Rathburn,1964a and 1964b, Reuter,1973 and Raut and Leon,1977) have started to seriously investigate leakage using different detection techniques that are based on various physical principles and most of which are described in the exhaustive report by Marr (1968). However, most methods involve the confinement of the test gasket by using additional members sealed with O-rings. This provides a chamber into which the test fluid leaks through the gaskets and is measured. Notwithstanding, 40 years later, the concept of leakage was introduced for the first time in the design procedure of gasket joints by the gasket manufacturer Klinger (Sauter,1982) who produced charts based on a leakage of 0.25 ml/min, which was considered to be the limit of a technically tight seal. Unfortunately, a unique value of leakage as a reference for sealability, is not sufficient with regards to the various applications and sizes of bolted flanged joints. So this unique quantification scheme can

not be regarded as a well established tightness accaptability criteria.

In 1979, a comprehensive program recommended by the PVRC and known as the Gasket Test Program II started with two main objectives; the development of more meaningful gasket design factors based on leakage and the elaboration of a standard tightness test procedure at room temperature. As a result of this comprehensive program, the concept of tightness was introduced as a non-dimensional tightness parameter T_p defined in various papers (Bazergui et al.,1985 and Payne et al.,1988) and used in a proposed ASME-like optimizing design procedure.

$$T_p = \frac{p}{p^*} \left[\frac{L^*_{RM}}{L_{RM}} \right]^{0.5} \qquad (2.1)$$

T_p combines the mass leak rate of gasket with fluid pressure and can be interpreted as the pressure (in atmospheres) required to cause a unit helium leak rate of 1 mg/sec in a 150 mm OD gasket. T_p depends on not only the operating gasket stress but also the initial gasket seating stress. As a direct consequence, the traditional "m" and "y" gasket factors, introduced several decades ago, were replaced by three new idealized constants G_b, a and G_s which characterize the real leakage performance of gaskets. These new factors will be described in detail Section in 2.3.3 . One of the key issues to the problem of leakage performance in bolted gasketed joints is the proper assessment of the stress remaining on the gasket after initial tightening of the joint and application of the operating pressure. Therefore, the bolt load requirements have to be precisely evaluated for both the initial gasket seating and the operating conditions. Gasket seating is the

condition which exists when the gasket is seated by applying an initial load with the bolts during assembly. The operating bolt load is the one required to resist the hydrostatic end force of the design pressure tending to part the joint, and to maintain sufficient compression on the gasket to ensure a tight joint. Hereafter, we present design procedures used in the ASME Code and a new suggested approach based on the concept of leakage.

2.2.1 ASME Code Procedure

The initial compression force applied to a joint must serve several purposes namely:

- It must be sufficient to initially seat the gasket by flowing the gasket material into the imperfections of the gasket seating surfaces regardless of operating conditions.

- It must be great enough to compensate for the total hydrostatic end force that will be present during operating conditions.

- It must be sufficient to maintain a residual load on the gasket-flange interface. The design seating bolt load is thus given by:

$$W_{m2} = \pi \; b \; G \; y \qquad (2.2)$$

From a practical standpoint, the residual gasket load must be `m´ times the internal pressure if a tight joint is to be maintained. This coefficient is called the "m"

factor in the ASME Code. The design operating bolt load is then:

$$W_{m1} = \frac{\pi}{4} G^2 p + 2b \pi G m p \qquad (2.3)$$

Bolts are then selected so that the actual bolt area A_b is equal to or greater than the minimum required bolt area A_m obtained from the ratio of the greater of W_{m1} and W_{m2} over the allowable bolt stress. The maximum stress on the gasket is therefore:

$$S_g = \frac{A_b S_a}{2\pi N G} \qquad (2.4)$$

2.2.2 The Klinger Procedure

In an other but similar procedure to the one used in the ASME Code, the Klinger method is based on recommended seating and in-service gasket stresses and was suggested by Sauter (1982). It employs different gasket factors "m′" and "y′". The "y′" factor is the minimum seating stress to which the pressure is added while the "m′" factor is a maintenance factor. These factors are the slope and intercept of a straight line B made asymptotic to the experimental curve A of in-service gasket stress versus internal pressure (Fig. 2.1). This experimental curve is obtained for an assumed technically tight seal with a constant leak rate of 0.25 ml/min. The minimum in-service gasket stress is:

$$L = y' + m' p \qquad (2.5)$$

The recommended initial seating stress on the gasket is the recommended in-service stress L to which the reduction in stress resulting from the hydrostatic end load is added:

$$S_g = y' + m'p + \frac{\pi}{4}\frac{G^2}{A_g}p \qquad (2.6)$$

2.3.3 Modified Gasket Design Procedure

The initial bolt load may be derived from a more modern method based on the design criterion of tightness. This method is the result of the extensive gasket leakage tests that have been carried out under the auspices of the PVRC (Bazergui and Payne,1984, Bazergui and Marchand,1984 and Payne et al.,1989a). Figure 2.2 shows the gasket stress S_g as a function of tightness T_p. Such a graph is essential for interpreting gasket sealing behavior in terms of gasket stress. It shows a complete test sequence with two parts, A and B, corresponding to initial loading and subsequent unloading -reloading cycles which are representative of the real operating conditions.

With some simplifying assumptions for design purposes, the tightness performance of gaskets is ideally characterized by three new constants G_b, a and G_s represented in Fig. 2.2. The two first constants G_b and a are the intercept at $T_p = 1$ and the slope associated with the part A seating load-sequence data for higher loads respectively, while G_s is the ambient intercept at $T_p = 1$ associated with all part B unload-reload sequences.

Of particular interest is how tightness increases with increasing initial gasket stress. For the same operating gasket stress S_g, the unloading-reloading loop from the initial gasket seating stress S_A gives higher tightness T_p than that from the initial gasket seating stress S_{Amin}.

In order to optimize the bolt load, a similar but more balanced iterative procedure that uses a variable tightness criteria (Alvaro,1990) was developed. This method optimizes the values of the ASME Code-like seating and operating design loads (W_{m1} and W_{m2}), taking into consideration certain physical constraints on the joint. First, the minimum gasket stress should always be greater than twice the pressure 2p and secondly, the seating stress S_{ya} is reduced by 1.5 so as to avoid higher allowable stresses for the assembly condition.

The minimum bolt load W_m is derived by satisfying both the seating and operating gasket stress requirements for the design value of minimum tightness T_{pmin} during operation, given a specified design pressure, gasket geometry and constants G_b, a and G_s, (Hsu et al.,1994) such that:

- The required theoretical seating stress, S_{ya} is:

$$S_{ya} = \frac{G_b}{0.75} [1.5\ T_{pmin}]^a \qquad (2.7)$$

- The design seating stress component, S_{m2} is:

$$S_{m2} = \frac{S_{ya}}{1.5} - p\,\frac{A_p}{A_g} \tag{2.8}$$

- The design operating stress component, S_{m1} is:

$$S_{m1} = G_s \left[0.75\,\frac{S_{ya}}{G_s} \right]^{\frac{1}{T_r}} \tag{2.9}$$

where
$$T_r = \frac{\log(1.5\ T_{pmin})}{\log(T_{pmin})} \tag{2.10}$$

- The minimum bolt load required, W_m, is;

$$W_m = p\ A_p + S_m\ A_g \tag{2.11}$$

where S_m is the greater of S_{m1} or S_{m2} or 2p.

2.3 ELEVATED TEMPERATURE BEHAVIOR OF BOLTED JOINTS

Some flanged joint assemblies may begin to leak some time following a successful hydrostatic test. One reason for this is that the gasket experiences a drop in its initial compressive stress due to creep relaxation behavior of the elements that constitute the

joint. Although it is widely acknowledged that creep relaxation of bolted flanged joints is increased by elevation of temperature, reports (Bazergui,1984) show that room-temperature relaxation can also be significant even at light loads. In reality, there exist several other factors that may contribute to the bolt load loss. The thermal degradation of the gasket and the difference between the thermal expansion of the joint members are among the most important factors that contribute to the gasket load change which in turn may lead to a serious increase in leakage and even a complete failure of the joint (blow-out).

The process of relaxation is somehow accelerated with higher temperature. In part, high temperature creates thermo-mechanical effects, expanding the metals, affecting the gasket material by promoting a creep relaxation phenomenon which is a permanent strain or relaxation of many soft materials under stress. In the one hand, creep causes relaxation of the gasket compression stress which increases leakage because of gasket thickness loss even though, while in the other hand it tends to fill all the gaps and capillary holes that may be the actual paths for leakage. The matter is made more complicated by the time-temperature aging effect of the gasket material. The mechanism leading to leakage is complex, and unless more research work is to be pursued, the elevated temperature behavior of gaskets and joints will remain a difficult and often unresolved matter for flange design engineers.

2.3.1 Creep in Bolted Joints

Creep analysis of bolted flanged connection was investigated by Bailey (1937), Marine (1938) and Waters (1938). Steady creep was assumed and only the interaction of the flanges and bolts was focused upon, ignoring the stiffening effects of the hub and cylinder and the effect of relaxation of the gasket. Stress decay in gaskets and its effect on the tightness of the joint was further studied by Thorn (1942) and Werkenthin et al. (1945) who conducted tests on rubber based gaskets. The experimental creep relaxation apparatus used to conduct such tests are described in the various papers (Tapsel,1939, Thorn,1949 and Farnam,1951). Smoley et al. (1963) examined the effect of relaxation on the bolt torque loss in a flange assembly.

With the introduction of improved computational techniques to the field of bolted flanged connections, a better understanding of the problem associated with creep has been made possible. Fessler and Swannell (1974) carried out a finite element analysis of a typical bolted flanged joint using a strain hardening creep law. Fairly accurate results would have been obtained if the gasket had been considered. However, its creep data was not available at the time. Such analyses are time consuming and costly; therefore, it is of interest to develop simpler analytical methods. Kraus (1980,1984) proposed a model to predict the time required by the bolts to relax from an initial stress to some final level. As the influence of other joint structures were not considered, Kraus found that the leakage over time prediction is half of what would be estimated using a finite element

analysis. Here again, the gasket creep relaxation behavior was not included in the analysis.

Thus, most investigators seem to have considered mainly the creep of the bolts and focused their attention on the interaction of the flanges and bolts only (Johson and Baily, 1954). The creep relaxation of the gasket is not usually accounted for (ASME, 1992). And, even if this is the case, the results obtained from many researchers in the field including the standard tests (ASTM,1993) available, are not really representative of the real gasket working conditions.

Gasket creep data are based on three types of tests. The first type is the creep test under constant gasket stress, the second type is a creep test under cyclic stress and a third type is a gasket stress relaxation test at constant gasket deflection. Of course, none of these tests (Vignaud et al. 1986 and Bazergui,1984) reproduce the true bolted joint situation which would involve simultaneous creep and relaxation with neither constant stress nor constant deflection. Also, the tests are carried out at room temperature and last only few hours, which may not be sufficient for some gasket types expected to operate for several years. The flexibility of the test bench in which the gaskets are tested is, in most cases, not representative of the standard flanges. The influence of the flange stiffness on the gasket stress relaxation was well established both experimentally and theoretically by Marchand et al. (1993) and Bouzid et al. (1994a).

Tests conducted by Bazergui (1984) at room temperature showed that most of the gasket relaxation occurred during the first 15 minutes after the tightening of the joint bolts and is more pronounced at low gasket stress levels particularly for Spiral-Wound gaskets. He also performed cyclic creep tests and found that most of the creep takes place in the first 25 cycles and a larger extent of creep is produced in comparison with constant stress tests because of ratcheting and cumulative deflection. The process is accelerated at higher temperatures. The mechanism which leads to leakage is complex because, on the one hand, relaxation of the gasket compression causes leakage to increase while, on the other hand, creep tends to densify the gasket material filling the gaps and porosities that constitute paths for leakage.

2.3.2 Thermal Degradation of Gaskets

Another recently investigated phenomenon, that takes place at high temperature, is the physical degradation of the gasket material. The elevated temperature exposure over time of certain gaskets, such those made of organic composite based materials and graphite, undergo changes in their physical and mechanical properties.

One of the first investigators on the subject was Chivers (1978) who observed time-dependent effects and deduced that three resulting phenomena that take place simultaneously, namely relaxation, creep and thermal degradation. He used the Arrhénius equation to predict the life time, L, of gaskets as a function of temperature, T:

$$L = \rho\ e^{\eta/T} \tag{2.12}$$

The coefficient ρ and η are temperature dependent. On-site tests conducted on asbestos filled spiral wound gaskets at 200 °C show up to a hundred time increase in leakage but this was attributed mainly to the gasket relaxation. However, the time-temperature exposure known as aging is a mechanism that may also lead to relaxation due to the reduction of gasket thickness resulting from a weight loss. The process involved is complex: the gasket material is degraded and decomposed by pyrolysis and oxidation (Garn,1965). This, in turn, reduces the material density and the gasket gradually becomes porous and looses its sealability.

In order to better characterise gaskets at high temperature and give an insight to the process of aging, Payne et al. (1989a, 1989b and 1990) under the auspices of the PVRC and MTI developed several test methods (ATRS, HATR, ARLA, HOTT and AHOT). These methods simulate the real high temperature working conditions closely, and give a realistic representation of the behavior of gaskets in bolted flanged joint. Residual tensile strength, load relaxation, thickness change, weight loss and sealability are some of the gasket properties that are sought from the tests conducted on these fixtures.

One of the test fixture developed to perform the high temperature gasket tests (the Universal Gasket Test Rig) is able to simulate a variety of flange rigidities including

ASME/ANSI B.16.5 and DIN 2632 flanges. This rig is currently used to perform hot blow-out tests (HOBT) for evaluating gasket tightness performance under extreme relaxation conditions (TTRL,1994).

More recently, Marchand et al. (1990a, 1990b and 1990c) and Derenne et al. (1994) showed the influence of thermal degradation on sealing performance of some sheet gaskets and found a strong correlation between the weight loss during thermal exposure and gasket properties such as relaxation, initial compression stress, thickness change, tensile strength, and tightness. Much of the study was conducted on fibre-reinforced sheet gasket materials (Marchand,1991). Marchand et al. (1992) have also established a correlation of the weight loss for sheet gasket materials with time and temperature of exposure and have successfully combined the two effects in a single time-temperature equation using, as reference, a 48 hours exposure:

$$w' = -\left(\frac{t}{48}\right)^{d} \frac{m_w}{1/T_0 - 1/T} \tag{2.13}$$

Equation (2.13) leads conveniently to the definition of an aging parameter A_p based on the weight loss correlation such that;

$$A_p \equiv \frac{w'}{m'(48^{0.6}/100)} \tag{2.14}$$

The combined effect of time and temperature on the damage of gasket materials

subjected to an oxidizing environment, was also defined by an equivalent aged exposure parameter A_e as determined by a multiple regression analysis:

$$A_e \equiv (T-T_t)\ t^c.\frac{100}{\kappa} \tag{2.15}$$

While A_p is a more accurate predictive parameter, A_e is simpler and is used for screening different gasket materials and setting the elevated temperature conditions. An empirical relation between these parameters and the gasket thickness loss would be of great use for an assessment of the bolt load loss.

2.3.3 Differential Thermal Expansion

Differential thermal expansion is a potential source of load change in gaskets and bolts. The temperature coefficient of expansion or contraction of the gasket being substantially different than that of other joint members, and particularly the bolts, any change in temperature has a direct impact on gasket compression. While cooler bolts tend to increase the gasket load, the relative stiffness of the joint and, in particular, the bending flexibility of the flange are some factors that determine the net loss or gain of gasket and bolt load. Bickford et al. (1988) who conducted a FE analysis of a head flange of a troublesome and difficult to seal heat exchanger unit, concluded that, in this particular case, the differential thermal expansion is the major contributor to the increase in bolt load.

Although high temperature is seen as a potential source of high stresses in structural applications involving different materials, up to now, very few investigations related to bolted flanges, have been carried out to establish a design method (Hayes and Roberts,1970 and Singh and Holtz,1979). Recently, Kumano et al. (1993) and Sawa et al. (1994) proposed a method for predicting bolt load change due to the difference in thermal coefficient of linear expansion based on a model of a joint made of two hollow cylinders fastened by a tap bolt. Better results would have been obtained if the flexibility of the flange was accounted for in the analysis. The need to give attention to the relaxation properties of the materials involved when designing a joint for high temperature service, especially in situations where thermal induced effects are the controlling factors in design, is recognized by the ASME Code, but no specific guidelines are given.

2.4 FLANGED JOINTS DESIGN METHODS

Some of the methods which are currently employed for the design of bolted flanged joints are reviewed and described in this section. The basis of each method is described giving the main parameters having an influence on the hypotheses and approximations used.

2.4.1 The Taylor-Forge Method

As already pointed out, this method was pioneered by Waters et al. (1937,1949) and is based on a complete elastic analysis of the whole flange assembly using the theory of "Beams on Elastic Foundation" in the pipe-hub and flange intersections and considering the flange as a circular plate with a central hole (Figs. 2.3-2.4). The method suggests values for the initial seating load and the load required to seal at operating pressure for a comprehensive range of gasket types.

For the bolting-up condition, the total flange moment is

$$M_f = W_m \frac{(C-G)}{2} \tag{2.16}$$

For the operating condition, the total flange moment is

$$M_f = F_D h_D + F_T h_T + F_G h_G \tag{2.17}$$

The evaluation of stresses in the flange takes account of a more detailed analysis which treats the flange, taper hub and shell separately. The hub is analyzed as a thin cylindrical shell of tapered thickness, the ring as a thin flat plate (Fig. 2.4). Edge moments and forces are introduced and compatibility of displacement and rotation are applied to the two discontinuity junctions. To simplify the analysis, it is assumed that the

radial displacement is zero at the thick end of the hub.

While the detailed mathematics are given in the paper by Waters et al. (1949), our present interest is in the basic assumptions of the method rather than in the finer detail of the laborious solution. In effect, no account is taken of possible change in bolt load on application of pressure and in fact no assessment of the load-deformation characteristics of the joint is made as pointed out by Wesstrom et al. (1951). Further, it neglects the normal pressure load on the inner surfaces of shell, hub and flange ring referred to as the pressure inflation effect and the zero radial displacement at the thick end of the hub.

In large diameter flanges, these account for more than 30% of maximum stress as has been shown later by Murray and stuart (1961) and, much recently, confirmed by Thomson (1987). Instead, the former presented an analysis for larger taper hub flanges which removed many of the earlier assumptions of the Taylor-Forge method. Their particular concern was larger flanges of over 5 feet in diameter. However, the major difficulty with its application lays in the complex manipulation of its equations and the iterative process involved. Nevertheless, with modern computers this task is obviously reduced in terms of time and a complete explanation of the technique can be found in the book by Singh and Soler (1984).

2.4.2 The Lake and Boyd Method

Engineers and researchers have long suspected that yield occurs at the junction between the shell and the hub or flange due to the high longitudinal bending stresses and argue that such stresses should not be limited to fictitious values derived by elastic analysis such as the one used in the ASME Code, but rather by the load capacity of the shell under plastic conditions. Based on some experimental evidence which showed that this method could produce adequate joints even by allowing hub and shell yielding and still performing satisfactorily, the Lake and Boyd (1957) method was adopted by the British Standard, BS 1500 (1990), to generally give lighter flanges and thus save substantial flange material.

Figure 2.5 shows the model used; noting the point of action of the equivalent moment M is at the middle surface of the flange ring and the point of zero radial displacement as regard to the Taylor Forge method, so that:

$$M = M_0 + P_0 t_f /2 \tag{2.18}$$

Having established the elastic solution, the analysis goes on to consider plastic conditions. First, yielding takes place due to longitudinal bending of the shell at the junction with the flange thus limiting the moment M_0 to $t_c^2 S_y/4$, where S_y is the uniaxial yield stress. Then the shell hoop stress at the extreme outer fibre reaches yielding while the flange ring remains fully elastic.

Although this method appears to represent an improvement over the Taylor-Forge method, the resulting greater flexibility and consequently higher angular flange rotation would make the joint difficult to seal (Gill,1970).

2.4.3 The DIN 2502 Method

The DIN 2505 method (1961) used in Germany is based on the work of Schwaigerer (1954 and 1961) and Anonymous (1967). Similar to the Lake and Boyd method, this method is based on an elasto-plastic analysis and requires a bolt/gasket load-deformation diagram to examine the joint sealing state for all design conditions. The difference in flange flexibility under assembly and pressure conditions together with the reduction in bolt and flange stiffness due to the decrease of the modulus of elasticity at increased temperature, are accounted for.

Referring to Fig. 2.6, it is assumed that the ring and shell adjacent to the ring are both fully plastic, the former under hoop stresses and the latter under longitudinal bending stresses. The plastic collapse moment M is determined as the sum of the resistance of these two components. For the ring alone, the external collapse moment M_1 gives rise to a bending moment $D_0M_1/2$ about axis xx which is limited to:

$$D_0 M_1 = (A-B) \frac{t_f^2 S_y}{4} \tag{2.19}$$

For the shell, the presence of longitudinal stresses due to the end load P_0 is accounted for by calculating a thickness t_{c1} sufficient to carry the end load:

$$t_{c1} = \frac{P_0}{\pi\ (B+t_c)\ S_y} \tag{2.20}$$

Then the external collapse moment M_2 is therefore

$$M_2 = (t_c^2 - t_{c1}^2)\ \frac{S_y}{4} \tag{2.21}$$

The tentative thickness of the flange t_f must be adjusted as necessary until the design condition on the external flange moment, being restricted to the 2/3 of the calculated collapse moment, is met. In common to the other methods already mentioned, this method assumes that the loading is simply an external moment applied to the flange ring and all other pressure effects are neglected. This method requires that a load-deformation diagram similar to the one given by Podhorsky and Vu (1984), be constructed to examine the overall behavior of the joint and to check that the gasket is capable of sealing under all design conditions. This diagram takes into account the difference in flange flexibility and the creep of the gasket at increased temperature.

Another flange design method referred to as TGL (TGL,1991) and originally developed in East Germany, is to be mentioned. It is based on the rotation of the flange and accounts for the scatter of the bolt loads. The effect of temperature in terms of the difference in dilatation of the joint members are also included. This method is presently being adopted by the EEC.

2.5 CONCLUSION

Bolted flanged joints must satisfy the requirements of both structural integrity and leakage tightness. Currently, the emphasis is placed on accurate predictions of stress levels for material saving purposes. Safe designs from a structural integrity point of view has never been a serious problem as there are no records of sudden and total failure of a flanged joint especially with the use of ductile materials. However, at the design level, little has been done with regards to joint leakage.

It is intuitively recognized that the interaction of the gasket, bolt and flange deformations plays an important part in the mechanism leading to leakage. However, the current design procedures of bolted flanged connections including the ASME Code design procedure are based on a stress criterion without limiting the extent of deformations. In this context, and owing to the fact that the previous discussed methods of gasket design are all based on a rigid flange theory, bolted joints have been the subject of criticism. The flexibility of the bolts and gasket together with the rotation of the flange, the friction between the gasket and the flange and the temperature induced effects have a strong influence on the final gasket compression and radial stress distribution (Bouzid et al.,1993,1994a and 1994b, Cascales and al.,1987, Cascales and Militello,1987 and Derenne et al.,1984) and have been ignored in the ASME Code design procedure. Although, a lot of emphasis is put towards studying all geometric and material parameters involved, a complete comprehensive model is not in sight. For example, a

recent study on a bolted flange joint (Chaaban et al.,1993) shows that the bolt torque and hence the gasket stress distribution is also greatly influenced by the type of bolt lubricant used. During the development of most design procedures, little consideration has been given to the creep relaxation of the gasket. The tests developed to obtain gasket properties are often not fully representative of the real gasket working conditions. It is thus necessary to account for most of the parameters that are required to be put in a rational model in order to better predict the problem of leakage.

Over the last decade, a substantial research effort has been dedicated to the study of flanged joints and the characterization of gasket behavior at room and elevated temperatures. To overcome the shortcomings of the present ASME Code approach and gain insight into gasket behavior, a great effort have been made by Bazergui, Marchand, Derenne and Payne since 1984. Through the auspices of the PVRC, the MTI and others, a fundamental understanding of gasket behavior has been achieved in parallel with the development of new gasket test methods.

The proper assessment of gasket performance requires that the mechanical and tightness properties of the gasket material be known at elevated temperature. What corrections have to be applied to the gasket constant, and how to account for time and temperature effect that induces thermal degradation of the gasket material are a few of the questions that have been raised and will be addressed in the present thesis.

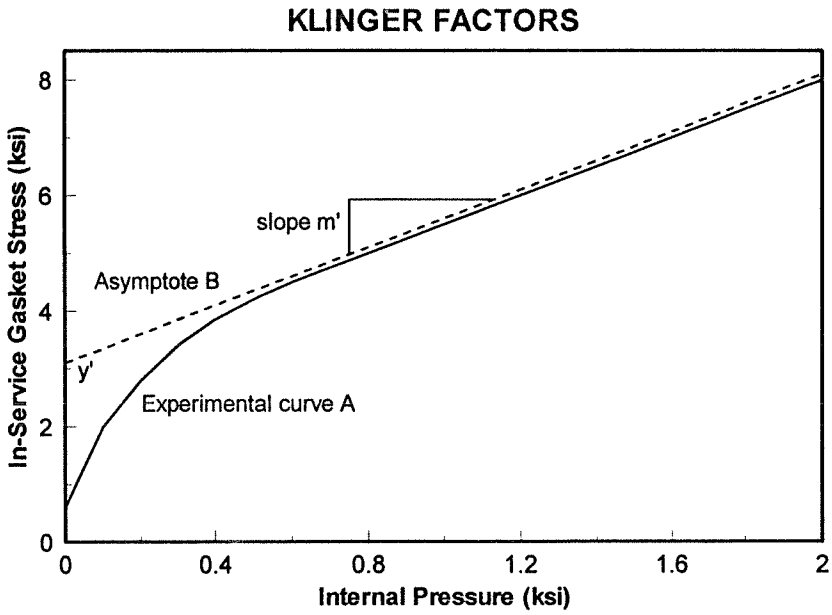

Figure 2.1 Klinger gasket factors m′ and y′ derivation

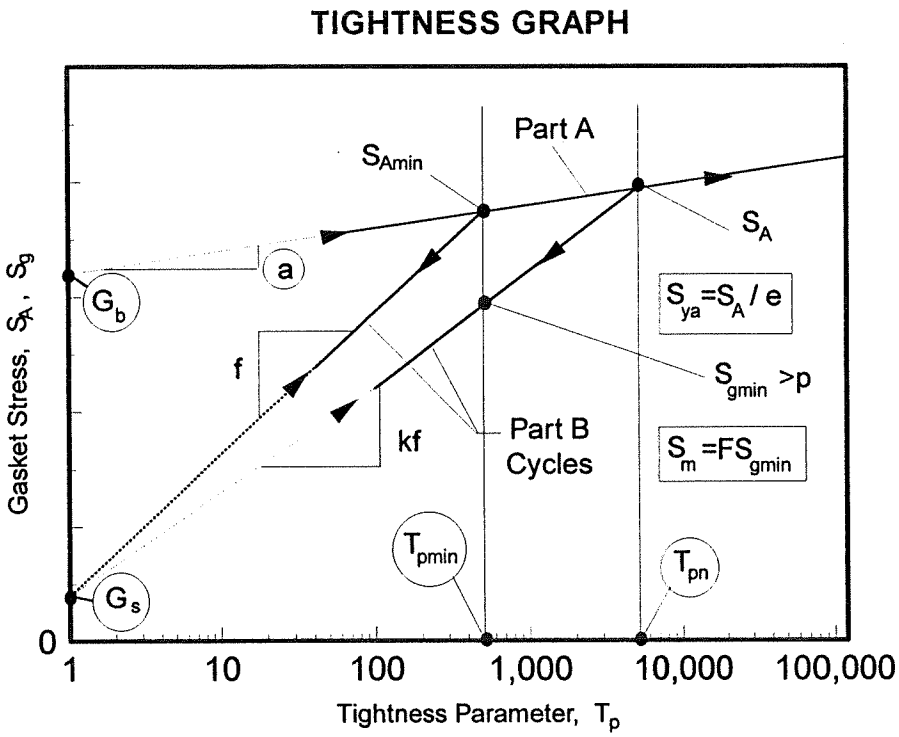

Figure 2.2 Idealized tightness graph from leakage data

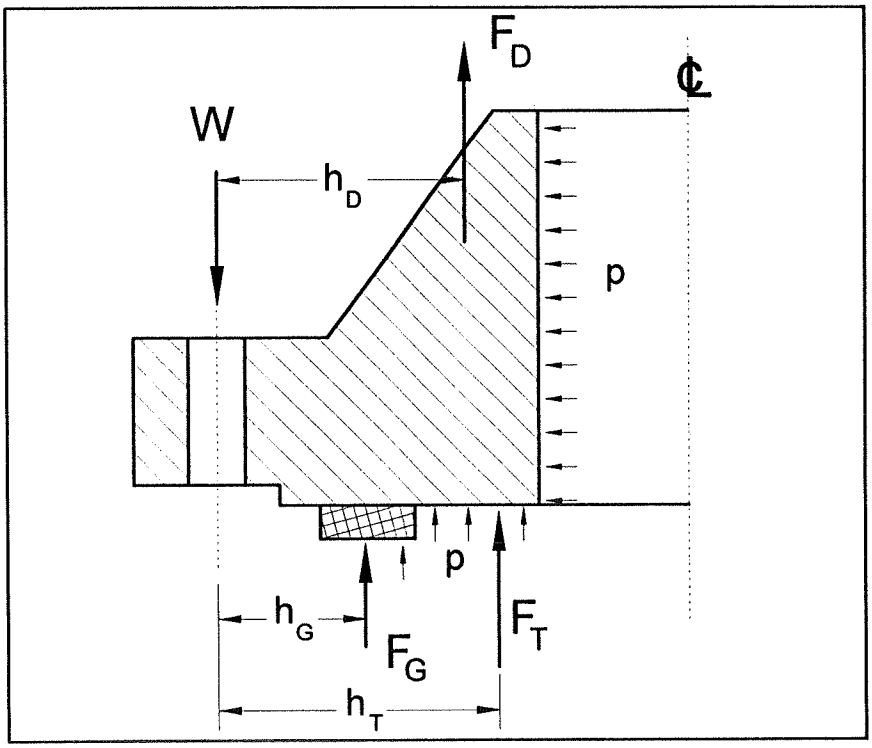

Figure 2.3 Loads considered in Taylor Forge model

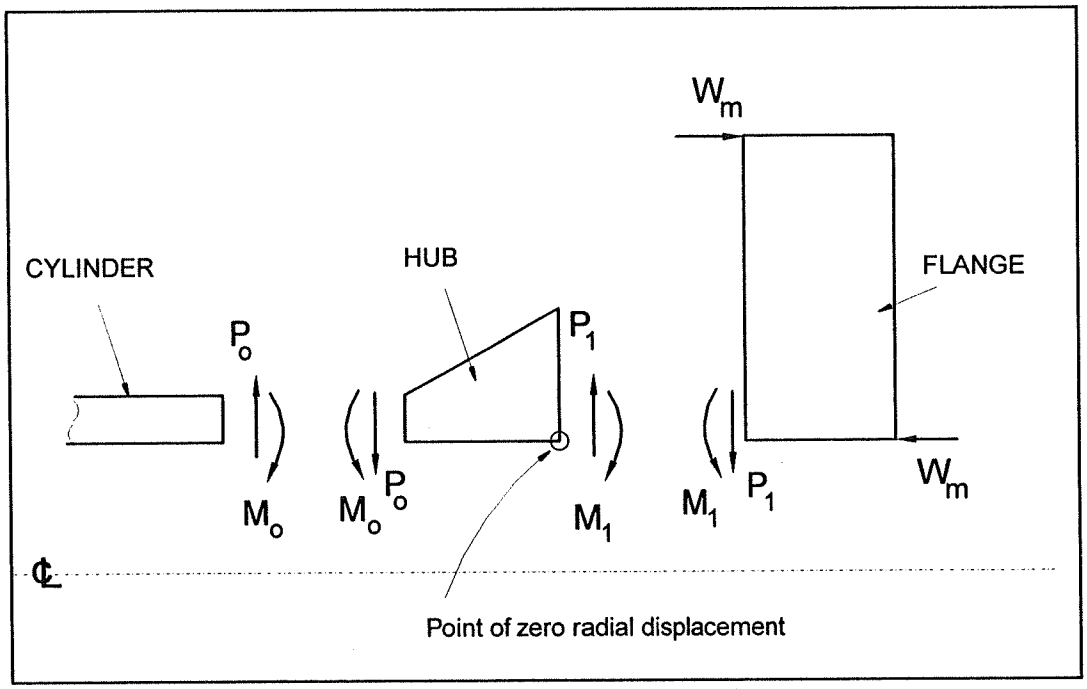

Figure 2.4 Taylor Forge model

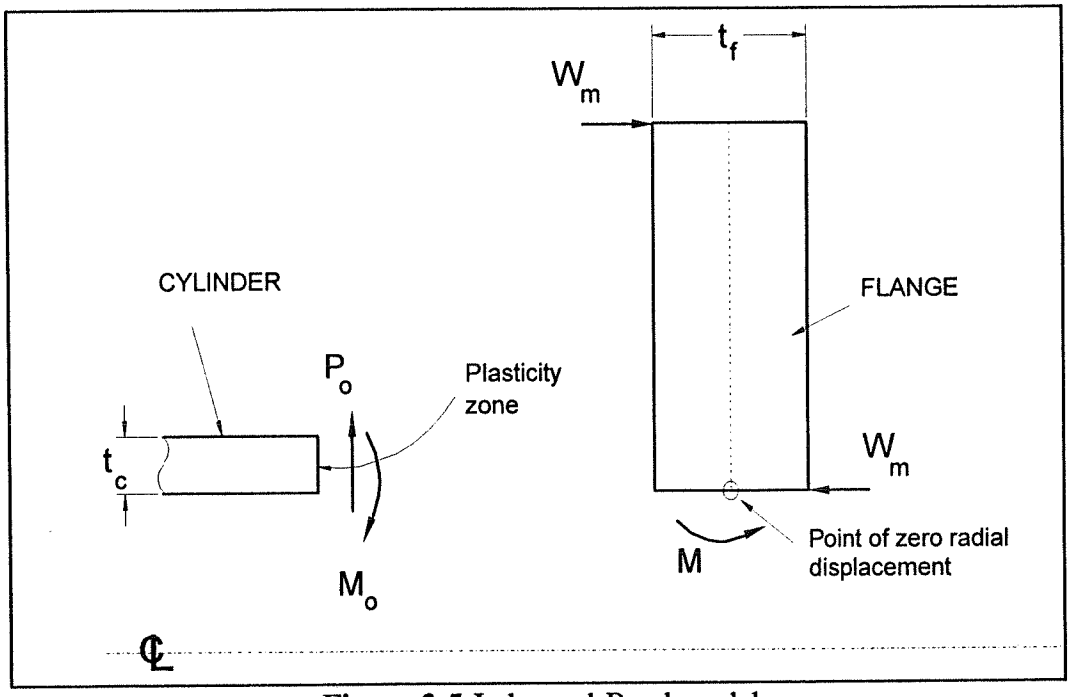

Figure 2.5 Lake and Boyd model

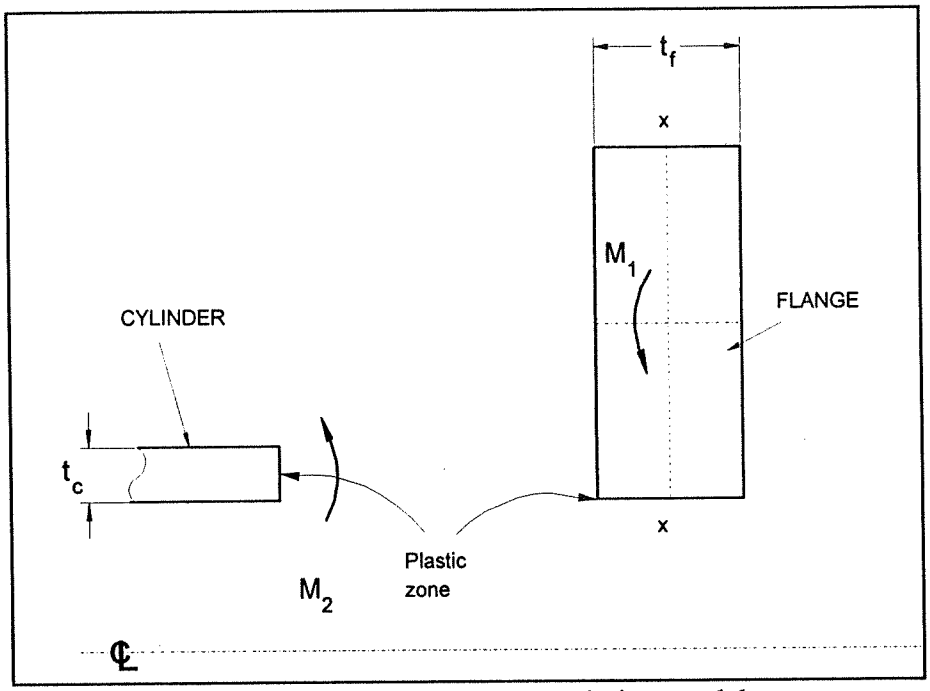

Figure 2.6 DIN 2505 flange design model

CHAPTER 3

EXPERIMENTAL AND NUMERICAL PROCEDURES

3.1 INTRODUCTION

To compare the results obtained from the analytical bolted flange model that will be presented in the next chapter, an experimental investigation together with numerical FEM analyses were performed. This chapter describes the experimental and numerical procedures of the different tests that have been conducted for the purpose of developing and validating the analytical model. Besides this, both methods will help understand some of the phenomena that govern the bolt-gasket-flange interaction. This should also give an indication of how complex the analytical model will have to be to provide a reasonable estimate of the major parameters that control leakage.

In order to avoid costly experimental tests, in one case it was found beneficial to use published results and compare them to the results obtained from our proposed analytical model. This was the case when comparisons were made in relation to the variation of the bolt load with internal fluid pressure obtained from the analytical model. The relevant experimental tests were conducted on real bolted flanged assemblies designed according to Japanese Standard JIS B2210-2217 as will be further discussed.

Most of the tests that we conducted were related to the seating conditions because the bolted flanged joint fixture (Fig. 3.1) used is designed to reduce the hydrostatic pressure end load. As will be seen later, for the purpose of simulating leakage through gaskets, the pressure is applied to a small annular chamber within the gasket inside diameter, and only a small amount of the resulting hydrostatic end force act to separate the flanges. Some other experimental tests, including pure creep tests, had to be carried out because the gasket material data was not available in the literature.

A series of studies were undertaken to identify the proper mix of the dominant parameters needed to verify the adequacy of the analytical approach and modeling of the type of flanges considered. In conducting this research work, a few parameters considered important have been identified, namely: the torque coefficient, the bolt load, the flange rotation, the gasket deflection and radial stress distribution, and the leakage rate. The numerical analyses utilize the ABAQUS general purpose FEM program for the evaluation of the above parameters.

3.2 EXPERIMENTAL PROCEDURES

Several experiments were conducted to validate the analytical approach and modeling. Several test fixtures and laboratory equipment were used in conjunction with the parameters under investigation. These fixtures are described in the following sections.

3.2.1 Bolted Flanged Rig

As shown in Fig. 3.1, a multipurpose experimental rig consisting of a pair of ANSI B16.5 type, NPS 4 Class 600 lb steel welding neck flanges with the raised faces machined off was used throughout this investigation. The bottom flange is bolted to a 3.75" (95.25 mm) diameter solid shaft at its hub small end. The solid shaft is fixed to the supporting base. Steel platens with standard raised faces are fitted between the two flanges, using o-rings to seal the space between the shaft and the flanges. An aluminium plate fitted with o-rings is used to seal a narrow annular chamber around the outside diameter of the gasket. The upper and lower platens are removable and may be remachined to the desired surface roughness. The rig is designed in such a way that the end force due to the fluid pressure is very small, thus the gasket load is almost equal to the measured bolt load.

For the experimental tests involving leakage measurements, 1/16" (1.6 mm) thick compressed asbestos sheet gaskets are used because their leakage is easily detectable using simple pressure variation techniques. The pressurized fluid was helium. For the relaxation tests, either of two PTFE based types gaskets of different thickness, 1/8" and 1/16" (3.2 and 1.6 mm), were used. The bolt loads, the gasket displacements, the pressures and temperatures are continuously monitored through a microcomputer based data acquisition system. The initial bolt load is applied by a torque wrench to each of the 7/8" (22.2 mm) diameter instrumented bolts. A full bridge with all four strain gages

carefully placed, was used to cancel out bending.

A special tightening procedure based on the criss-cross pattern shown in Fig. 3.2 was developed to apply the required torque to each bolt to produce approximately the same load on all bolts. Four displacement transducers positioned in diametrally opposed pairs monitor the gasket deflection as well as the flange rotation. Since the solid shaft cancels out the hydrostatic end pressure, only the variables related to seating conditions could be varied. Results relevant to operating conditions have been obtained from other experimental investigations available in the literature.

3.2.1.1 Displacement and Rotation Measurements

Four high-sensitivity Linear-Voltage-Differential-Transformer deflectometers having a precision of 0.00001" (0.254 μm) positioned in diametrally opposed pairs are used to monitor gasket displacement, as well as the rotation of the flange. Since the readings are not taken at the mid gasket location, a correction, taking into account the flange rotation, is applied to the gasket displacement. The local deformation of the flange due to bearing stress of the gasket is not significant and is neglected. Regarding the thickness of the flange, it is reasonable to assume that the flexural bending effect is very small and the flange ring may be considered to rotate rigidly around its centroid.

3.2.1.2 Leakage Measurements

A few experimental leak tests were performed to study the effect of certain key parameters believed to control the leakage of a real joint. Leak detection is achieved by measuring pressure and temperature variations, over a given time interval in the annular chamber (Fig. 3.1). Knowing the volume of the leakage collection circuit, and applying the perfect gas law, the volume leak rate is computed for standard atmospheric conditions, 14.7 psi and 32°F, (1 atm. and 0°C) and is transformed to a mass leak rate L_{RM} expressed in mg/sec. Sufficient time is allowed for the leak rate to stabilize. As mentioned previously, the rig is designed in such a way that the gas pressure needed to perform leakage measurements is limited to a small annular chamber so that the pressure end effect is small and can be neglected.

3.2.2 Torque Coefficient Test Rig

This part of the investigation, referred to as the Torque Coefficient Tests, was to evaluate the so called "nut factor" for various types of oil and grease used as bolt lubricants. A series of tests was performed with four different bolt lubricants that were provided by the Fel-Pro company. Two other tests were performed; one degreased bolts and the other with as received bolts and nuts. The tests were conducted on the simple test fixture shown schematically in Fig. 3.3. Since the same bolt is used for five of the six tests, in order to avoid lubricant interaction even after cleaning, a specified order was

followed:

1- C5-A lubricant,

2- N-5000 lubricant,

3- N-5000 improved lubricant,

4- C-670 lubricant,

5- Bolts without any lubricant (degreased),

6- As received bolts and nuts.

The torque coefficient test fixture is composed of an instrumented bolt which is used to evaluate the nut factor for the first 5 cases. For case 6, a new "as received" bolt was used, on which strain gages were mounted while keeping the original grease on it. With a similar bolt as that used by the bolted joint rig, the type of bolt tested is also a 7/8" (22.2 mm) diameter, 9 threads/inch SAE grade 8, machined as shown in Fig. 3.3 so as to allow strain gages to be mounted. Before applying the lubricant to the bolt (case 1 to 4) tests, an ultrasonic cleaning of the bolt has been performed using carbon tetrachloride as solvent. For case 6, no thread cleaning was, obviously, required.

For each case considered in this part of the investigation, three tests were performed and average values were obtained. Torque was applied gradually using a torque wrench and, the induced bolt load was measured from the strain gage measurements, without reaching any plastic deformation.

3.2.3 Study of the DynaForce Sensor System

Throughout the history of bolted sealing flange design, various methods and techniques have been used to study and understand the stress distributions within these systems as reported by Czernik and Miszczak (1991). These techniques were not highly developed until recent years. Most of these methods are based on a post treatment of impressions, images and sometimes deformations left after loading. They use paper made of carbon or NCR, deformed lead pellets and impression color density films to determine mating flange contact stress distributions. However, even these techniques provide only limited information because of their inherent constraints. Their major deficiency is that they record maximum applied force and do not give any indication of the joint element interaction that occurs during the bolt tightening sequence. Any reduction in stress during the torquing sequence due to flange rocking or from external applied forces, is not reflected in the impressions.

In this study, a contact pressure sensing system referred to as DynaForce sensor system, which offers the potential to acquire real time static as well as dynamic pressures, was investigated to acquire the gasket compressive stress distribution in a real bolted flanged joint. The new technology behind the sensing device (Czernick and Miszczak,1991) may be briefly described as follows. A grid of conductive traces of which each intersection forms an independent sensing cell is separated by a thin pressure sensitive semi-conductive ink coating which provides an electrical resistance-conductance

between intersecting contacts (Fig. 3.4). The grid is protected by two thin polyester sheets.

Of major importance is the electrical resistance which changes with applied external force. The sensor can be made of any shape and for the purpose of this study, it is of circular shape having an inside diameter 3.5" (88.9 mm) and an outside diameter 5.5" (139.7 mm), and is thin enough, 0.004" (0.1 mm), not to disrupt the interface between the gasket and the flange. The sensor is nevertheless removed during leakage measurements which may be altered by its presence.

Gasket stress measurements are recorded at each intersecting point through proprietary data acquisition software that includes a specially developed graphics option. It provides two and three dimensional visual dynamic contact stress distribution representations as well as total compressive force, on the sensor, in real time. Changes in intersecting point loads can be observed, measured, and recorded throughout the test. This may provide a powerful engineering tool. Yet, so far, this new technology has not reached the level of reliability that is required for a measuring device; the major problem is associated with its highly nonlinear behavior, large hysteresis, and a lack of repeatability. Unless a reasonably accurate method of calibrating DynaForce system is found, gasket stress distribution may only be accessed qualitatively.

3.2.3.1 Sensor Calibration and Data Correction

The DynaForce software so far only provides a linear calibration algorithm. Thus limiting its effective use to cases where the stresses in the sensor are all within a small range so that a single scale factor for all sensor outputs may be applied. Unfortunately, the gasket contact pressure range involved in this study is beyond the limited range of linearity of the sensor. Gasket contact pressures obtained during a test range from 0 psi (0 MPa) at the inner and outer diameters to some 30 ksi (207 MPa) near the outside diameter.

To obtain more accurate quantitative contact pressures, a calibration method that accounts for the nonlinearity of the sensor must be used. Every sensing cell obtained by conductive particles suspended randomly in a polymer based binder has a different electrical resistance with a different output response to the same load. In addition, as these particles are brought together with applied force, the electrical resistance through the ink is reduced. Therefore, ideally, the calibration of each cell should be performed separately. The problem encountered in such a case is the application of the same pressure on each cell. One possible solution is to hydrostatically pressurize the sensor in a confined chamber. However, the design and fabrication of such a confinement would not be an easy task to do since it is required to withstand pressures of up to 30 ksi (207 MPa).

A simpler method, involving the compression of a small area of the sensor could be an interesting alternative to the ideal calibration. The nonlinear calibration curve presented in Fig. 3.5 was obtained by compressing a small area of the sensor of 0.4 in^2 (258 mm^2) on a universal testing machine. In order to improve the uniformity of the pressure distribution during the calibration, a soft material was placed between the gasket and the sensor.

Results from the calibration test performed on a small sensor area (Fig. 3.5) can be used to compute stress correction factor as the ones given in Table 3.1. When the sensor is used to perform a test on a real flange, a computerized correction of the stress values is applied to the ASCII output file. Note that in Fig. 3.5, it can be noted that a difference exists between the loading and unloading calibration curves due to the hysteresis of the DynaForce sensor. This behavior of the sensor is not helpful since when utilised in a real bolted joint, locally, the different sectors of the gasket are subjected to several loadings and unloadings due to the elastic interaction. However, for the purpose of our investigation and simplicity, only the loading part of curve is considered.

3.2.3.2 Lubricant Effect on Gasket Stress Distribution

This part of the investigation, involved the evaluation of the stress distribution on the gasket and the load scatter in the bolts while tightening the flange in an actual bolted-flanged assembly. The same flange rig of Fig. 3.1 was used in conjunction with non-

asbestos 1/16" (1.6 mm) thick sheet gaskets. During these tests, The DynaForce sensor was used to measure the gasket contact stress distribution. Since the eight instrumented bolts give the load variation from bolt to bolt, the sensor will be split into 8 equal sectors so that integrated load corresponding to each bolt load can be evaluated. The same lubricant test order, specified in section 3.2.2, was followed, and the tightening sequence of the bolts was the "criss-cross" order as specified in Fig. 3.2.

To determine the gasket stress distribution, the DynaForce sensor was introduced between the gasket and the flange facings. For the "as received" bolts and nuts case (case 6), the test was carried out without strain gages fitted to any of the eight flange bolts. For the other cases, a data acquisition system red the bolt strains. At the same time, the gasket stress distribution was recorded through the DynaForce system and the correction factors obtained by calibration were later applied to the output files.

The lubricant test order and cleaning procedure was followed as described in the previous part. The bolt torque was applied in three stages, namely 1/3, 2/3 and full bolt maximum allowable stress value which was limited to 50% of yield. On the basis of the bolt yield load, approximately 50000 lbs (222.4 kN), the corresponding three torque levels for each lubricant were obtained directly from the previous torque test results. For each test, and after the application of each level of torque, the load in each bolt and the normal stress distribution on the gasket were recorded.

3.2.4 Relaxation Tests

Here again, the bolted joint rig of Fig. 3.1 was used to undertake the relaxation tests for later comparison with the analytical model. This type of test, performed on real flanges, reflects the true creep relaxation behavior that is present in most bolted joints. Two PTFE material based types gaskets (PTFE Virgin 'A' and Gylon blue 'B', Table 3.2) of different thicknesses, 1/8" and 1/16" (3.2 and 1.6 mm) were used. Due to the relatively high creep rate of this material the experiments could be run within a few hours.

The loads were applied through the strain gaged bolts with a torque wrench using a slightly modified sequence to the known criss cross sequence developed for the purpose of obtaining an initial load on each bolt within a few minutes and with a reasonable accuracy of $\pm$500 lb ($\pm$2.22 kN). The modified tightening sequence consists of applying the same torque to two diametrally opposed bolts at the same time. The bolt load with gasket material 'A' was initially set at 65,000 lbs (289.1 kN) while the bolt load with gasket material 'B' was initially 53,000 lbs (235.7 kN) which corresponds respectively to an initial gasket stress of about 7200 and 6100 psi (49 and 42 MPa). Once the target load is set, the automatic data logger is triggered to collect and store the data in files. A predetermined varying time intervals were fed to the computer prior to initial tightening in order to start recording as quickly as possible with a consistent data range over approximately a five hours period.

3.2.5 Creep Tests

The modeling of relaxation in a bolted joint is based on gasket pure creep curves as will be shown in Chapter 6. Since little relevant information is available on the two selected gasket PTFE materials listed in Table 3.2, creep tests were undertaken and limited in time so that the complete test lasted a day. For consistency and reproduction of the real conditions as much as possible, the load was applied to the entire surface of the gasket. The tests were carried out on the Amsler servohydraulic testing machine under the load control option. The gasket deflection is averaged from three recorded LVDT measurements placed at 120 degree from each other. The movement of the loading platens was therefore monitored with a resolution of 0.00001" (0.254 μm). The LVDT's are set to zero after the application of a small stress of about 50 psi (0.35 MPa) on the gasket.

The gaskets were compressed to a sufficiently high stress level, of about 8000 psi (55.2 MPa), based on the initial full gasket area, to cover the range of stresses typically encountered in practice with such gasket types. In a typical series of tests, each of four stresses 900, 3000, 5400 and 7800 psi (6.2, 20.7, 37.2 and 53.8 MPa) was applied on a new gasket through smooth rigid platens. The load was held constant while the deflection was recorded at predetermined programmed time intervals ranging from 60 seconds at the beginning of the test to 600 secondes at the end.

3.3 FEM ANALYSES

The general purpose finite element computer program ABAQUS was used to simulate the tri-dimensional behavior of a bolted flanged gasketed joint and study the radial distribution of the gasket contact stress and its variation with flange rotation. The axisymmetric finite element model shown in Fig. 3.6 represents a bolted joint of the same dimensions as the weld neck NPS 4 class 600 lb test rig. The FEM model was developed using 2-D isoparametric 8-nodes axisymmetric elements having two degrees of freedom at each node. The flange and gasket loads and displacements, the rotation of the flange and the radial gasket stress distributions were determined together with the evolution of some of these parameters with time in the presence of gasket creep. In view of the symmetry of the geometry and applied load, only half of the joint including one flange together with half of the gasket and bolt were modeled. The cylinder was long enough not to disturb the discontinuity effects at the junction with the hub.

The Modulus of Elasticity E_{hole} for the bolt hole circle region bounded by the diameters $C+d_h$ and $C-d_h$ is reduced by the volume ratio of the bolt holes to the total volume without holes. The resulted Modulus of Elasticity for the bolt hole region is:

$$E_{hole} = E_f \left[1 - \frac{n\, d_h}{4\, C} \right] \tag{3.1}$$

where d_h is the diameter of bolt holes and E_f is the flange Modulus of Elasticity. If the flange is made out of steel of Modulus of elasticity of 30×10^6 psi (207 GPa), then the

bolt hole region is represented by a Modulus of elasticity of $23.6x10^6$ psi (162.5 GPa). The bolt is replaced by a solid ring with an equivalent axial section modulus with no radial nor circumferential resistance and eventually fixed to the upper surface of the flange. Although, the simulated bolt ring and part of the flange that represents the hole region may appear to occupy the same space, they are independent bodies in which only axial force is transmitted through the common upper surface where the bolt head comes in contact with the flange. This appears clearly in the typical amplified deformed shape of the bolted joint in Fig. 3.7.

The purpose of the numerical study was to better evaluate the importance of the following parameters and their influence on the overall behavior of the joint with particular emphasis on the leakage tightness including the gasket and bolt loads, the flange rotation, the gasket radial stress distribution, the static differential thermal expansion between joint members, the creep relaxation of the gasket and the bolts and the rigidity of the joint.

3.3.1 Modeling of the Gasket Mechanical Properties

For comparison purposes, both linear and nonlinear gasket material models were considered in the evaluation of the flange rotation. However, for further studies, only the linear stress displacement relationship is considered relevant to the gasket behavior because the gasket is usually subjected to several high stress fluctuations during the initial

tightening (seating) due to the torquing sequence and the loading and unloading gasket compression test showed the behavior to be quite linear. This will be explained further in the next chapter.

While the linear modeling is a very straight forward task to apply in most general-purpose FEM programs, nonlinear modeling is also used. One of the approaches which accommodates nonlinear modeling quite well through the specification of different key points that prescribe the complex stress strain material behavior. Linear interpolations between successive points are done by the program. Adequate approximation of the nonlinear behavior of the gasket is thus obtained, and may lead to satisfactory results.

General purpose FEM programs such as ABAQUS give the possibility of defining the gasket mechanical properties in three directions rather than the simple relationship between the force and the displacement in the axial direction. However, due to the limited published mechanical data on gaskets and even though the gasket properties are, in general, anisotropic, isotropic material properties have been assumed for simplicity.

The movement of the gasket is partially restrained in the radial direction due to friction. This has the effect of introducing additional deformation in the axial direction due to the Poisson's effect in the radial and circumferential directions, and disturbing the simple stress strain relationship in the axial direction. Therefore, the choice of Poisson's ratio and friction coefficient values greatly influences the final results. A value of 0.4 for

Poisson's ratio seems reasonable for the type of gasket used in this case and was considered in the present study.

Due to the lack of data on the subject, friction tests were performed on three rectangular specimens made of sheet gasket materials (asbestos, PTFE and elastomer) in contact with a steel plate with surface roughnesses of 275 μin RAAH (7μm) which is within the code recommended range. The results are shown in Table 3.3. Practically, the surface roughness has some influence especially with higher loads causing gasket material penetration. The tests were performed on a fixture capable of applying a maximum stress of 50 psi (0.35 MPa), compared to the very high values, 10000 psi (68.9 MPa) that are present in typical joints causing strong adhesion. This is more important when looking at the gasket radial expansion in terms of resistance to blow-outs and even to buckling.

3.3.2 Applied Loading

The loading of the bolt is somewhat complicated to represent in the FEM model. Because the bolt load will vary with the application of pressure and time due to the creep relaxation of the gasket, one cannot apply a constant value. In order to avoid specifying a constant bolt load acting on the assembly, the load was applied to the bolt symmetrical plane through fixed displacement which has the effect of stretching the bolt equivalent ring elements to produce internal tensile stresses. In this way, a compressive reaction on the gasket was achieved. Such a system adjusts itself as the pressure is applied and

continues during the time at which the creep of the gasket takes place. Formerly, a separate run corresponding to the initial seating condition with the effective initial bolt load applied to the free end was necessary to evaluate the exact initial displacement to be specified for subsequent runs. This new method is advantageous when compared to the application of a temperature difference to the bolt ring which involves several runs before there was convergence towards the required bolt load for seating. For the operating condition, the total hydrostatic end force is applied to the cylinder shell and flange face through an equivalent axial circumferential force uniformly distributed through the cylinder thickness and area of flange inside the mid gasket location. At the same time, however, the prescribed displacement on the lower end of the bolt ring corresponding to the preload are maintained.

3.3.3 Boundary Conditions

Only the axial displacement of the gasket mid plane was constrained while the radial displacement was conditioned by the state of the contact surface between the gasket and the flange. This was simulated using interface elements capable of imposing some defined friction between the mating surfaces. Typically, a coefficient of friction of 0.25 obtained from the few experimental tests was considered between the gasket and flange, although higher values for cases of rougher flange surface finish were also considered. The bolt symmetrical plane is free to move in the radial direction while the rotation about a plane perpendicular to the flange axial direction is fixed.

Table 3.1 Corrected scale for Dynaforce representation

DynaForce Gasket Stress (kpsi)	Corrected Gasket Stress (kpsi)	Correction Factor
0.3	0.11	0.38
1.5	1.14	0.76
2.7	2.51	0.93
3.8	4.03	1.06
5.0	6.05	1.21
6.0	7.80	1.30
7.2	10.15	1.41
8.3	12.37	1.49
9.5	14.92	1.57
10.5	17.33	1.65
11.7	20.12	1.72
12.8	22.91	1.79
14.0	26.04	1.86
15.0	28.65	1.91

Table 3.2 Gasket types and dimensions

Designation	Materials and construction details
A 1/8	PTFE virgin 1/8 Dimensions (in): 4.85 ID, 5.935 OD, 0.125 thick
A 1/16	PTFE virgin 1/16 Dimensions (in): 4.935 ID, 5.925 OD, 0.125 thick
B 1/8	Gylon blue 1/8 Dimensions (in): 4.81 ID, 5.825 OD, 0.125 thick
B 1/16	Gylon blue 1/16 Dimensions (in): 4.925 ID, 5.955 OD, 0.125 thick

Table 3.3 Friction coefficient

Gasket material	Friction coefficient
PTFE Virgin on steel	0.25
NBR/Asbestos on steel	0.3
NBR/Aramid on steel	0.31
Steel on steel	0.5
Copper on steel	0.3

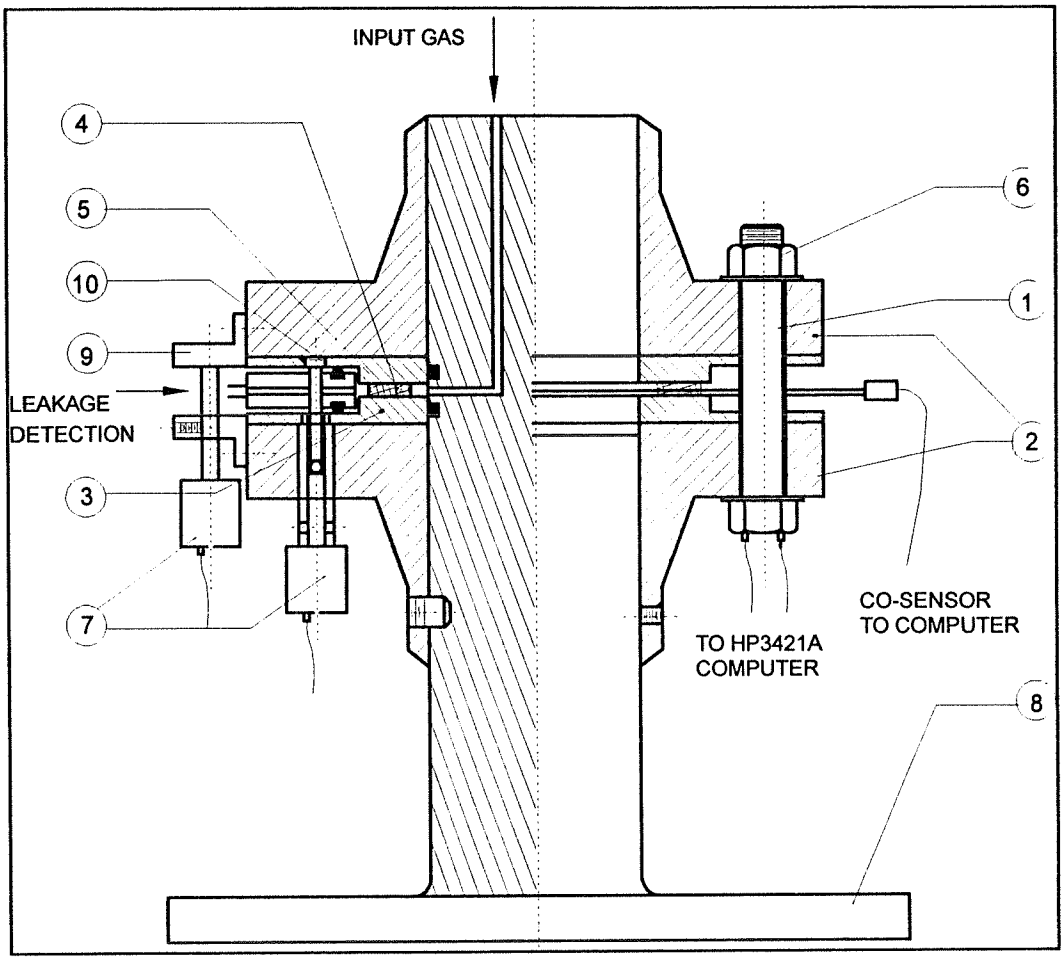

1	Strain gaged bolt	6	Nut
2	Flanges	7	LVDT
3	lower platen	8	Supporting base
4	Gasket	9	LVDT supports
5	Upper platen	10	Leakage sensing system

Figure 3.1 Experimental bolted flanged rig (Bazergui et al. 1985)

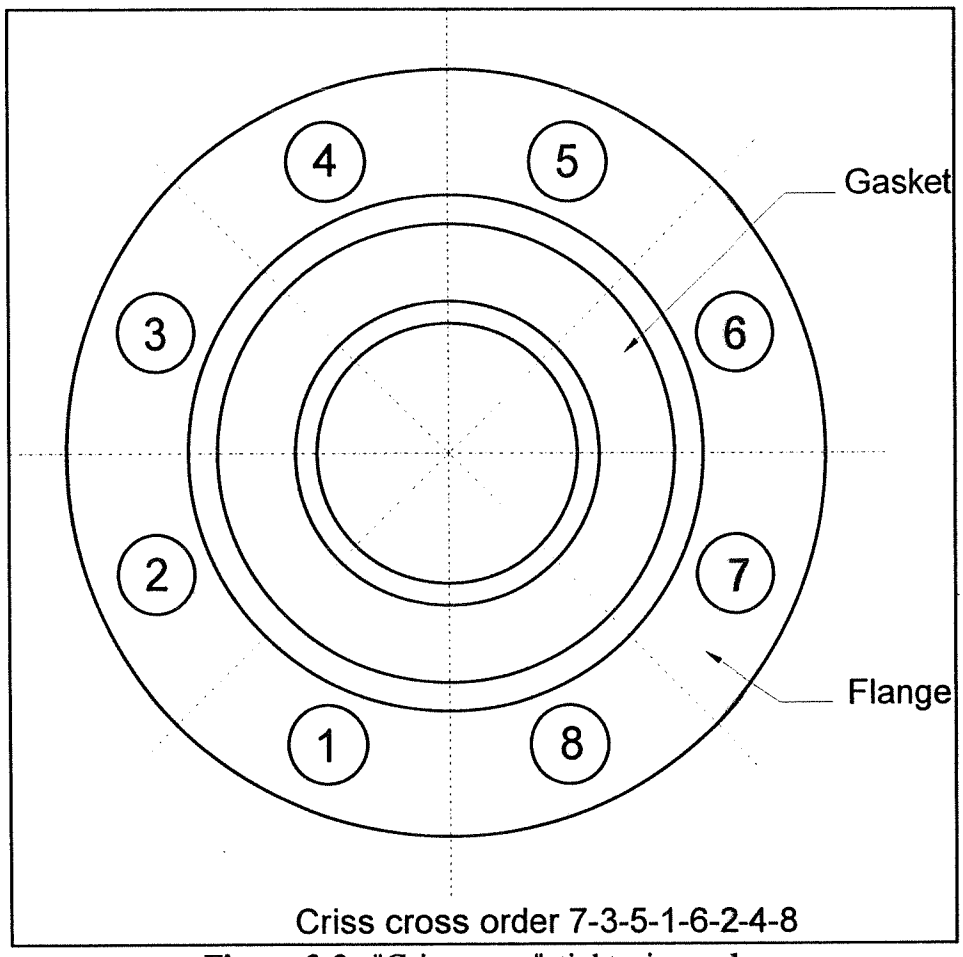

Figure 3.2 "Criss cross" tightening order

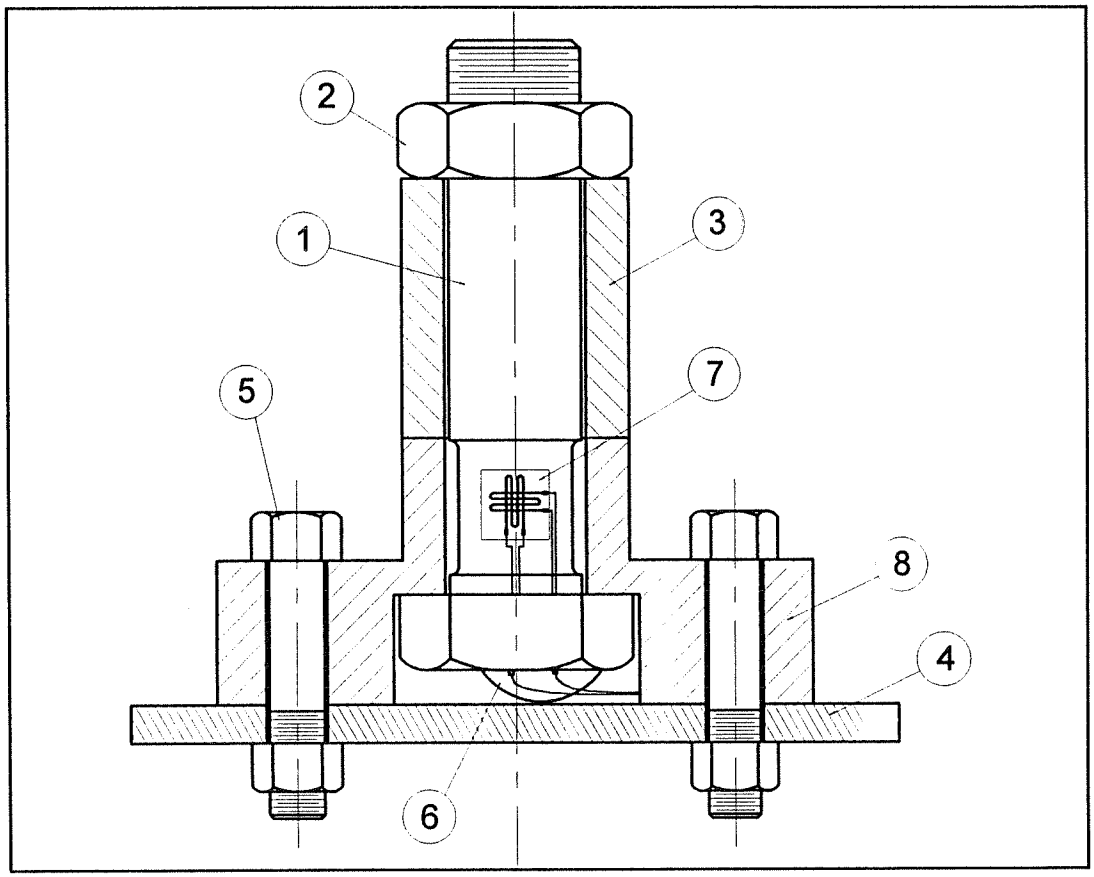

1	Strain gaged bolt	5	Fixation bolt
2	Nut	6	Silicon protection
3	Cylinder	7	Strain gage
4	Base	8	Support

Figure 3.3 Experimental rig used for torque coefficient tests

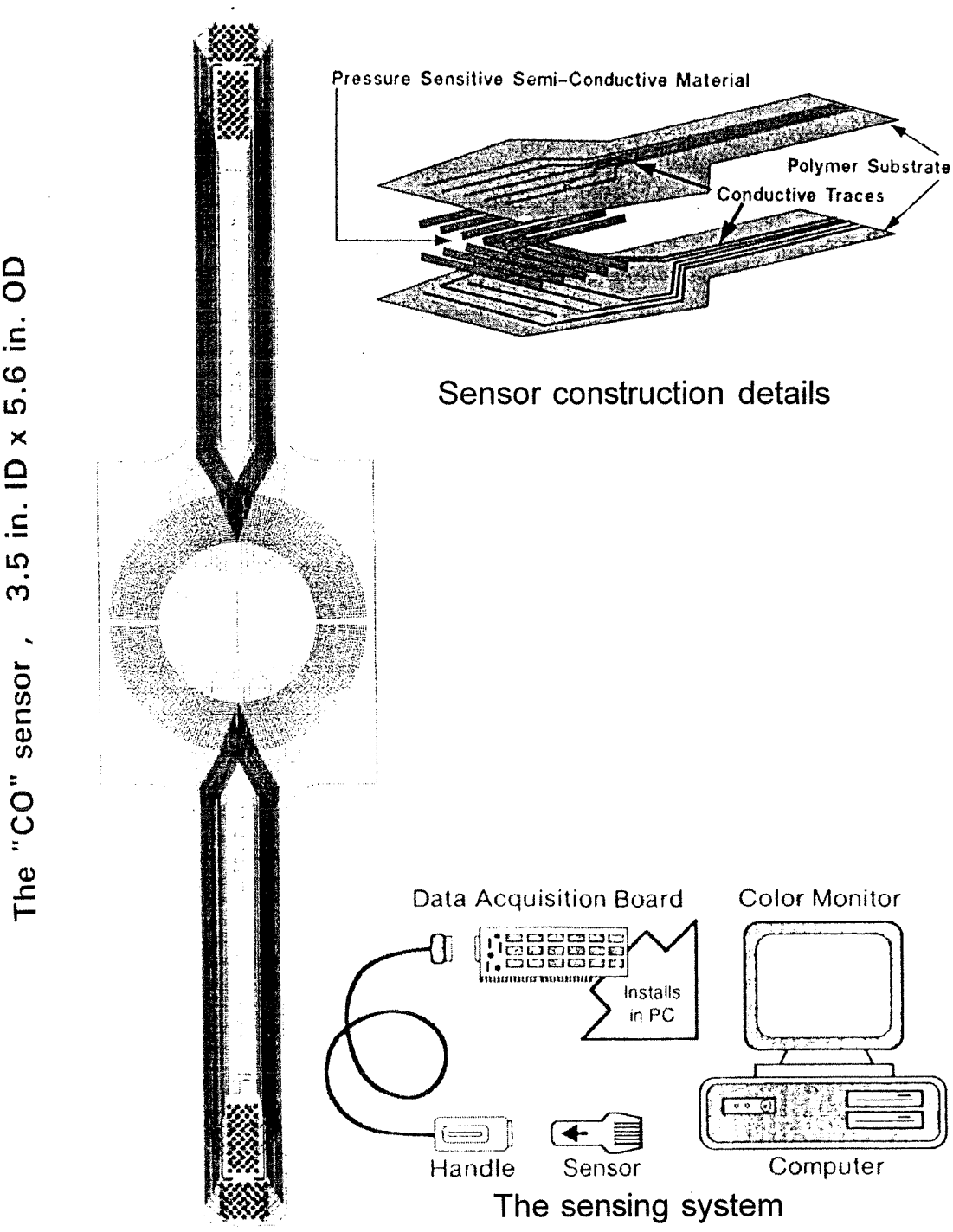

Figure 3.4 DynaForce sensor used in this study

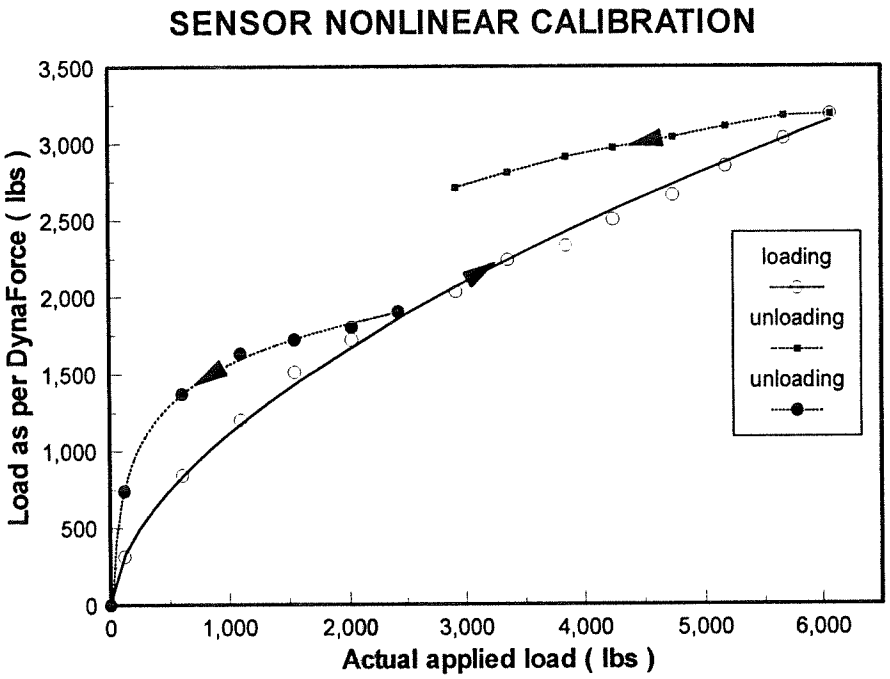

Figure 3.5 DynaForce sensor calibration curves

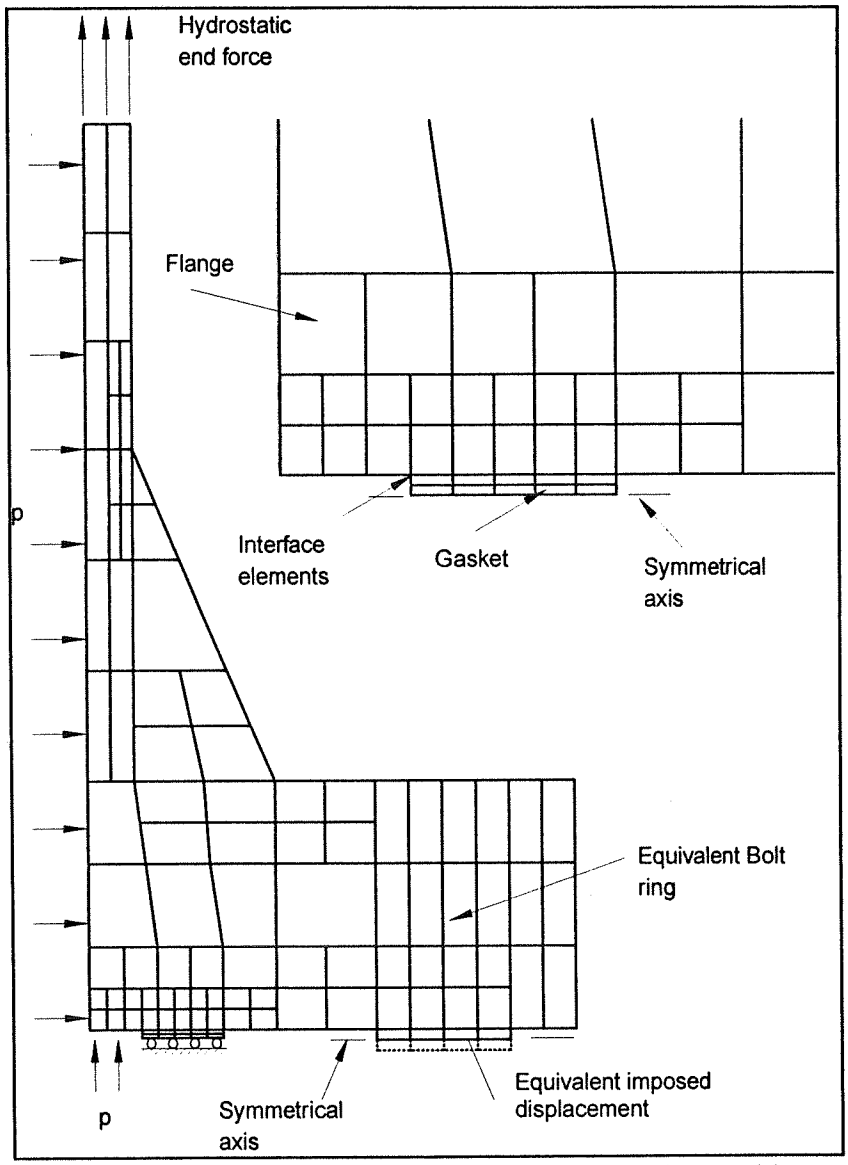

Figure 3.6 FE modeling of the bolted flanged assembly

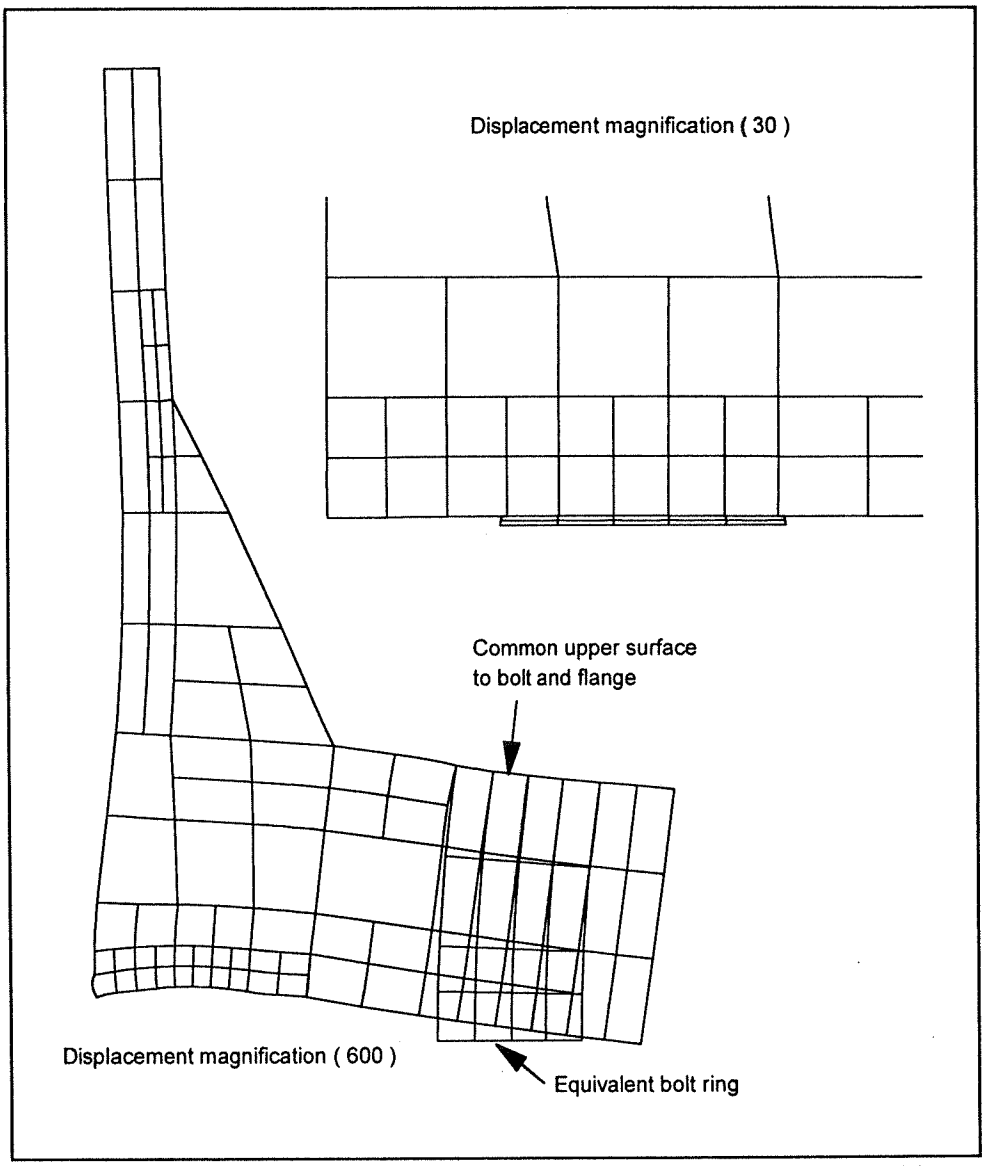

Figure 3.7 Typical deformed shape of the bolted flanged assembly

CHAPTER 4

A METHOD OF ANALYSIS OF BOLTED FLANGED JOINTS BASED ON ELASTIC INTERACTION

4.1 INTRODUCTION

In most flange design methods, the definitions of bolt and gasket loads under pressurised conditions are not sufficient to investigate leakage in detail. As indicated previously, it is necessary to make a precise evaluation of the bolt and gasket loads in order to be able to predict leakage accurately and proceed with the optimization of bolted flange joint. This chapter presents a simple analytical model based on an extension of the Taylor-Forge approach taking into account flange rotation, flexibility of both the gasket and the bolts and, when applicable, the stiffness of the end closure. While the rigid flange approach considers that the bolt load always increases with increasing pressure, some examples, based on an elastic interaction approach, will show that this load may either decrease or remain constant with an increasing pressure, depending on the joint elastic characteristics.

Bolted flanged joints are subdivided into three major categories, namely: ring flange, tapered hub (welding neck) flange and lap-joint flange. Our work, however, will concentrate mainly on the first two types of flanges. The principles and techniques are

equally applicable to other flange types with some modifications.

The first basic development was to analyze the actual force relationship and examine carefully the interdependence between the bolt loads during initial seating and final operation. Figure 4.1 shows an exaggerated view of the deformed shape of a loaded joint. The deformation of each element of the joint may have an impact in the final results and should thus not be neglected in the analysis.

4.2 ANALYTICAL MODEL

One of our objectives while developing the model was that it remain consistent with the ASME Code design philosophy, bearing always in mind two important factors; structural integrity and leakage tightness.

4.2.1 Modeling of the Gasket Mechanical Behavior

The proper modeling of the gasket is a key factor to obtaining reliable analytical results. The gasket compression and its reaction application point have a strong influence on the flange rotation and affect the leakage performance of raised faced flanges. From a typical gasket compression test, Fig. 4.2, one may appreciate the highly nonlinear behavior when loading the gasket for the first time. This nonlinearity is observed in most

types of gaskets in a more or less pronounced way.

Since the control of leakage is a major concern, the gasket characteristics during the operating condition are of most interest. Fortunately, the gasket stress-deformation curve of Fig. 4.2 shows a linear behavior during unloading which a gasket always exhibits at the operating condition. This feature of linearity, typically present in most gaskets, becomes more apparent for subsequent unloading-reloading. The real gasket behavior when mounted in a bolted joint is somewhat different from that obtained from an ideal compression test. However, during the tightening of a bolted joint, the sequence and the number of passes used to achieve the required preload involves a number of loadings, unloadings and reloadings of the gasket in the vicinity of a bolt. Thus on assumption of linear behavior may be considered as being satisfactory for most gaskets. A Modulus of Elasticity can be determined from the slope of the unloading-reloading portion of the curve and will be defined as the "Modulus of Decompression", E_g as in the paper by Bazergui (1985) such that:

$$E_g = \frac{dS_g}{dD_g} (t_g - D_{gmax}) \tag{4.1}$$

4.2.2 Presentation of the Analytical Model

The model used to simulate the joint is shown in Fig. 4.3 . The three essential mechanical elements, gasket, bolt and flange are represented by simple elastic springs

of linear stiffness K_g, linear stiffness K_b, and rotational stiffness K_f respectively. For cases involving blind cover plates, a plate stiffness K_p will be included. The force-displacement relations for the gasket and the bolt are:

$$u_g = \frac{F_g}{K_g} \tag{4.2}$$

$$u_b = \frac{F_b}{K_b} \tag{4.3}$$

For the flange whose stiffness accounts for the reinforcing effect of the cylinder and hub, the rotation is given by:

$$\theta_f = \frac{M_f}{K_f} \tag{4.4}$$

The applied loads, moments, displacements and rotations for each element are determined in the following section.

4.3 THEORETICAL ANALYSIS

Although figure 4.4 shows schematically the two flange geometries considered in the present study, namely: the symmetrical joint with two identical flanges, and the joint involving a flange with a blind cover, both ring flanges and weld neck flanges are

considered. The two following assumptions have been used:

1) Since the gasket is modeled by a single linear spring, the stress on the gasket will be assumed to be uniform across its width,

2) The flange rotates rigidly without distortion with respect to the point of gasket reaction located in the gasket-flange contact region.

The flange is decomposed into separate elements. In the case of a ring flange, the annular plate is welded to the cylindrical shell, while in the welding neck flange, the annular ring is integral with a short tapered hub to which the small end is butt welded to the cylindrical shell. Figure 4.5 shows the separate flange elements and the junction forces and moments. The anatomy of the flange leads to a standard problem in stress analysis near geometric discontinuities. In order to solve for the discontinuity forces and moments, governing equations for each structural element together with the compatibility of geometry at the interface boundaries, have to be considered. Before laying down the individual joint elements analyses, a brief overview on how these elements are treated, will be given:

- The cylindrical shell is be treated as "beam on an elastic foundation"

- The flange is considered to be either a circular plate with a central hole for small flanges or a circular ring for larger diameter flanges.

- The hub is treated using the theory of cylindrical shell with linearly varying thickness employing four constants of integration and a particular integral, and no assumption is made with regards to the point of zero radial deflection.

- The bolt is represented by a linear elastic spring

- The gasket is initially modeled by a single linear elastic spring and then the radial location is adjusted. This is equivalent to dividing it into several elements so as to simulate a series of identical linear elastic springs (see Section 5.8.3).

- The gasket radial stiffness together with the frictional resistance between the flange and gasket may also be considered as an optional feature.

- The difference in thermal expansion, creep and thermal degradation are simulated through an equivalent relative axial displacement of the gasket, the bolt and the flange.

4.3.1 Cylinder Theory

The long thin cylindrical part of the assembly (Fig. 5.4) is subject to internal pressure and its end is subjected to the discontinuity edge moment M and shear force P per unit circumference. For a long cylinder, the resultant radial displacement w_c (positive if directed radially outwards) and slope θ_c (positive clockwise) of the cylinder at any location x are given by the theory of beams on elastic foundation (Harvey, 1980), i.e.:

$$w_c = -\frac{e^{-\beta_c x}}{2\beta_c^3 D_c}\left[\beta_c M\,(\cos\beta_c x - \sin\beta_c x) + P\cos\beta_c x\right] + \frac{(2-\nu_c)B^2 p}{8E_c t_c} \qquad (4.5)$$

$$\theta_c = \frac{dw_c}{dx} = \frac{e^{-\beta_c x}}{2\beta_c^2 D_c}\left[2\beta_c M\cos\beta_c x - \frac{P}{2}(\sin\beta_c x + \cos\beta_c x)\right] \qquad (4.6)$$

$$\text{where} \qquad \beta_c = \left[\frac{12(1-\nu_c^2)}{B^2 t_c^2}\right]^{1/4}$$

$$\text{and} \qquad D_c = \frac{E_c t_c^3}{12(1-\nu_c^2)}$$

The end deflection and rotation are obtained by replacing the value of x by zero and substituting for D_c in the above equations giving:

$$w_c = \frac{6(1-\nu_c^2)}{E_c t_c^3 \beta_c^3} P - \frac{6(1-\nu_c^2)}{E_c t_c^3 \beta_c^2} M + \frac{(2-\nu_c)B^2}{8E_c t_c} p \qquad (4.7)$$

$$\text{and} \qquad \theta_c = \frac{12(1-\nu_c^2)}{E_c t_c^3 \beta_c} M - \frac{6(1-\nu_c^2)}{E_c t_c^3 \beta_c^2} P \qquad (4.8)$$

4.3.2 Hub Theory

The hub is considered to be a cylindrical shell with a linearly varying thickness; its radial displacement w_h is governed by the following differential equation (Timoshenko, 1930):

$$\frac{d^2}{dx^2}\left[x^2 \frac{d^2 w_h}{dx^2}\right] + \frac{12(1-\nu_h^2)}{\alpha^2 a_h^2} x\, w_h = \frac{12(1-\nu_h^2)}{E_h \alpha^3} p\, (1-\frac{\nu_h}{2}) \qquad (4.9)$$

Equation (4.9) differs from that used by Waters et al. (1937) because the term on the right hand side has been included. The homogeneous solution together with the

particular solution for the displacement w_h is expressed in terms of the longitudinal coordinate x, measured from the point of zero thickness, may be written as follows:

$$w_h = x^{-½} [C_1\psi_1'(\varepsilon)+C_2\psi_2'(\varepsilon)+C_3\psi_3'(\varepsilon)+C_4\psi_4'(\varepsilon)] + \frac{pa_h^2}{2E_h\alpha\, x}(2-\nu_h) \qquad (4.10)$$

The taper may be expressed in terms of the thickness of the cylindrical shell as $\alpha x_1 = t_c$ allowing the hub thickness t_h at any location to be expressed in terms of x and α so that $t_h = \alpha\, x$

$$\text{also} \quad \varepsilon = 2\rho\sqrt{x} \qquad \text{and} \qquad \rho = \left[\frac{12(1-\nu_h^2)}{\alpha^2 a_h^2}\right]^{1/4}$$

a_h is the hub mean radius. C_1 to C_4 are arbitrary constants of integration which must be established from the boundary conditions, and the ψ's are the Schleicher functions, proportional to the well known Kelvin functions. By successive differentiation the following relations for the rotation θ_x, moment M_x and shear force P_x emerge (Flugge,1973):

$$\theta_x = \frac{x^{-3/2}}{2} [C_1S_1(\varepsilon)-C_2S_2(\varepsilon)+C_3S_3(\varepsilon)-C_4S_4(\varepsilon)] - \frac{(2-\nu_h)\, a_h^2\, p}{2E_h\, \alpha\, x^2} \qquad (4.11)$$

$$M_x = \frac{E_h\alpha^3\, x^{1/2}}{48(1-\nu_h^2)} [C_1S_5(\varepsilon)-C_2S_6(\varepsilon)+C_3S_7(\varepsilon)-C_4S_8(\varepsilon)] + \frac{(2-\nu_h)\, a_h^2\, p}{12(1-\nu_h^2)} \qquad (4.12)$$

$$P_x = -\frac{E_h\alpha^3\rho^2\, x^{1/2}}{24(1-\nu_h^2)} [C_1S_2(\varepsilon)+C_2S_1(\varepsilon)+C_3S_4(\varepsilon)+C_4S_3(\varepsilon)] \qquad (4.13)$$

The S coefficients are a combination of Schleicher functions and their derivatives and are given in Appendix I while the arbitrary functions C_1 to C_4 are related to the edge moments and shears and the expressions which establish this relationship can be obtained by substituting the appropriate values of x, namely x_1 and x_2 into Eqs. (4.10) to (4.13).

4.3.3 Flange Theory

For small diameter flanges, Kirchoff's plate bending equations better characterize their behavior while for larger diameter flanges, the ring theory is more accurate. Use of the exact "thick plate" theory would lead to a very complex analysis which from practical viewpoint will be disregarded.

4.3.3.1 Plate Theory

The governing equation for small deflection of an axisymmetrically loaded thin plate is given by the so called Poisson-Kirchoff equation (Timoshenko,1959 and Roark,1988):

$$\left[\frac{d^2}{dr^2} + \frac{1}{r}\frac{d}{dr}\right]\left[\frac{d^2}{dr^2} + \frac{1}{r}\frac{d}{dr}\right] u = 0 \qquad (4.14)$$

The complete solution for the displacement u has four integration constants such that:

$$u = C_1 r^2 \ln r + C_2 r^2 + C_3 \ln r + C_4 \tag{4.15}$$

Once the expression for u is solved, by successive differentiation, equations for radial moment M_r and rotation θ_f are obtained from:

$$M_r = D_f \left(\frac{d^2u}{dr^2} + \frac{\nu_f}{r}\frac{du}{dr} \right) \tag{4.16}$$

$$M_t = D_f \left(\frac{1}{r}\frac{du}{dr} + \nu_f \frac{d^2u}{dr^2} \right) \tag{4.17}$$

$$Q = - D_f \frac{d}{dr} \left[\frac{1}{r}\frac{d}{dr} \left(r\frac{du}{dr} \right) \right] \tag{4.18}$$

$$\text{and} \qquad \theta_f = \frac{du}{dr} \tag{4.19}$$

The solution for the four constants, three of which serve in the derivative of Eq. (4.15), are found by applying the appropriate boundary conditions to a circular plate with a central hole subjected to an equivalent circumferential twisting couple M_f located at the inside and outside diameters of the flange. The following relation between M_{r1} and θ_f, at the inside radius of the flange ring, as obtained by Timoshenko (1959) is:

$$M_{r1} = \frac{1-K^2}{\left[\frac{1+\nu_f}{1-\nu_f}\right]K^2+1}\left[(1+\nu_f)\frac{2D_f\theta_f}{B} + M_f\left[\frac{1}{2}+\left[\frac{1+\nu_f}{1-\nu_f}\right]\frac{K^2}{K^2-1}\ln K\right]\right] \qquad (4.20)$$

where $K = \frac{A}{B}$

and $D_f = \frac{E_f t_f^3}{12(1-\nu_f^2)}$

For a loose type flange with no attachment to the pipe, the three known boundary conditions which serve in the derivation of Eq. (4.20) are:

at $r = \frac{A}{2}$ $\quad M_{r1} = 0$

$\quad Q = -\frac{M_f}{A/2}$

at $r = \frac{B}{2}$ $\quad M_{r1} = 0$

The flange rotation θ_f may therefore be obtained:

$$\theta_f = \frac{B\pi Y M_f}{E_f t_f^3} \qquad (4.21)$$

where $Y = \frac{1}{K-1}\left[\frac{3}{\pi}(1-\nu_f) + \frac{6}{\pi}(1+\nu_f)\frac{K^2 \ln K}{(K^2-1)}\right]$

The radial displacement of the flange w_f at the junction with the hub or cylinder may be calculated by considering thick-walled cylinder theory (Timoshenko, 1930). The total displacement is made up of the expansion due the pressure p, the shear force P, the frictional force V_g and the rotation θ_f due M_f given by:

$$w_f = \frac{B\gamma}{2E_f} p - \frac{B\gamma}{2t_f E_f} P + \frac{\gamma}{2\pi t_f E_f} V_g + \frac{t_f}{2}\theta_f \qquad (4.22)$$

where $$\gamma = \frac{A^2+B^2}{A^2-B^2} + \nu_f$$

4.3.3.2 Ring Theory

Considering the flange to be made up of a circular ring of uniform rectangular cross section twisted by couples uniformly distributed around its center line, the condition of equilibrium of the ring, gives the bending moment acting on each section as (Harvey, 1980):

$$M = \int_0^{\pi/2} M_f \sin\phi \frac{D_0}{2} d\phi = M_f \frac{D_0}{2} \qquad (4.23)$$

Where D_0 is the ring mean diameter and M_f is the twisting couple per unit length of the circumference. If we assume that the deformation of the ring consists of a rotation of its cross section through an angle θ_f, the elongation e of a fibre at radius r and distance y from section center and the corresponding stress σ are:

$$e = \frac{\theta_f y}{r}$$

and $$\sigma = \frac{E_f \theta_f y}{r}$$

The moment equilibrium equation becomes:

$$M = \int_{+t_f/2}^{-t_f/2} \int_{B/2}^{A/2} \frac{E_f \theta_f y^2 \, dr \, dy}{r}$$

and which upon integration yields

$$\theta_f = \frac{6\ M_f\ D_0}{E_f\ t_f^3\ \ln K} \tag{4.24}$$

Similarly, the radial displacement of the ring at its junction with the hub or cylinder is given by:

$$w_f = \frac{(K+1)^2\ B}{2(K-1)\ E_f}\ p - \frac{(K+1)^2\ B}{2(K-1)\ t_f E_f}\ P + \frac{(K+1)^2\ B}{4\pi(K-1)\ t_f E_f}\ V_g + \frac{t_f}{2}\theta_f \tag{4.25}$$

There are four terms in Eq. (4.25), the first one is due to the internal pressure p, the second and third are due to the discontinuity edge force P and the friction force V_g which is considered uniformly distributed over the thickness of the flange, and the last term is due to the flange rotation about its centroid (Fig. 4.8).

4.3.4 Blind Cover

An equivalent system to the blind cover plate shown in Fig. 4.6, is considered for a more precise evaluation of its axial displacement. This is achieved by the superposition of three simple cases of a flexible circular plate simply supported at the flange outside diameter: 1) the plate is subjected to a ring load F_g distributed along the effective gasket diameter G, 2) an operating pressure p distributed over the inner part of the plate bounded by the same circle of diameter G and 3) a plate subjected to a ring load F_b distributed along the bolt circle diameter C. Then, the components of displacement due

to F_g, p and F_b, given by Szilard (1974), are:

$$u_p = u_p(F_g) + u_p(p) - u_p(F_b) \tag{4.26}$$

with $$u_p(p) = a_0\, p \tag{4.27}$$

$$a_0 = \frac{A^4}{1024 D_p}\left\{1+[4-5\alpha^2+4(2+\alpha^2)\ln\alpha]\alpha^2+2\left(\frac{k_3}{1+\nu}\right)C_1-C_0\right\}$$

and $$u_p(F_g) = F_g \,/\, K_p' \tag{4.28}$$

where $$K_p' = \frac{64\pi D_p\,(1+\nu_p)}{[k_1-k_2+k_2C_1]}$$

with $\alpha = G/A$; $C_0 = 1 - \alpha^2$ and $C_1 = 1 - \alpha^4$

The quantity D_p is the plate flexural rigidity:

$$D_p = \frac{E_p t_p^3}{12(1-\nu_p^2)}$$

The constants k_i are defined as:

$$K_1 = (3+\nu)(1-\alpha^2) + 2(1+\nu)\alpha^2 \ln \alpha$$

$$K_2 = (1-\nu)(1-\alpha^2) - 2(1+\nu) \ln \alpha$$

$$K_3 = [4-(1-\nu)\alpha^2 + 4(1+\nu) \ln \alpha]\, \alpha^2$$

Similarly, the expression for $u_p(F_b)$ may be obtained by replacing, in Eq. (4.28) F_g by F_b and K_p' by K_p'' which is obtained by replacing $\alpha = C/A$ instead of G/A in all previous involved expressions. Therefore:

$$u_p(F_b) = F_b / K_p'' \tag{4.29}$$

4.3.5 Equilibrium

For the purpose of the analysis, a free body diagram of the bolted joint is required. As an example, a flange with a blind cover (case 1) is shown in Fig. 4.7 for both the seating and operating conditions. Within the framework of the previous considerations, a system of equations considering the force and moment equilibriums together with geometric compatibility may be derived in the manner described by Gill (1970). Based on Fig. 4.7, the axial equilibrium of external forces are obtained for the initial seating "i" and final operating "f" conditions respectively:

$$F_b^i = F_g^i \tag{4.30}$$

$$F_b^f = F_g^f + p\ A_p \tag{4.31}$$

$$N_l = p\ \frac{B}{4} \tag{4.32}$$

a) For the case of a ring type flange, (Fig. 4.5b);

-cylinder to ring junction

$$M = M_0 \qquad \text{and} \qquad P = P_0 \tag{4.33}$$

b) For the case of welding neck flange, (Fig. 4.5a);

-cylinder to hub junction

$$M_{x1} = M_1 \qquad \text{and} \qquad P_{x1} = P_1 \tag{4.34}$$

-hub to ring junction

$$M_{x2} = M_2 \qquad \text{and} \qquad P_{x2} = P_2 \tag{4.35}$$

4.3.6 Flange Loading

In order to simplify the analysis, some approximations must be made in the representation of the flange loading. The gasket and bolt loads are uniformly distributed around the circumferences of circles of diameters corresponding to their lines of reaction. Referring to Fig. 4.8, the resulting twisting couple M_f can be obtained from considering the equilibrium about the flange centroid as:

$$M_f = -\frac{B}{D_0} M - \frac{B}{D_0}\frac{t_f}{2} P + \frac{G}{D_0}\frac{(D_0-G)}{2}\frac{F_g}{\pi G} + \frac{C}{D_0}\frac{(C-D_0)}{2}\frac{F_b}{\pi C} - \frac{G}{D_0}\frac{t_f}{2}\frac{V_g}{\pi G} + \left[\frac{(G-B)}{4}+\frac{(D_0-G)}{2}\right]\frac{\pi}{4}\frac{(G^2-B^2)}{\pi D_0} p + \frac{B}{D_0}\frac{(D_0-B)}{2} N_1 \tag{4.36}$$

Substituting for F_g and N_1 from Eqs. (4.31) and (4.32), the expression for M_f from Eq. (4.36) will reduce to:

$$M_f = -\frac{B}{D_0}M - \frac{Bt_f}{2D_0}P + \frac{(C-G)}{2\pi D_0}F_b - \frac{t_f}{2\pi D_0}V_g + \frac{(G-B)}{16D_0}(G^2+B^2)p \tag{4.37}$$

M and P are the discontinuity or edge force and moment acting on the flange and may be equal to M_0 and P_0 or M_2 and P_2 depending on the flange type considered (see Fig. 4.5).

4.3.7 Geometrical Compatibility

Geometrical compatibility equations are used to determine the discontinuity force and moment variables at the junctions between the cylinder, the hub, and the flange.

4.3.7.1 Compatibility of Displacement and Rotation

The equations for compatibility requiring continuity of both, rotation and displacement, can be combined with equations of equilibrium to give a system of equations with five unknowns, M_0, P_0, V_g, θ_f and F_b, for the ring type flange and eleven unknowns, M_1, P_1, M_2, P_2, C_1, C_2, C_3, C_4, V_g, θ_f and F_b, for the welding neck type flange. Depending on whether we have seating or operating condition, one or two additional equations are needed to solve for the unknowns. Before the application of pressure, the bolt initial force F_b^i, which is the required bolt load to satisfy both the requirements of seating and operating conditions (Wm_1 and Wm_2), should be previously defined and consequently our system will be reduced by one unknown. However, upon application of pressure, the bolt force will change to an unknown value F_b^f requiring an additional equation to solve the system. The geometrical compatibility equations are:

a) For the case of a ring type flange;

-cylinder to ring junction

$$w_c = w_f \qquad \text{and} \qquad \theta_c = \theta_f \tag{4.38}$$

b) For the case of a welding neck flange;

-cylinder to hub junction

$$w_c = w_h \qquad \text{and} \qquad \theta_c = \theta_h \tag{4.39}$$

-hub to ring junction

$$w_h = w_f \qquad \text{and} \qquad \theta_h = \theta_f \tag{4.40}$$

4.3.7.2 Gasket and Flange Radial Constraints

In the Taylor-Forge method, it is assumed that the radial displacement is zero at the thick end of the hub to reduce the number of unknowns and shorten the arithmetics. Clearly, the resultant shear force P and the frictional force V_g (the latter not being introduced in the calculations) are the most important loads beside the pressure, for evaluating the radial and hoop stresses in the flange.

Beside Poisson's effect, the application of the internal pressure tends to displace the gasket radially outwards. However, this movement is to some extent restricted by the radial rigidity of the gasket together with the frictional resistance that is present between the gasket and the flange faces. This radial friction is generated because of the difference of radial resistance between the gasket and flange and may be of great importance in

evaluating leakage conditions especially when reaching blow-up situations.

Consequently, an additional equation can be derived by considering the radial displacement of the flange and the gasket at their contact location. In our model, this condition which will enable the development of a relation between the quantities P, V_g and θ_f shown in Fig. 4.8. The radial displacement of the flange w_f produced by the edge loads P and V_g, the pressure p and the flange rotation θ_f due to M_f must equal the radial displacement of the gasket w_g produced by the pressure p, the frictional force V_g and the gasket load F_g if the frictional resistance is important enough to prevent any relative radial displacement at the gasket contact area.

Hereafter, a method of introducing the effect of gasket radial resistance and the friction at the interface in the original elastic model is laid out. But first, let us point out that two possible situations may occur with regards to the above considerations (see Fig. 4.9). The first situation corresponds to the condition of no slip, as already pointed out, where radial relative movement between the mating surfaces is not possible. This is due to either high gasket loads or high surface roughness that may cause the flange material to deeply penetrate the gasket, thus preventing any radial relative movement. The second situation corresponds to the condition of full slip where the internal pressure is supported only by the gasket radial resistance or hoop stress developed in the gasket, in which case the frictional force V_g is not considered in the analysis.

4.3.7.2.1 Gasket Radial Displacement

The application of the internal pressure together with the axial gasket load tend to displace the gasket radially outward while the gasket friction force tends to bring the gasket radially inwards (see Fig. 4.10). Both loads tend to displace the gasket outward and, therefore, the total radial displacement of the gasket (positive inwards) is:

$$w_g = - w_g(p) + w_g(V_g) - w_g(F_g) \tag{4.41}$$

The radial displacement at a point of radius r due to the internal pressure p only is given by the theory of thick cylinders, such that:

$$w_g(p) = \frac{(1+\nu_g)\, a_g^2\, b_g^2}{E_g\, r\, (a_g^2 - b_g^2)}\, p \tag{4.42}$$

where a_g and b_g denote the gasket inside and outside diameters respectively.

Similarly, using the same expression as above, the radial displacement of the gasket due to the frictional force V_g is:

$$w_g(V_g) = \frac{(1+\nu_g)\, a_g^2\, b_g^2}{E_g r\, (a_g^2 - b_g^2)\, \pi G\, t_g}\, V_g \tag{4.43}$$

The radial displacement of the gasket at due to the squeezing effect produced by an axial force F_g is obtained by considering ring theory and is given by:

$$w_g(F_g) = \frac{\nu_g\, F_g}{2\pi E_g l_g} \tag{4.44}$$

Substituting F_g by F_b and p from Eq. (4.31) in Eq. (4.44), gives the expression for the total gasket radial displacement as:

$$w_g = -\frac{\nu_g}{2\pi E_g l_g} F_b + \frac{\eta_g}{\pi E_g t_g} V_g + \left[\frac{\nu_g A_p}{2\pi E_g l_g} - \frac{\eta_g G}{2E_g} \right] p \qquad (4.45)$$

where $$\eta_g = \frac{4(1+\nu_g)\, a_g^2\, b_g^2}{G^2(a_g^2 - b_g^2)}$$

4.3.7.2.2 Flange Radial Displacement

The radial displacement of the flange, $w_f(p)$, at the mid-gasket location due to an internal pressure p, is given by the thick cylinder theory such that:

$$w_f(p) = \frac{G\, \eta_f}{2E_f} p \qquad (4.46)$$

where $$\eta_f = \frac{(A^2/G^2)(1+\nu_f) + (1-\nu_f)}{K^2-1}$$

The flange, at the mid-gasket location G, is also subjected to radial displacement (positive inwards) due to other loads, namely the discontinuity edge force P, the frictional force V_g and the rotation θ_f such that:

$$w_f = - w_f(p) + w_f(P) - w_f(V_g) + \frac{t_f}{2}\theta_f \qquad (4.47)$$

Treating all loads as equivalent radial pressures, the total radial displacement of the flange is therefore:

$$w_f = -\frac{G\eta_f}{2E_f}p + \frac{G\eta_f}{2E_f t_f}P - \frac{\eta_f}{2E_f}\frac{V_g}{\pi t_f} + \frac{t_f}{2}\theta_f \qquad (4.48)$$

4.3.7.2.3 Blind Cover Radial Displacement

In the case of a blind cover, the radial displacement at the mid-gasket location G, is also considered in the analysis, although its effect could be negligible when the thickness becomes relatively larger. The expression for this displacement due to the frictional force V_g, at a radial position r, is obtained by considering disk theory and is given by the following expression:

$$w_p(V_g) = \left[1-\nu^2+(1-\nu)^2\frac{r^2}{(A/2)^2}\right]\frac{r}{2E_p t_p}\frac{V_g}{\pi G} \qquad (4.49)$$

$$\text{at } r = \frac{G}{2} \qquad w_p(V_g) = \frac{\eta_p}{4\pi E_p t_p}V_g \qquad (4.50)$$

$$\text{where} \qquad \eta_p = 1-\nu_p^2 + (1-\nu_p)^2\frac{G^2}{A^2}$$

After studying the radial displacement of the flange, the gasket and the blind cover, we are in a position to analyze the two joint types considered. First, for the case of an identical pair of flanges, the condition that the gasket follows the flange radial displacement must be satisfied:

$$w_g = w_f \qquad (4.51)$$

and, therefore, after substitution and rearrangement, Eq. (4.51) becomes:

$$\frac{G\eta_f}{2E_f t_f} P + \frac{t_f}{2}\theta_f - \left(\frac{\eta_f}{2\pi E_f t_f} - \frac{\eta_g}{\pi t_g E_g} \right) V_g + \frac{\nu_g}{2\pi E_g l_g} F_b = \left(- \frac{\eta_g G}{2E_g} + \frac{\nu_g A_p}{2\pi E_g l_g} + \frac{\eta_f G}{2E_f} \right) p \tag{4.52}$$

Second, for the case of a joint with a blind cover, the condition at the two interfaces is not identical since, at the mid-gasket location, the flange and the cover plate have different radial displacements. At the top and bottom surfaces, if no slip occurs, the gasket will tend to follow both mating surfaces. In such a case, the overall gasket radial displacement is assumed to take the average value such that:

$$w_g = \frac{1}{2} (w_f + w_p) \tag{4.53}$$

Similarly, after substitution and rearrangement, Eq. (4.53) becomes:

$$\frac{G\eta_f}{4E_f t_f} P + \frac{t_f}{4}\theta_f - \left(\frac{\eta_f}{4\pi E_f t_f} - \frac{\eta_g}{\pi t_g E_g} + \frac{\eta_h}{8\pi E_h t_h} \right) V_g + \frac{\nu_g}{2\pi E_g l_g} F_b = \left(-\frac{\eta_g G}{2E_g} + \frac{\nu_g A_p}{2\pi E_g l_g} + \frac{\eta_f G}{4E_f} \right) p \tag{4.54}$$

4.3.7.3 Axial Compatibility

The still unknown final bolt load F_b^f for the operating condition may be obtained from the geometric compatibility consideration in the axial direction. The axial displacement of the nut Δ_n which represents the amount by which the nut would axially move and corresponding to the actual number of turns necessary to achieve the required preload, must be the same in the initial pre-tightening state (i) and after the final pressurisation state (f). In fact, this nut axial displacement, being equivalent to the number of turns, is fixed and does not change when the pressure is released. It can be shown that it is the sum of the axial displacement of all joint elements involved, including the elongation of the bolt, the compression of the gasket, the displacement due to flange rotation and, when applicable, the deflection of the blind cover. For clarity, Fig. 4.11 shows schematically all amplified joint displacement components including gasket thickness that are involved in obtaining the geometric axial compatibility equation:

$$\Delta_n = \sum_{e=1}^{4} u_e^i = \sum_{e=1}^{4} u_e^f = \text{Const.} \tag{4.55}$$

$$\text{i.e.,} \quad \Delta_n = u_g^i + u_b^i + u_p^i + u_f^i = u_g^f + u_b^f + u_p^f + u_f^f \tag{4.56}$$

$$\text{where} \quad u_e = \frac{F_e}{K_e} \tag{4.57}$$

The expression for the nut displacement Δ_n involves the axial rigidity of all joint members as obtained by linear force-displacement relationships. The index "e" denotes

the joint element under consideration and may be the bolt b, the gasket g, the flange f, or the blind cover p. F_e represents the resultant axial force on the joint element while K_e represents the axial element stiffness. For the symmetrical case of a pair of identical flanges, K_p is replaced by K_f in the analysis.

The axial displacement, u, of the different joint members are obtained as follows:

a) The force-displacement relationships for the assumed linear behaviour of the gasket and bolt as established by Eq. (4.3), can be written as follows:

$$\text{for the gasket} \qquad u_g = \frac{F_g}{K_g} \tag{4.58}$$

$$\text{with} \qquad K_g = \frac{A_g E_g}{t_g} \qquad \text{and} \qquad A_g = \pi G N$$

$$\text{and for the bolt} \qquad u_b = \frac{F_b}{K_b} \tag{4.59}$$

$$\text{with} \qquad K_b = \frac{n A_b E_b}{l_b}$$

b) As can be seen from Fig. 4.11, the flange axial displacement u_f may be obtained from the rigid rotation of the flange around the gasket reaction point such that:

$$u_f = \left(\frac{C-G}{2}\right) \theta_f \tag{4.60}$$

c) In case of blind cover, it can be shown that Eq. (4.26) may lead to the axial displacement being:

$$u_p = \frac{F_g}{K_p'} - \frac{F_b}{K_p''} - a_0 p \tag{4.61}$$

4.4 BOLT LOADS RELATIONSHIP

After assembling the above equations, a system of 5 or 11 unknowns is obtained depending on the flange type considered. The complete set of equations is set in matrix form as detailed in Appendix II. Starting with the axial compatibility Eq. (4.56) and substituting for the element displacements u, it can be shown that an relationship between the seating and operating conditions exists. For case 2 of Fig. 4.4, the final bolt load may be expressed in terms of the initial bolt load as shown by the following equation:

$$F_b^f = F_b^i + \frac{\left[\frac{1}{K_g}+\frac{1}{K_p'}-\frac{a_0}{A_p}\right]}{\left[\frac{1}{K_g}+\frac{1}{K_b}+\frac{1}{K_p'}-\frac{1}{K_p''}\right]} A_p p + \frac{(C-G)}{2\left[\frac{1}{K_g}+\frac{1}{K_b}+\frac{1}{K_p'}-\frac{1}{K_p''}\right]}(\theta_f^i-\theta_f^f) \quad (4.62)$$

In case 1 of a symmetrical bolted joint of Fig. 4.4, only half of the joint system including half of the gasket as well as half of the bolt may be considered in the analytical model. The problem is then tackled in a similar manner to the previous case 1, with the blind cover considered as being rigid.

And therefore, the expression for the final bolt load will reduce to:

$$F_b^f = F_b^i + \frac{\frac{1}{K_g}}{\left[\frac{1}{K_g}+\frac{1}{K_b}\right]} A_p p + \frac{C-G}{\left[\frac{1}{K_g}+\frac{1}{K_b}\right]}(\theta_f^i-\theta_f^f) \quad (4.63)$$

By neglecting the discontinuity force and moment at the cylinder to flange junction, the gasket to flange frictional resistance and, the flexibility of the flange and blind cover, all terms including K_p as well as θ_f are to be dropped out from the previous expression of the final bolt load, leading to the well known rigid flange expression (Roberts and Jeannette, 1950):

$$F_b^f = F_b^i + \frac{1}{\left[1+\frac{K_g}{K_b}\right]} A_p\, p \qquad (4.64)$$

From the examination of the second term sign of the left-hand side of Eq. (4.64), it indicates that the force in the bolts will always increase with increasing pressure during operation which is not the case in some real assemblies as mentioned before.

4.5 RESULTS AND DISCUSSION

A computer program, "POLYFLG" based on the elastic interaction model as described in this chapter and consistent with the ASME code approach, has been developed and implemented to give precise values of final joint loads and allow, therefore, a better and more accurate estimation of the joint tightness. The detailed program together with its flow-charts are presented in Appendix III. The data is processed on a PC and the required information about the loads and distortion of the flanges are then printed out. In addition, the program provides the gasket and bolt

stresses, the flange rotation and stresses and, also, the stresses in the cylinder. With this information the possibility of the gasket leakage can be examined on a tightness graph obtained by a ROTT test.

Based on an initial bolt loading obtained from the tightness or leakage concept using the new gasket factors G_b, a and G_s, the final bolt and gasket loads and stresses are obtained for the two types of flanges considered. We have considered three cases wherein two standard intermediate and large ANSI B16.5 class 1500 flanges as well as a relatively large diameter flange, are used either in pairs or with blind cover plates in conjunction with three pressurized pipes NPS 12, 24 and 42. The flange thicknesses are 4.88", 8" and 6.5" (124, 203.2 and 165.1 mm) respectively and the flange material is carbon steel SA 105 with a Modulus of Elasticity equal to 29.9 E+6 psi (206 GPa) throughout.

The design pressures are 1500 psi (10.3 MPa) for the two ANSI B16.5 flanges cases and 925 psi (6.4 MPa) for the large diameter flange case and the design temperature is 70 °F (21 °C) in all cases. Appropriate size double jacketed mica-filled gaskets with G_b = 2900 psi (20 MPa), a = 0.23 and G_s = 14.69 psi (0.1 MPa) (Bickford, 1990) with a decompression modulus E_g = 234 ksi (1.614 GPa) were used in all cases. Standard tightness class T2 corresponding to a mass unit leak rate of 1/500 mg/s per millimetre of gasket circumference was used in evaluating bolt loads for the three cases.

Table 4.1 summarizes the results obtained for the bolt and gasket loads based on elastic interaction of all joint elements. This approach gives a more accurate evaluation of the final bolt and gasket loads as a function of the initial bolt loads, taking into account the flexibility of the gasket, the bolts and the flanges. With this method, the bolt and gasket stresses could also be evaluated.

The final forces in the bolts and gasket obtained with the proposed equations are found to be higher than those predicted by the rigid flange method (see ASME Code) in all cases. An estimation of the frictional force existing between the flange and the gasket contact area is also given. On the one hand, this force, being very small in magnitude as compared to the gasket load, was found to have a small effect on flange rotation and stresses. On the other hand, it offers a resistance to the radial expansion produced by the internal pressure and increase the blow-out resistance and is important to include as an option. This effect is more important in case of metallic gaskets having higher resistance. Another point worth mentioning is that the flange rotation does not exceed 0.2 deg. in all cases. In the two cases of the ANSI B16.5 class 1500 flanges, the rotations are rather low, less than 0.07 deg., even with the slip-on type, owing to the fact that the 1500 class flanges are rather stiff. All cases involving a blind cover plate result in higher rotations explaining in part, perhaps, why such joint configuration are found difficult to seal. Also, the higher values of bolt and gasket loads obtained with such cases are due to the relatively higher cover plate rigidity as compared to the flange. However, further comparison with numerical FE and experimental results will be given in the next chapter.

While the above examples show an increase in bolt load due to the application of pressure, as is predicted by the rigid flange approach, there are several examples where the bolt load remains constant or even decreases with increasing pressure as indicated in cases presented by Kohmura (1985) and Sawa et al. (1991). Figures 4.12 and 4.13 show the results obtained with the proposed method as compared to those measured on real bolted flanged joints by these two researchers. The flange dimensions are given in these figures. Kohmura tested two types of symmetrical joints made out of steel and aluminium. These joints were used in conjunction with PTFE gaskets reinforced by inorganic fillers. The dimensions of the gaskets were ID=167 mm, OD=220 mm, and 2 mm thick. Sawa tested an aluminium gasket of ID=50 mm, OD=105 mm and 5 mm thick, mounted on a steel flange with symmetrical configuration.

Depending on the characteristics of the joint and the flange rotation, effectively, the analytical flange model is capable of predicting with reasonable accuracy, within 4% in the two cases previously considered, the decrease of the final bolt load when the pressure is increased. Based on the results presented in table 4.1, it is clear that the design calculations based on the rigid flange approach do not indicate the conditions that actually exist in a flange joint, but merely represent some arbitrary stage in the tightening of the bolts. As long as this concept of design remains uppermost in the minds of designers no real progress can be made in understanding the manner in which flange joints function.

Table 4.1 Gasket and bolt loads.

FLANGE SIZE AND TYPE	NPS-12		NPS-24		NPS-42	
	W. Neck	Slip-On	W. Neck	Slip-On	W. Neck	Slip-On
Pressure, (psi)	1500	1500	1500	1500	925	925
Design bolt load, (lb)	309 686	309 686	970 824	970 824	1 898 456	1 898 456
Maximum bolt load, (lb)	472 232	472 232	1 396 700	1 396 700	1 900 000	1 900 000
Final gasket load (ASME code),(lb)	90 598	90 598	234 513	234 245	492 245	492 245
Final bolt load (POLYFLG), (lb)	401 297	373 259	1 141 980	1 099 210	2 138 380	2 065 230
	437 770*	420 459*	1 331 590*	1 289 940*	2 349 230*	2 280 060*
Final gasket load (POLYFLG), (lb)	182 209	154 171	405 666	362 904	724 530	651 377
	218 682*	201 371*	595 282*	553 634*	933 134*	866 205*
Frictional force (POLYFLG), (lb)	4 269	4 244	7 686	7 677	8 331	8 309
	4 311*	4 293*	7 803*	7 782*	8 407*	8 378*
Flange rotation (POLYFLG), (deg)	0.026	0.047	0.039	0.059	0.146	0.173
	0.028*	0.052*	0.044*	0.068*	0.156*	0.194*

* with blind cover

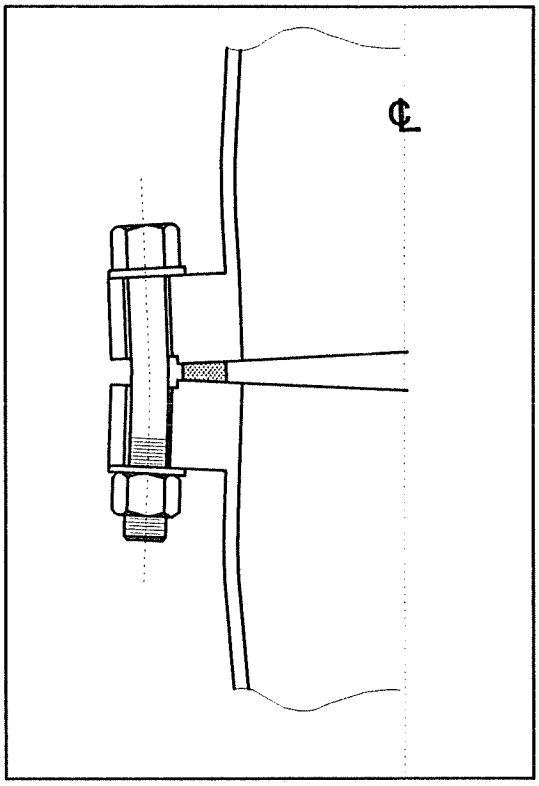

Figure 4.1 Deformed shape of a joint

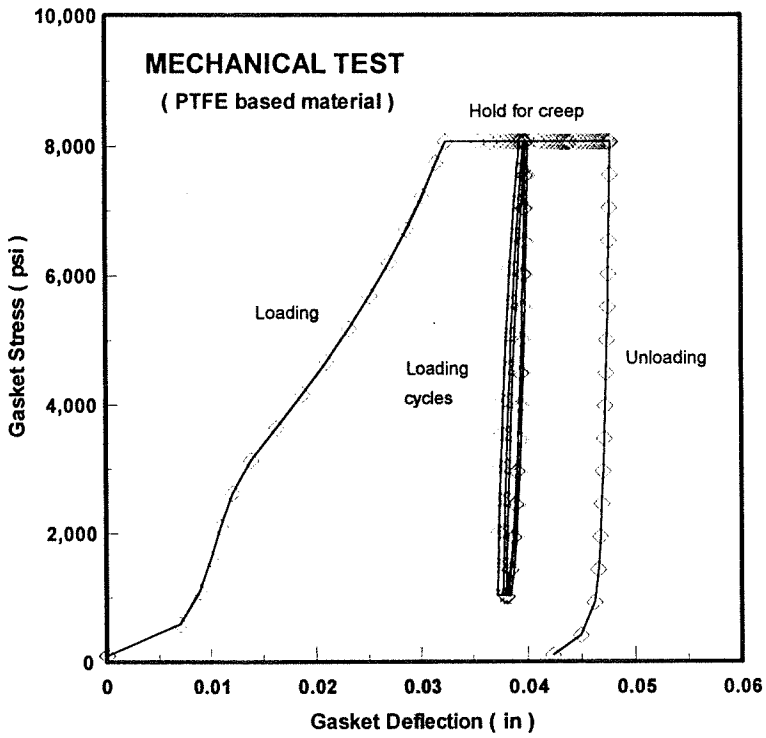

Figure 4.2 Typical PTFE gasket stress-deformation

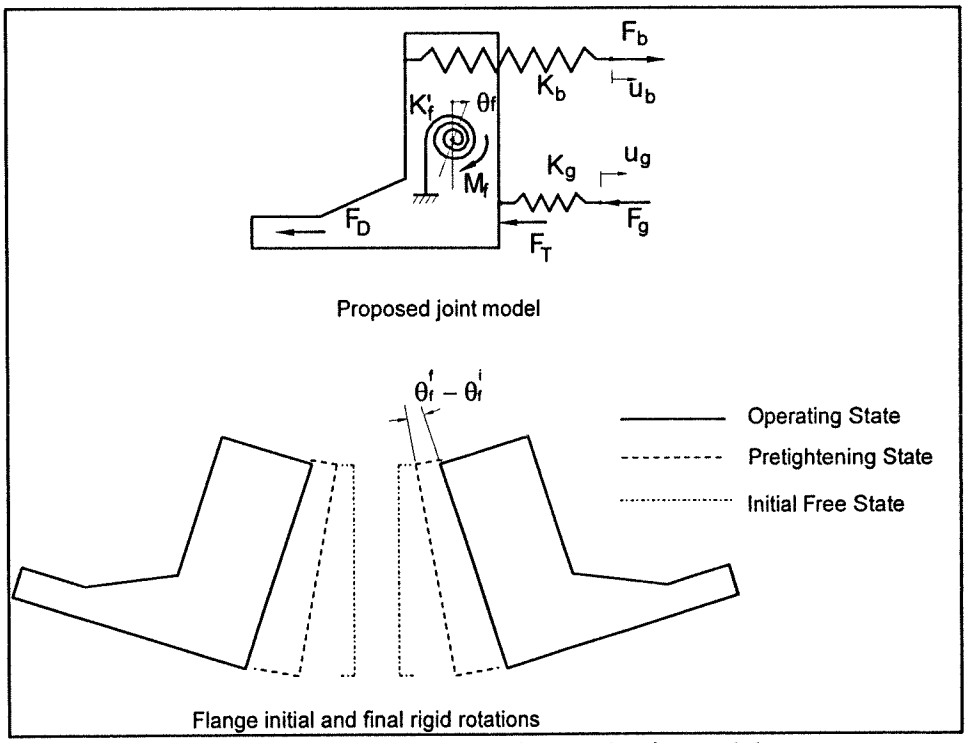

Figure 4.3 Proposed linear elastic model

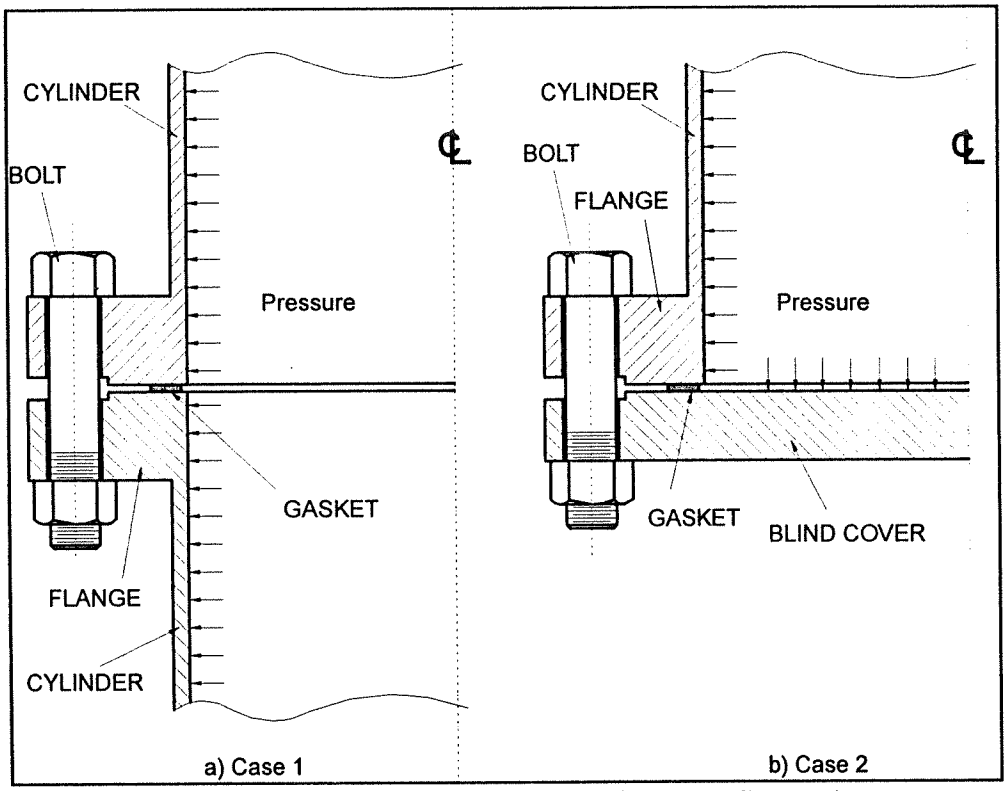

Figure 4.4 Two studied cases (ring type flanges)

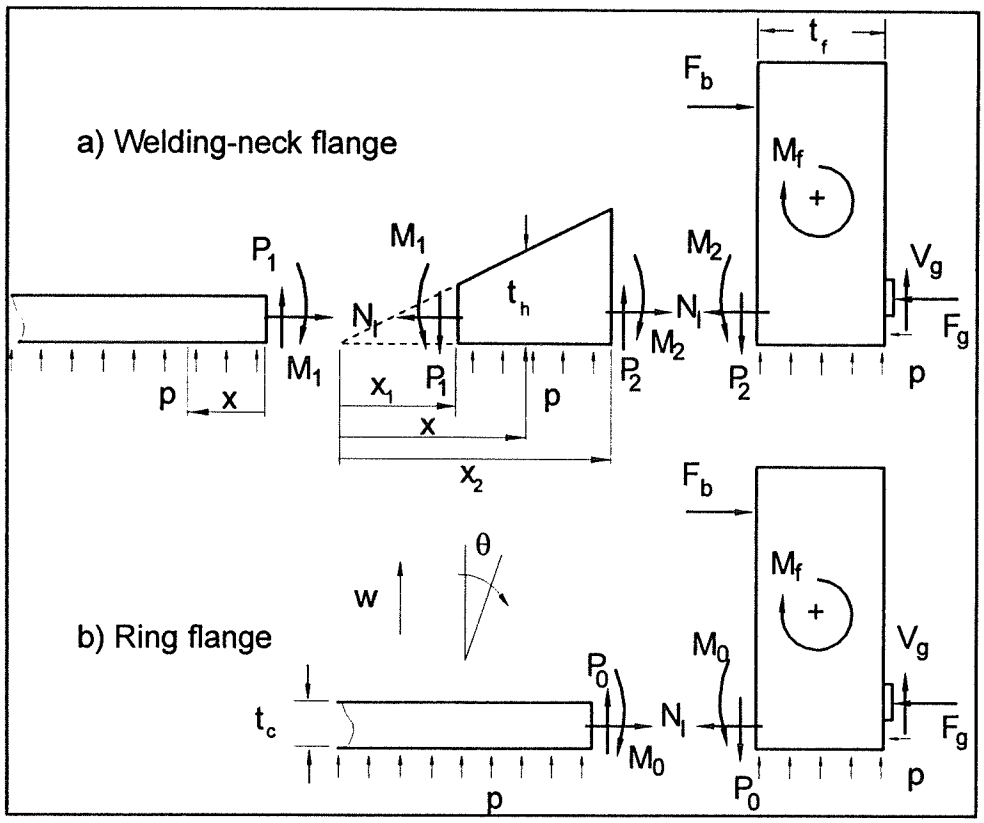

Figure 4.5 Flanges separation into elements

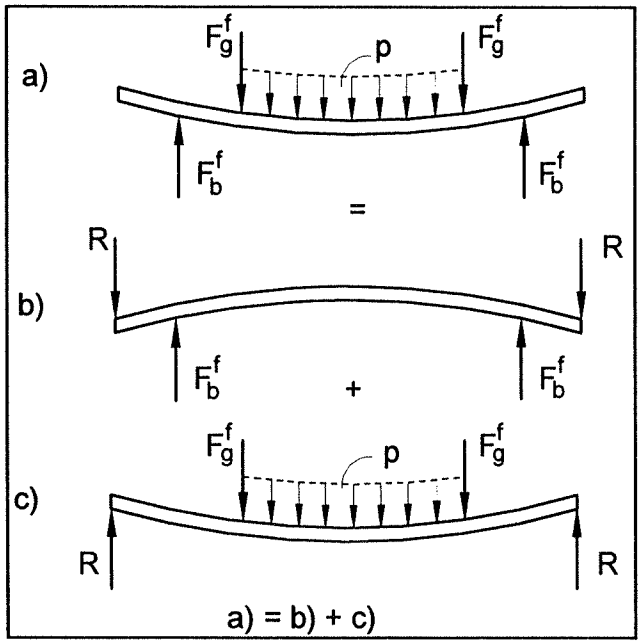

Figure 4.6 Equivalent plate for blind cover

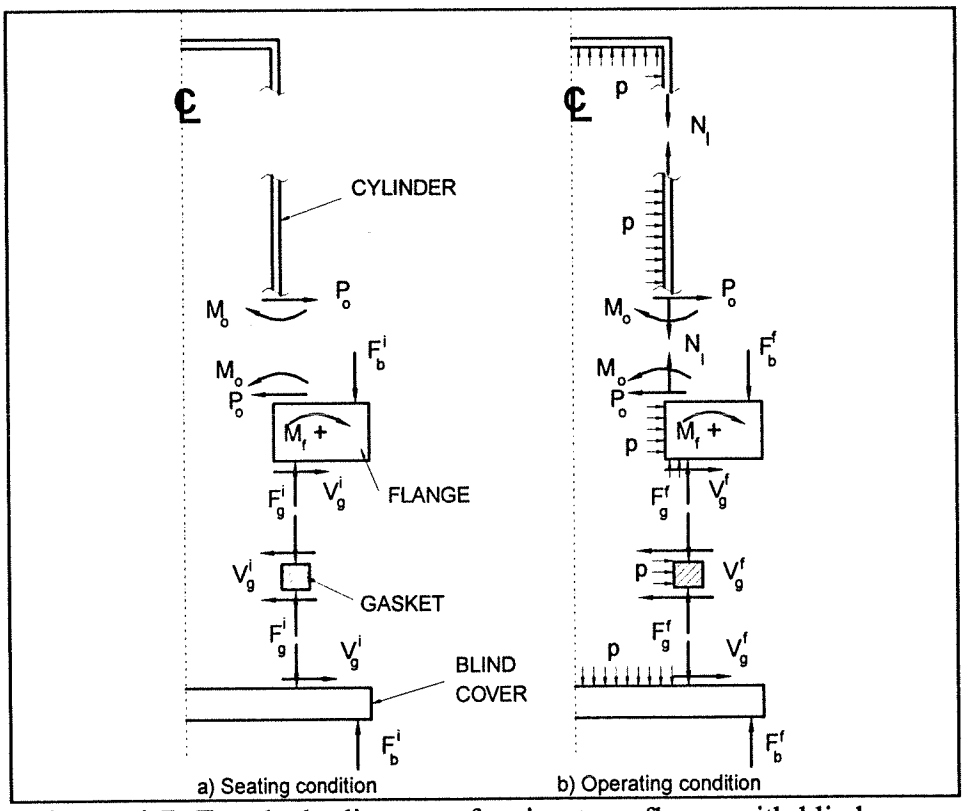

Figure 4.7 Free body diagram of a ring type flange with blind cover

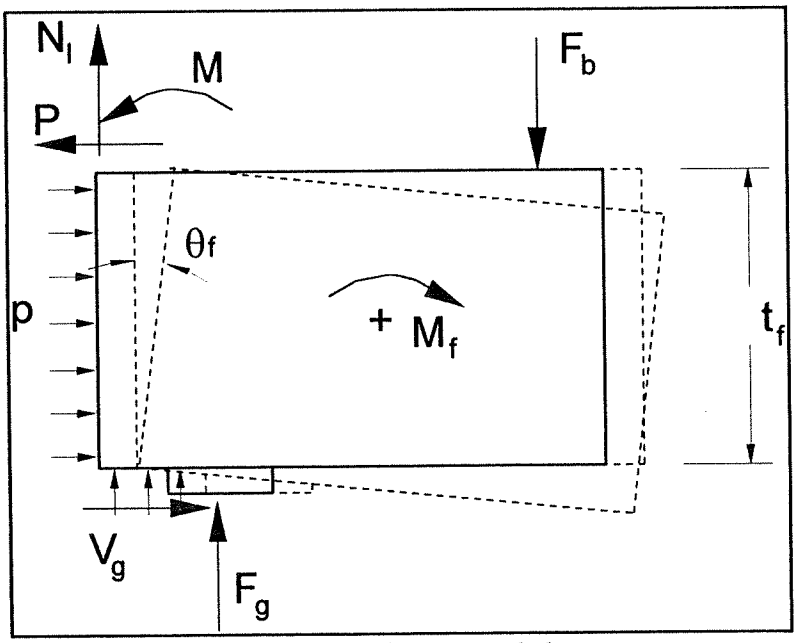

Figure 4.8 Flange pivoting around the contact zone

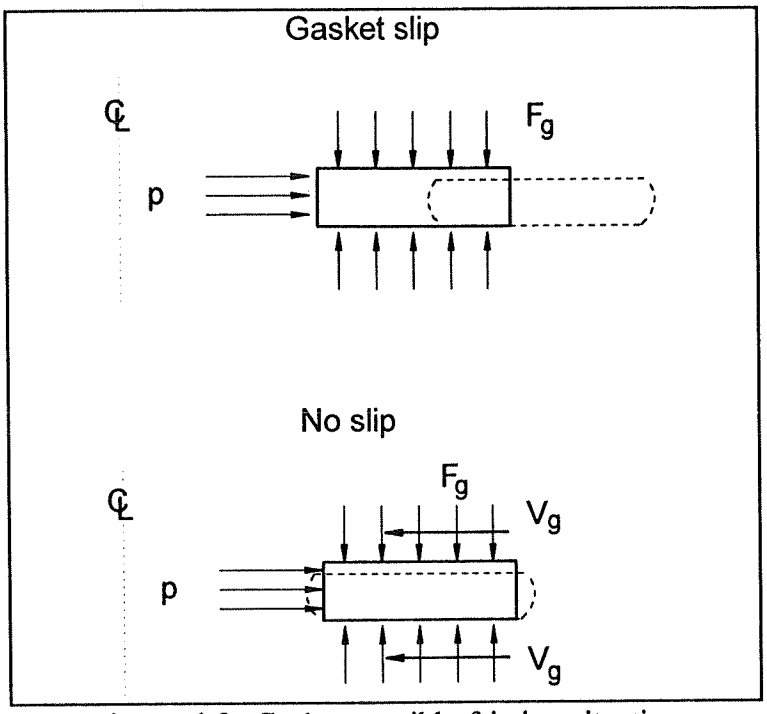

Figure 4.9 Gasket possible friction situation

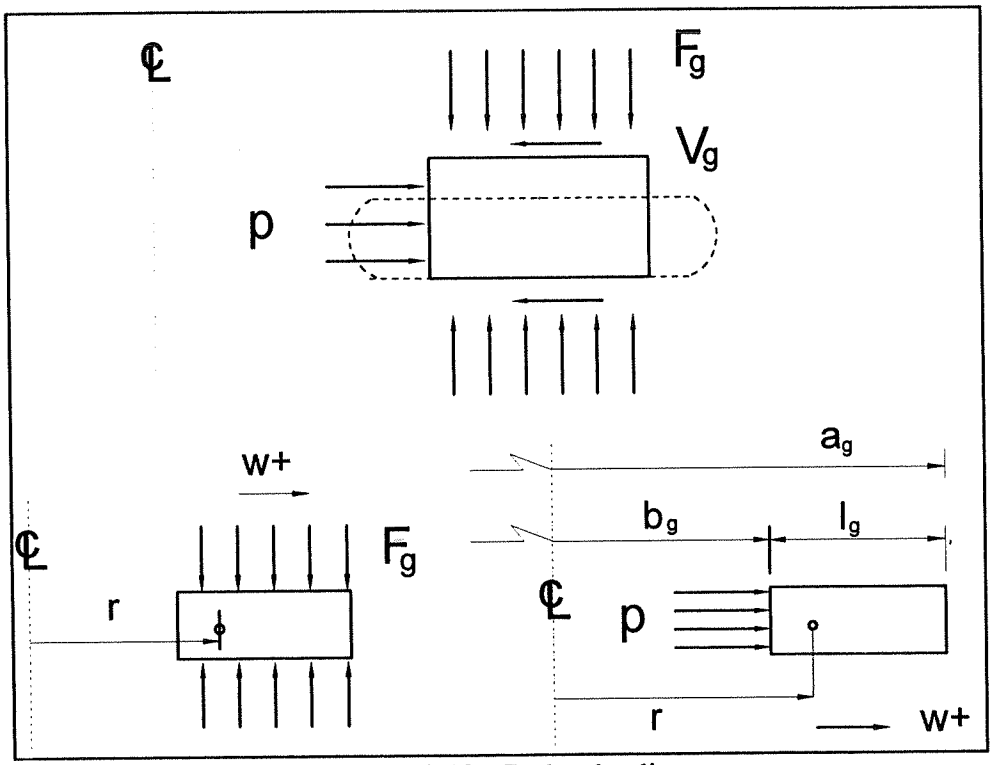

Figure 4.10 Gasket loading

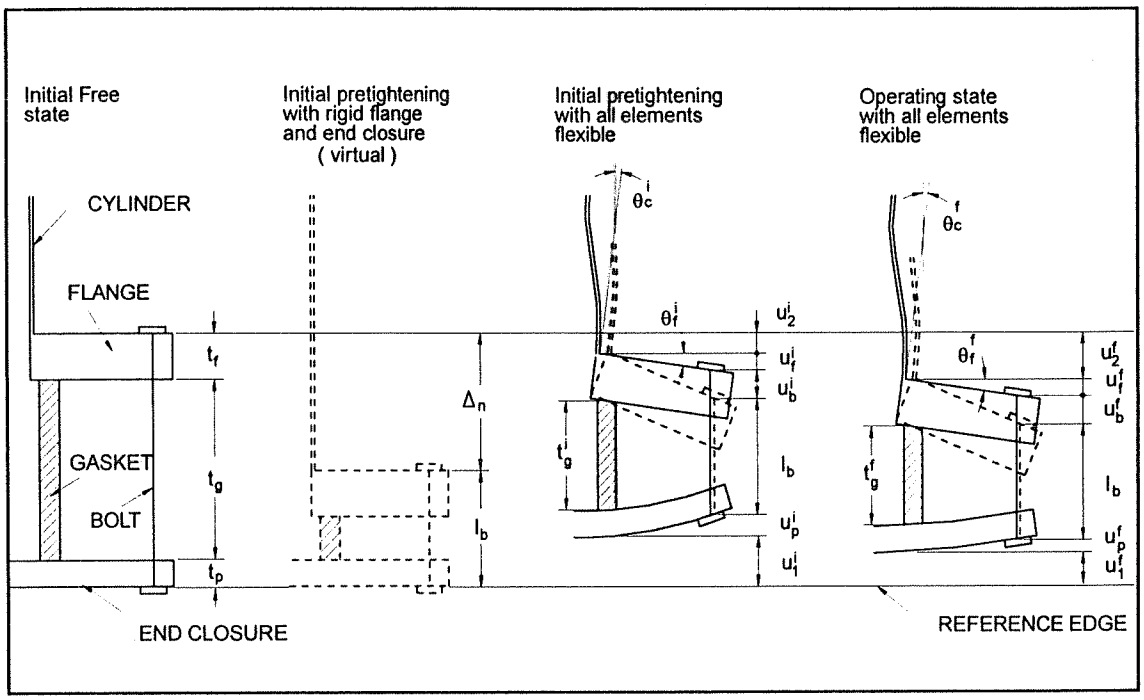

$$l_b + \Delta_n = l_b + u_b^i + u_1^i + u_2^i + u_f^i + u_p^i = l_b + u_b^f + u_1^f + u_2^f + u_f^f + u_p^f$$

$$\text{or} \quad u_g^i = u_1^i + u_2^i \quad \text{and} \quad u_g^f = u_1^f + u_2^f$$

$$\text{then} \quad \Delta_n = u_b^i + u_g^i + u_f^i + u_p^i = u_b^f + u_g^f + u_f^f + u_p^f$$

Figure 4.11 Different states including joint element displacements

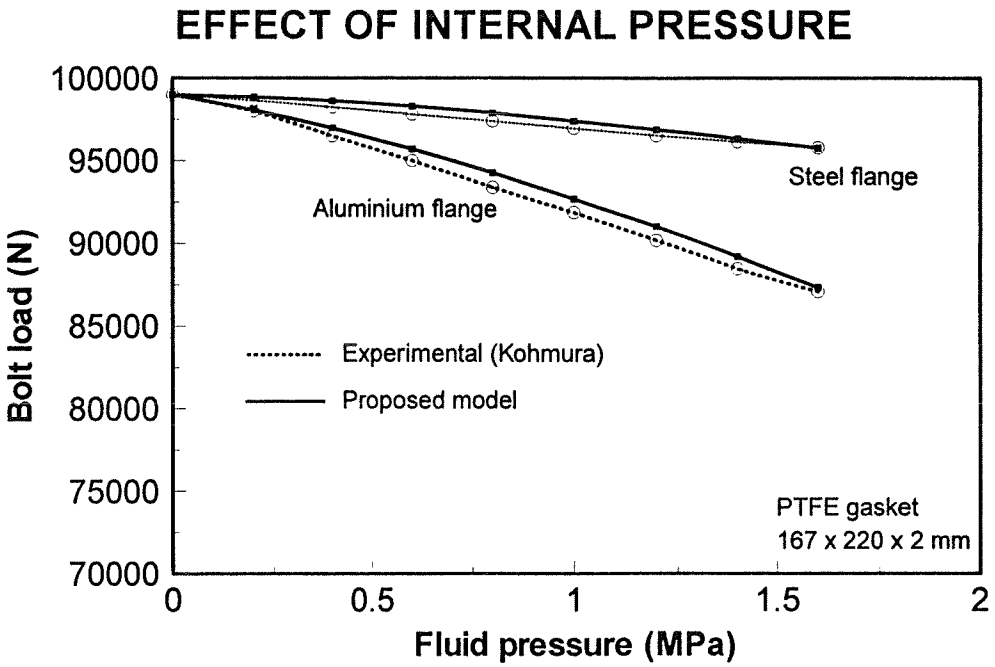

Figure 4.12 Decreasing bolt load with pressure

A=280, B=151, t_c=7, t_f=22.5, g_1=16 and x=45.6 mm

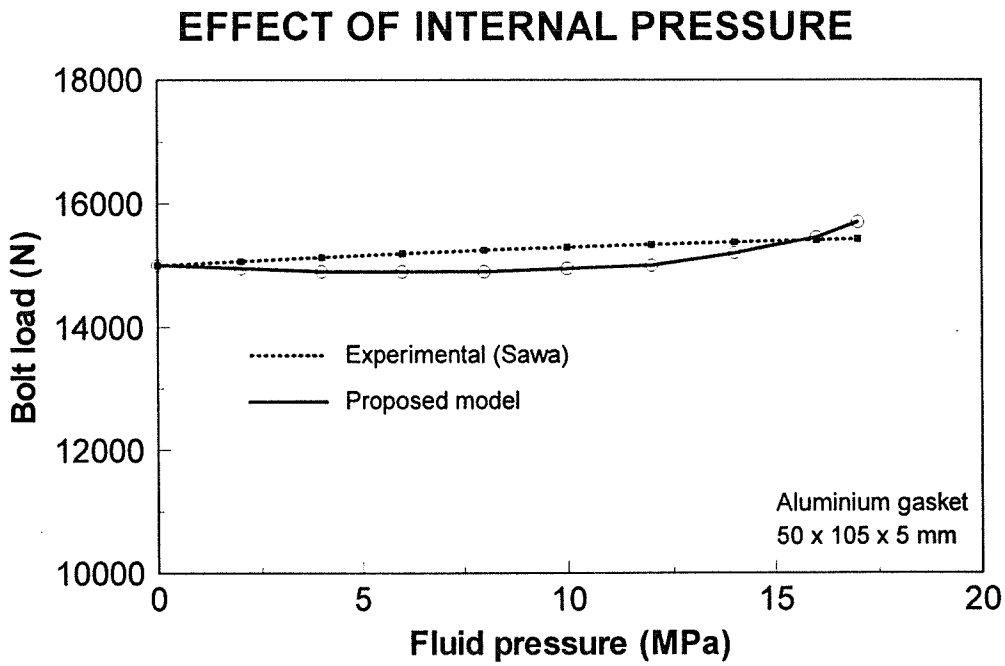

Figure 4.13 Constant bolt load with pressure

A=165, B=50, t_c=10, t_f=26, g_1=20 and x=42 mm

CHAPTER 5

GASKET STRESS DISTRIBUTION

PART A: USE OF THE DYNAFORCE SENSING SYSTEM TO STUDY THE GASKET STRESS DISTRIBUTION

5.1 INTRODUCTION

One of the important factors that influences the load distribution in bolts and on the gasket face of a flanged joint, when the bolts are tightened with an applied torque, is the type of bolt lubricant used. For a given bolt lubricant and load in a bolted flanged joint, it is difficult to determine the normal stress field on the gasket due to the many geometric and material parameters involved. In order to calculate final loads in the assembly, it is often assumed that this normal stress is uniform and therefore the bolt loads are almost equal. In the field, however, to ensure a tight seal while working under time constraints, mechanics may ignore recommended torque values and associated lubricants and tighten the bolt until the leak stops. This can cause too much bolt load, which can lead to stress corrosion cracking, thread stripping, damaged gaskets, and leakage caused by excessive flange rotation, as pointed out by Short (1992).

Part A of Chapter 5 deals with a study of a new pressure sensing system used to measure the actual gasket contact stresses and considers the effect of lubricants in an actual assembly of a bolted flanged joint. Thus, the first section describes an investigation to determine the torque coefficients of some typical industrial lubricants and the second section evaluates the stress distribution on a typical gasket by using a DynaForce sensing system. A summary of the results obtained in both parts of the investigation is presented and discussed.

5.2 TORQUE COEFFICIENTS TESTS

Figure 5.1 summarizes the results of the bolt load versus applied torque obtained experimentally for each lubricant using the rig of Fig. 3.3 . A straight line, averaging the experimental data, was fitted in all cases. Based on this figure, the superiority of the C-670 lubricant is evident. However, it is to be noted that, in three repeated tests, a relatively larger scatter was found to exist at higher torques in the case of the C-670 lubricant as compared to others as may be appreciated from Table 5.1. As a result, and since all data has been averaged and linearized, care should be taken when interpreting the curves of Fig. 5.1, particularly at higher torques where the behavior is nonlinear due to the plastic deformation of the threaded region of the bolt. The degreased bolt curve labelled "none", which represents the base line of comparison, is well below the others.

The inverse of the slope C of each line of Fig. 5.1 represents the torque coefficient, such that:

$$T_b = F_b \frac{1}{C} \tag{5.1}$$

where T_b = applied torque, lb.in (N.m),

F_b = applied bolt load, lb (N),

C = slope obtained from load vs torque curves, in^{-1} (m^{-1}).

Alternatively, the torque-preload Eq. (5.1) can be written in terms of the nominal bolt diameter D such that:

$$T_b = F_b (K \quad D) \tag{5.2}$$

where K is the dimensionless nut factor which is a general-purpose experimental constant obtained as the ratio between the torque and preload and includes all relevant parameters such as friction, torsion, bending, plastic deformation of threads and any other factor that may or may not have been anticipated. Many investigators have found that nut factors determined on a sample or prototype joint, can often differ significantly with a scatter of more than 26% in the preload achieved at a given input torque. This merely reflects the fact that the nut factor does indeed summarize such things as tool accuracy, operator skill besides the more obvious factors such as lubricity and condition of threads.

The nut factor is, therefore, given by:

$$K = \frac{1/C}{D} \tag{5.3}$$

Table 5.1 shows the minimum, average, and maximum values of K (K_{min}, K_{av}, K_{max}) as well as the slopes C (C_{min}, C_{av} and C_{max}) for each lubricant compared to the values given in the literature (Bickford, 1990). There is relatively good agreement between the two sets of results.

5.3 GASKET STRESS DISTRIBUTION

Figures 5.2 (a,b,c) show typical plots of the load values recorded by the strain gages for the eight assembly bolts at three levels of applied torque. The tests were run on the bolted rig of Fig 3.1 using asbestos type gaskets with a criss-cross tightening sequence (7-3-5-1-6-2-4-8) as shown in Fig. 3.2. The decrease in load of the first tightened bolts (3,5 and 1) is the result of elastic interaction between the various joint components which includes the flange, bolts and gasket. The general loading pattern is the same for all lubricants, with lower bolt loads for lubricants with smaller nut factors (K). For each lubricant, we have selected measurements which correspond to only one semi-circular portion of the sensor and represent the stress distributions at level of full torque. The full torque is the torque required to achieve 50% of yield in the bolt.

As an example, Fig. 5.3 shows a typical gasket stress distributions, as given by the DynaForce sensor presentation software. The sensor is divided into several small pixels, the color of which represents the contact stress level in the corresponding gasket region. Because the DynaForce sensor is nonlinear in the pressure range applied to the gasket, the linear calibration method used by the software underestimates the actual contact pressure. To compensate for the nonlinear behavior of the sensor, a new nonlinear calibration curve was applied to all the DynaForce stress values. The basis for the nonlinear calibration method and the resultant pressure scale was explained in Section 3.2.3.1.

5.4 RESULTS AND DISCUSSION

In order to represent and analyze the results obtained by the DynaForce system, MATLAB software was used to calculate the corrected gasket stress distribution. This software allows us to not only apply the stress correction factors but to manipulate the matrices of the DynaForce ASCII output files. In the following, we describe the final state of load in the bolted-flanged system for each case studied.

Figure 5.4 presents a typical histogram of the percentage of area occupied by each specific level of stress for the different lubricants. Although the target average contact stress was 15 ksi (103.4 MPa) as would be expected from the bolt torques of Table 5.2,

only a small percentage of the gasket area is at that stress. Most loaded cells are either at higher or lower stress values; suggesting that an important variation in the radial distribution of contact stress due to flange rotation is present.

Figure 5.5 shows a mean stress on a radius at every 2.86 degree portion, for the different lubricants. A fluctuating contact stress distribution around the circumference of the gasket is observed throughout. This is partly due to the method used to average the cells contact stresses lying in the bolt triangular portion. When working with a triangular portion of a matrix, it is not clear how to account for the matrix elements located at the boundaries. Looking at the DynaForce sensor, although the grid of cells is arranged in a circular fashion, the corresponding output data is stored in a square matrix. An element of the square matrix is not the value of the cell being at the corresponding polar location, but an average value of the cells being within the same region. The transformation of the polar cells mesh into the rectangular matrix form by the DynaForce software is not appropriate because of the difficulty in matching the corresponding positions.

The C-670 lubricant shows a lower stress distribution. A considerable variation of the average contact stress is observed at the junction between the two parts of the sensor as shown in Fig. 5.5 at the 90 and 180 degrees angular position. This is a boundary problem caused by the difference in readings when passing from one side of the data acquisition connection to the other. In deed, only one socket is used to read both sensor connections (Fig. 3.4). However, in most cases the error is relatively small.

A comparison has been made between the results obtained from the instrumented bolts and the DynaForce system. The flange has been divided into eight equal sectors corresponding to the eight bolt regions. The comparison is based on the average contact stress obtained over a gasket area limited by a bolt portion as illustrated typically by the curves of Figs. 5.6 a, b, c and d. Most of these curves show a large difference between the stresses given by the DynaForce sensing system and those determined with the more reliable instrumented bolts. This difference reaches a maximum of 50% for bolt 5 in the test with C-670 lubricant (see Fig. 5.6a).

As discussed previously, the highly nonlinear behavior of the sensor is the main reason for this difference. In fact, the use of the loading part of the calibration curve to readjust the load cell readings is not quite correct, since, in reality, every cell within the gasket region is subjected to few loadings and unloadings caused by the elastic interaction. When the load in a single bolt is increased, the bolt load in some of the previously loaded bolts in the joint will decrease. Therefore, the loading part of the calibration curve of Fig. 3.6 used to evaluate the cell load is not entirely correct. The problem is made more complicated since each cell follows a different loading-unloading path depending on the level of stress reached. To check the repeatability of the sensor, some tests were repeated up to three times as shown in Fig. 5.7 where the maximum percentage difference is about 15% with machine oil. Differences up to 37% were observed, however, in some other cases during the experimentation.

5.5 CONCLUSION

The effect of the type of bolt lubricant on the tightening of a bolted-joint assembly has been studied. Five types of common lubricants have been considered and compared for bolt load uniformity and ease of tightening. This study shows that, although some lubricants such as the C-670 lubricant made of molybdenum have the capacity of transmitting higher load for the same applied torque, their ability to maintain the achieved preload in a bolted joint is rather poor. With, such a lubricant, most of the transmitted bolt load drops rapidly due to the relatively low coefficient of friction and the elastic interaction between the various joint components. While a more uniform contact stress distribution is obtained with the N-5000 lubricant, the higher stresses are obtained with the machine oil lubricant.

From the results obtained and the comparisons made with the bolt stain measurements, the DynaForce sensing system has not proven to be a valuable quantitative tool for studying gasket contact stresses because of the hysteresis and poor repeatability of results. However, it is an interesting tool for a qualitative tri-dimensional visualisation giving a general trend of the gasket contact stresses. In an attempt to have more meaningful results, a nonlinear calibration method was employed. The new calibration method represents an improvement in comparison to the integrated DynaForce software calibration method. However, for the purpose of accurate stress measurements, a proper method of calibration of the sensor taking into account the nonlinearity and the hysteresis

effects preferably for each individual cell has to be developed. The DynaForce pressure sensing device cannot be used in its present form as a reliable measuring instrument.

PART B: GASKET MODELING AND EVALUATION OF THE RADIAL DISTRIBUTION OF THE GASKET CONTACT STRESS

5.6 INTRODUCTION

Structural integrity and leakage tightness are the two basic requirements of a properly designed bolted flange joint. Although bolted flange joints generally perform well structurally, their ability to seal efficiently is often a cause of concern. The gasket contact stress distribution, the key factor in sealing performance, is affected by both the flexibility of the flange and the extent of its rotation.

In this second part of Chapter 5, a simple approach to evaluate the radial distribution of the gasket stress and easily integrated in the analytical model or the "POLYFLG" program, is presented. It is based on a good estimation of the flange ring rotation. Some results obtained using this approach will be compared to those measured experimentally on an NPS 4 class-600 lb flange rig and to those calculated using an axisymmetric finite element model. The influence of the flange rotation on the radial distribution of the gasket contact stress and thus on the leakage tightness will be demonstrated.

5.7 EXPERIMENTAL AND FEM INVESTIGATIONS

Most of experimental leakage tests reported in the literature are performed with rigid fixtures for which only the average gasket stress is taken into account. However, studies (Marchand,1982 and Bouzid,1994b) show that the gasket stress distribution and flange rotation appear to have some effect on the joint sealing performance. Leakage is suspected of being more dependent on the local maximum stress in the gasket than on its average value.

The development of a simple method for predicting the rotation of the flange and the actual stress distribution in the gasket, through analytical modelling of the joint and considering the elastic interaction between all joint members is of great interest in predicting joint leakage.

5.7.1 Experimental Observations

The gasket reaction location, the flange rotation and the gasket width are important and interrelated parameters that should be considered when evaluating the gasket stress distribution and the leakage performance of a bolted joint. Figure 5.8 shows the effect of the gasket width made of asbestos material on the leakage performance as measured on the joint rig of Fig. 3.1. From this figure, it can be seen that, at constant gasket stress S_g, the mass leak rate L_{RM} decreases linearly on semi-logarithmic plot as the

gasket width increases. Since a higher bolt load is required when increasing the gasket width in order to generate the same average stress on the gasket, there is, of course, an upper practical limit on the gasket width.

Figure 5.9 shows a typical example of the gasket contact stress distribution as determined by the DynaForce system on the flange rig of Fig. 3.1. Circumferentially, the stress distribution is seen to be fairly uniform suggesting that the effect of bolt spacing is not significant. This is due to the fact that the number of bolts together with the type and the class of flange used (ANSI NPS 4 class 600) makes the joint rather rigid. Yet, there is a broad unevenness of the stress distribution indicating the effect of the overall rotation (or tilt) of the two. Radially, the stress distribution is shown to vary almost linearly, due to the rotation of the flange with the higher value being located at the outer perimeter of the gasket while the lower value being near the inside perimeter.

The effect of gasket width on the flange rotation as measured on the NPS 4 class 600 lb flange rig of Fig. 3.1 is shown in Fig. 5.10. The different gasket widths were obtained by varying the outside diameter while maintaining a constant inside diameter of 4" (102 mm); this causes the shift of the gasket reaction location towards the bolt circle especially for wider gaskets. This explains why for the same bolt load, a wider gasket produces less rotation. Such an influence is not negligible and have to be considered for an accurate analysis.

5.7.2 FEM Analysis on a NPS 4 Class 600 lb Flange

As expected, from the FEM findings (see Section 3.3), the radial distribution of stress of the asbestos gasket is of trapezoidal nature with the resultant slope varying linearly with respect to the gasket load as shown in Fig. 5.11. This slope is shown to slightly increase with gasket width. This was to be expected since for the same average stress, a greater bolt load, and hence a greater flange rotation, is obtained when increasing the gasket width. Also, Fig. 5.12 shows a linear correlation between the gasket maximum and mean stress and, obviously, the same conclusion could also be drawn for the slope which increases with increasing gasket width.

Therefore, the foregoing considerations and findings point to the possibility of the development of a simple approach to determine the radial distribution of the gasket stress and the gasket reaction location including a more accurate evaluation of the rotation in a flanged joint, and to determine whether the joint leakage performance is acceptable under the imposed conditions of testing and service. The method presented in the next section is intended to fill this need.

5.8 ANALYTICAL APPROACH

Most flange designs consider that the gasket pressure resultant acts at a known radial position and is independent of the flange rotation. In the previous chapters, the

analysis has considered the gasket as a linear element with the gasket reaction located at the mid-gasket location, diameter G. This chapter focuses on development of a simple analysis method which can be applied to ring type gaskets to better predict flange rotation and give an approximate solution to the radial distribution of the contact stress in the gasket. Using the same arguments as before, the gasket behavior is presumed to be linear in nature.

The idea of representing the gasket by several springs with linear and nonlinear compression stiffness placed in series was investigated by some researchers. In 1980, Soler conducted a computerized nonlinear analysis of a full face gasket. The detailed program is given in the book by Singh and Soler (1984). Boneh et al. (1986) developed a similar computer code with the nonlinear option for the gasket material properties. All these methods involve the sectioning of the gasket into several spring elements introducing time-consuming computation due the numerous variables involved.

Instead of simulating the gasket with several identical springs placed in parallel, it is much simpler to represent the gasket with only a single spring having an adjustable location that depends on the gasket pressure distribution estimated from the flange rotational flexibility. The analytical model developed for the calculation of the flange rotation is the same as that used in Chapter 4. An accurate evaluation of the rotation is, of course, necessary in order to better predict the radial distribution of the gasket stress.

5.8.1 Flange Rotation

The rotation of a flange or better known as the slope of the curvature, θ_f , when considered as a circular plate with central hole, may be expressed in terms of the total equivalent flange moment M_f acting on the flange, Eq. (4.21):

$$\theta_f = \frac{BY}{E_f t_f^3} M_f \qquad (5.4)$$

where $Y = \frac{3}{K-1}\left[(1-\nu_f) + 2(1+\nu_f)\frac{K^2 \ln K}{(K^2-1)}\right]$ for a plate (5.5)

with $K = A/B$

Equation (5.4) is evaluated at the junction between the cylinder and the flange. However, the slope of the circular plate varies with the radial position "r" according to Eq. (5.6) below, (Timoshenko,1930).

$$\theta_f = \frac{N\,A}{4\,D}\, r \left[\ln\left(\frac{A}{2r}\right) + \frac{1}{1+\nu_f} + \frac{1}{K^2-1} \ln K + \frac{1+\nu_f}{1-\nu_f} \frac{A^2}{4r^2} \frac{\ln K}{K^2-1} \right] \qquad (5.6)$$

The variation is relatively small, as shown in Table 5.3 where the relative differences in rotation between the values at the flange centroid θ_{fc} and the cylinder to flange junction θ_f are presented. It can be shown that the evaluation of the flange rotation can be greatly simplified, without introducing large errors, using the ring bending theory (θ_{fr}) instead of the circular plate theory (θ_{fp}) to represent the flange. For relatively large diameter flanges having a smaller value for K, the agreement is quite good as may be appreciated from Table 5.4. Hence referring to Eq. 4.24, Y will be simply :

$$Y = \frac{6}{\ln K} \tag{5.7}$$

Therefore the use of ring theory, in accordance with the prediction of stresses in flanges developed in the ASME Code, will be used and the ring portion of the flange will be assumed to rotate, but not to distort, when subjected to the flange moment M_f .

5.8.2 Radial Gasket Displacement and Stress Variations

The predicted rotation may be used to evaluate the radial variation of the gasket compression. In fact, for the analytical gasket model, only the average displacement of the gasket u_{gm} at the radial mid location need to be evaluated. Assuming the flange material to be rigid compared to the gasket material, the flange local surface deformation at the gasket contact region is relatively negligible. As a result, the displacement of the gasket u_g may be obtained at any radial position "z" measured from the gasket mid-location (see Fig. 5.13), according to the linear relation:

$$u_g = u_{gm} \pm k\, z\, \theta_f \tag{5.8}$$

where k is a factor that depends on the type of flange considered. For a symmetrical joint k is equal to 2 while for a joint with an assumed rigid blind cover k is equal to 1.

Finally, from the gasket stress-deflection curve, the contact stress at any radial location may be estimated as:

$$S_g = [\, u_{gm} \pm k\, z\, \theta_f \,] \frac{E_g}{t_g} \tag{5.9}$$

5.8.3 Adjustment of Gasket Reaction Location

Flange rotation causes a non-uniform gasket stress distribution which shifts the radius of application of the gasket reaction towards the outer gasket periphery. A simplified method to account for this effect is developed by assuming the gasket stress to be linearly proportional to the gasket displacement and considering the local flange contact surface with the gasket to be rigid. The expression of the gasket displacement Eq. (5.8) at any radial position x as defined from Fig. 5.14, is given by:

$$u_g = k \times \theta_f \tag{5.10}$$

Distance x depends on whether the gasket is partially loaded or fully loaded, Fig. 5.14 (a & b). The applicable case may be found by considering the displacement of the gasket at the gasket linear spring model location together with the flange rotation and summarized by the following conditions:

- For a fully compressed gasket

$$G_n - 2\,x_{n+1} > G_0 - l_g$$

$$\text{or} \quad G_n - 2\,\frac{u_{g_{n+1}}}{k\,\theta_f} > G_0 - l_g$$

- For a partially compressed gasket

$$G_n - 2\,x_{n+1} < G_0 - l_g$$

$$\text{or} \quad G_n - 2\,\frac{u_{g_{n+1}}}{k\,\theta_f} < G_0 - l_g$$

The gasket reaction location may be evaluated using a rapidly converging iterative method. First, the gasket reaction is assumed to act at the mid gasket location of

diameter G_0. With a first estimate of flange rotation θ_{f0}, the gasket displacement centroid which is the same as the new gasket reaction location G_n is then evaluated. With this new value, the new flange rotation θ_{fn} is recalculated to obtain the new gasket reaction location G_{n+1}. The whole process is repeated until the required convergence is achieved which, in general, is obtained after three or four iterations (see Appendix III).

5.8.3.1 Fully Compressed Gasket

Let $\bar{y}_n$ be the distance from the outer gasket diameter to the displacement centroid after n iterations. Referring to Figs. 5.13 and 5.14a for a symmetrical joint, the position of the centroid of a trapezoidally deformed shape of dimensions a, b and c is given by:

$$\bar{y}_n = \frac{c}{2}\left[\frac{a+b/3}{a+b/2}\right] \tag{5.11}$$

In case of the gasket geometry of Fig. 5.13a, substituting for a, b and c gives the position of the centroid $\bar{y}_n$:

$$c = l_g\,, \qquad b = l_g\,\theta_{fn}\,, \qquad a = \frac{u_{gn}}{k} - \frac{\theta_{fn}}{2}\,(G_n - G_0 + l_g)$$

$$\bar{y}_n = \frac{l_g}{2}\left[1 - \frac{\theta_{fn}\,l_g}{6\left[\frac{u_{gn}}{k} - \frac{\theta_{fn}}{2}\,(G_n - G_0)\right]}\right] \tag{5.12}$$

where the factor k has the same definition as before (see Eq. 5.8).

The new estimated gasket reaction after n iterations is therefore:

$$G_{n+1} = G_0 + \frac{1}{6}\left[\frac{\theta_{fn} l_g^2}{\frac{u_{gn}}{k} - \theta_{fn}\,(G_n - G_0)}\right] \tag{5.13}$$

5.8.3.2 Partially Compressed Gasket

Similarly, let $\bar{y}_n$ be the distance from the outer diameter to the centroid. Referring to Fig. 5.13 and 5.14 b, the position of the centroid of a triangular deformed shape is just at one third of its base. Therefore, in case of the gasket geometry of Fig. 5.14 (b), the position of the centroid is:

$$\bar{y}_n = \frac{1}{3}\left[\frac{G_0}{2} + \frac{l_g}{2} - \frac{G_n}{2} + \frac{u_{gn}}{k\,\theta_{fn}}\right] \tag{5.14}$$

The gasket reaction, after n iterations, is therefore:

$$G_{n+1} = \frac{1}{3}\left[2\,G_0 + G_n + 2\,l_g - 2\,\frac{u_{gn}}{k\,\theta_{fn}}\right] \tag{5.15}$$

5.9 RESULTS AND DISCUSSION

The flange rotation and contact stress distribution in the gasket may be calculated using the proposed simple analytical model of the flange joint. Figure 5.15 shows that the flange rotation calculated by considering simple elastic linear interaction of all joint members is in good agreement with the FEM and the experimental studies. The finite

element study has confirmed that the same flange rotation is obtained whether considering the linear or nonlinear gasket material behavior. In fact the flange rotation does not depend on the gasket material but rather on the bolt load. The importance of including the hub in the analytical model is demonstrated; the omission of the hub produces a less rigid joint and, therefore, the rotation of the flange is overestimated. From the axial gasket and flange displacements shown amplified in Fig. 5.16, both the proposed method and the FE method are shown to be in good agreement. Even at very high loads resulting in gasket stresses of 15 ksi (103.4 MPa), only very small flange distortion is present and rigid flange rotation can be safely considered.

Apart from the gasket edge effects which impose the rapid drop in gasket stress to zero, it can be seen in Fig. 5.17 that the linear radial distribution of the contact stress obtained from the analytical model compares well with that obtained from the elastic gasket material FEM model for the different bolt loads. The maximum gasket stress is at the outer gasket perimeter and is a result of the flange rotation as already pointed out. The importance of and need for proper evaluation of the residual gasket stress is seen to be necessary with regards to improvement of Code design procedures to account for leakage. A model capable of taking into account most of the parameters involved for a leak safe design has been developed. A more precise evaluation of the gasket residual stresses can be obtained with this simple approach in order to better predict gasketed joint leakage behavior.

Table 5.1 Comparison of nut coefficients

	Our Results						Bickford, 1990		
Lubricant	C_{min}	C_{av}	C_{max}	K_{min}	K_{av}	K_{max}	K_{min}	K_{av}	K_{max}
C-670	128.32	158.73	175.06	.078	.086	.107	.08	.095	.15
Improved N5000	89.7	97.63	104.63	.131	.140	.153	N/A	N/A	N/A
N5000	86.67	93.71	96.2	.143	.146	.158	.13	.15	.27
C5-A	65.45	80.06	80.86	.170	.171	.210	.10	.21	.225
As Received	75.79	80.91	90.65	.151	.169	.181	.158	.2	.267
None	-	31.28	-	-	.432	-	N/A	N/A	N/A

Table 5.2 Applied torque used for lubricant tests (Fig. 5.1).

Lubricant	1/3 torque (lb.ft)	2/3 torque (lb.ft)	Full torque (lb.ft)
C-670	102	205	307
Improved N5000	160	320	480
N5000	172	343	515
C5-A	187	376	564
As Received	208	415	624

Table 5.3 Variation of the flange rotation with radius

K	1.01	1.1	1.2	1.3	1.4	1.5	1.6	2.0	3.0	4.0
θ_{fc}/θ_f	0.998	0.986	0.972	0.96	0.949	0.939	0.93	0.902	0.877	0.886

Table 5.4 Comparison of rotation as per ring and flange theories

K	1.01	1.1	1.2	1.3	1.4	1.5	1.6	2.0	3.0	4.0
θ_{fp}/θ_{fr}	1.002	1.014	1.026	1.037	1.046	1.053	1.06	1.075	1.075	1.050

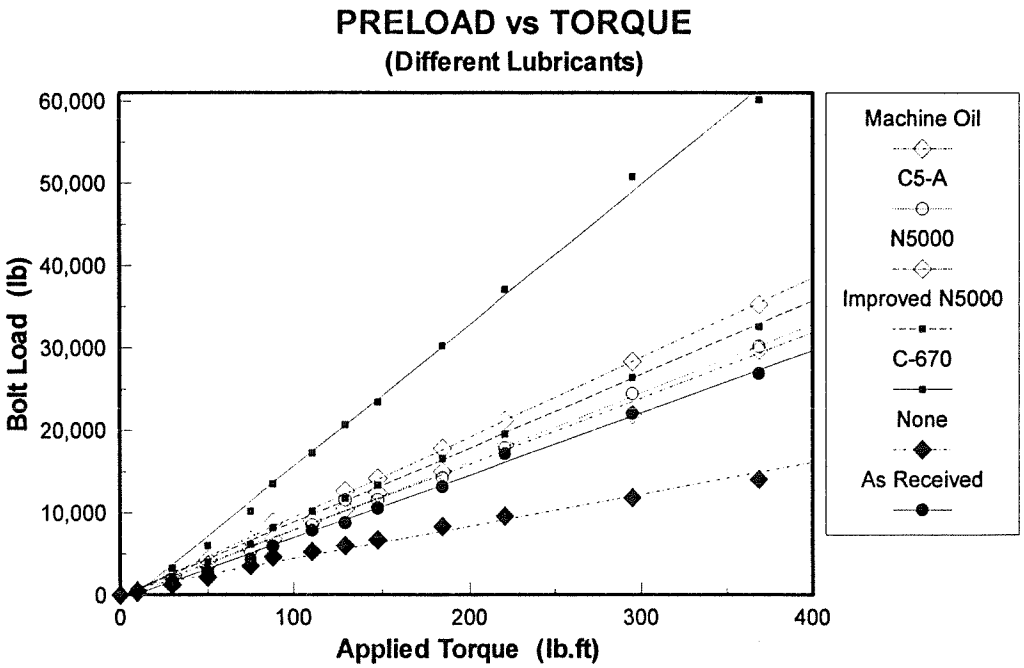

Figure 5.1 Preload vs applied torque for all lubricants (average)

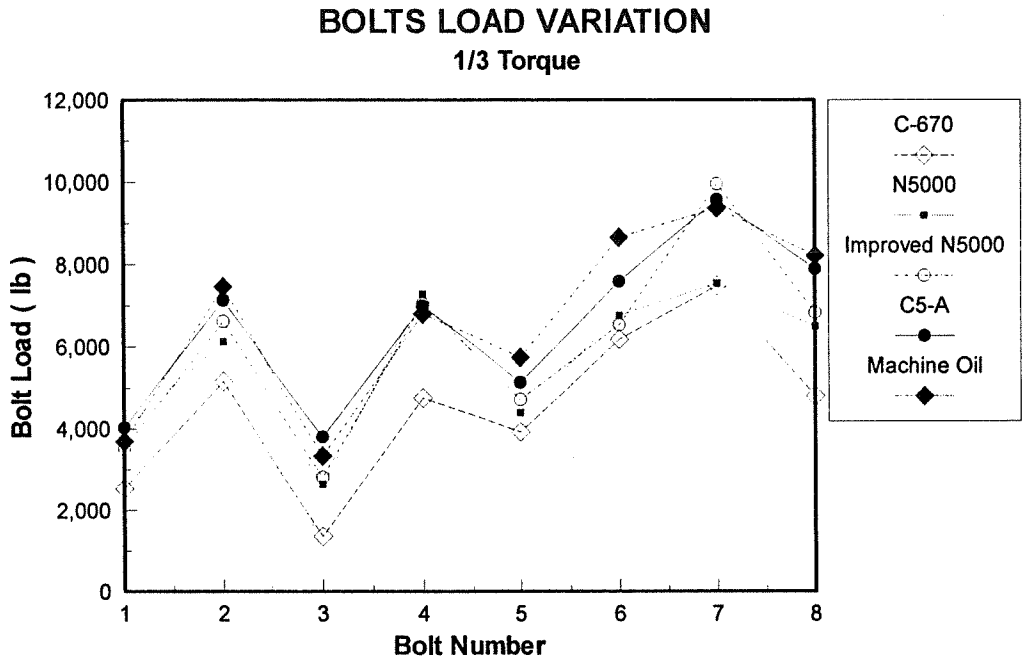

Figure 5.2a Bolt load variation at 1/3 torque

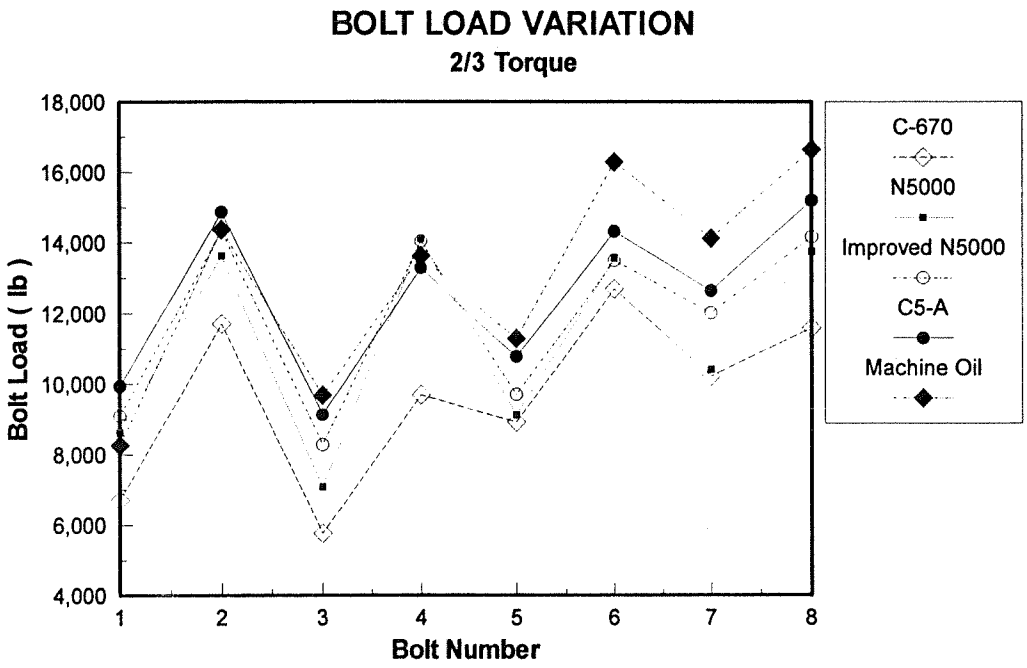

Figure 5.2b Bolt load variation at 2/3 torque

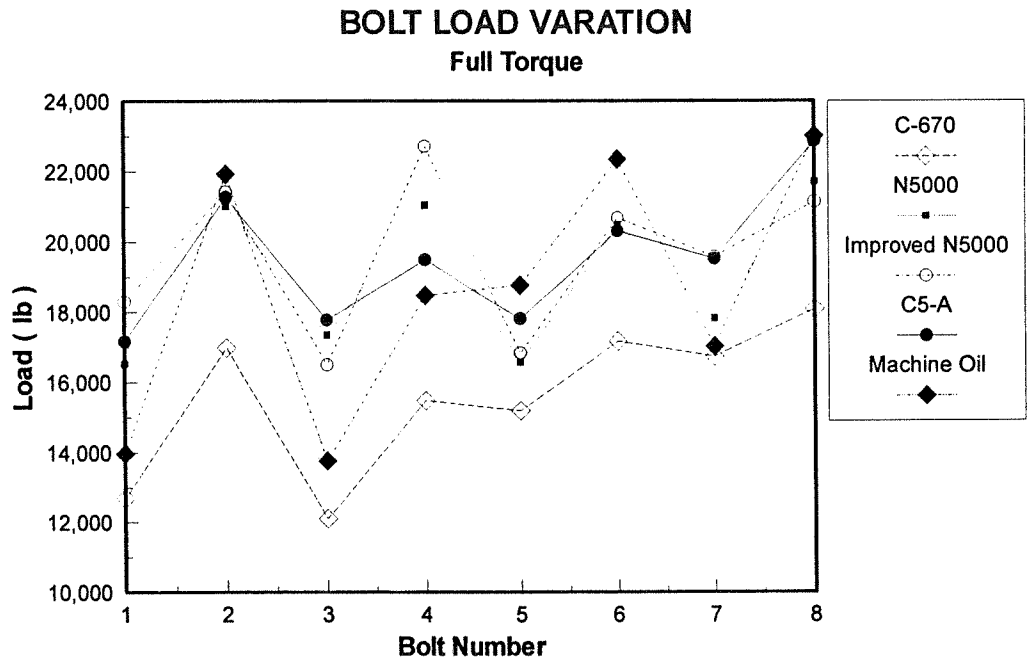

Figure 5.2c Bolt load variation at full torque

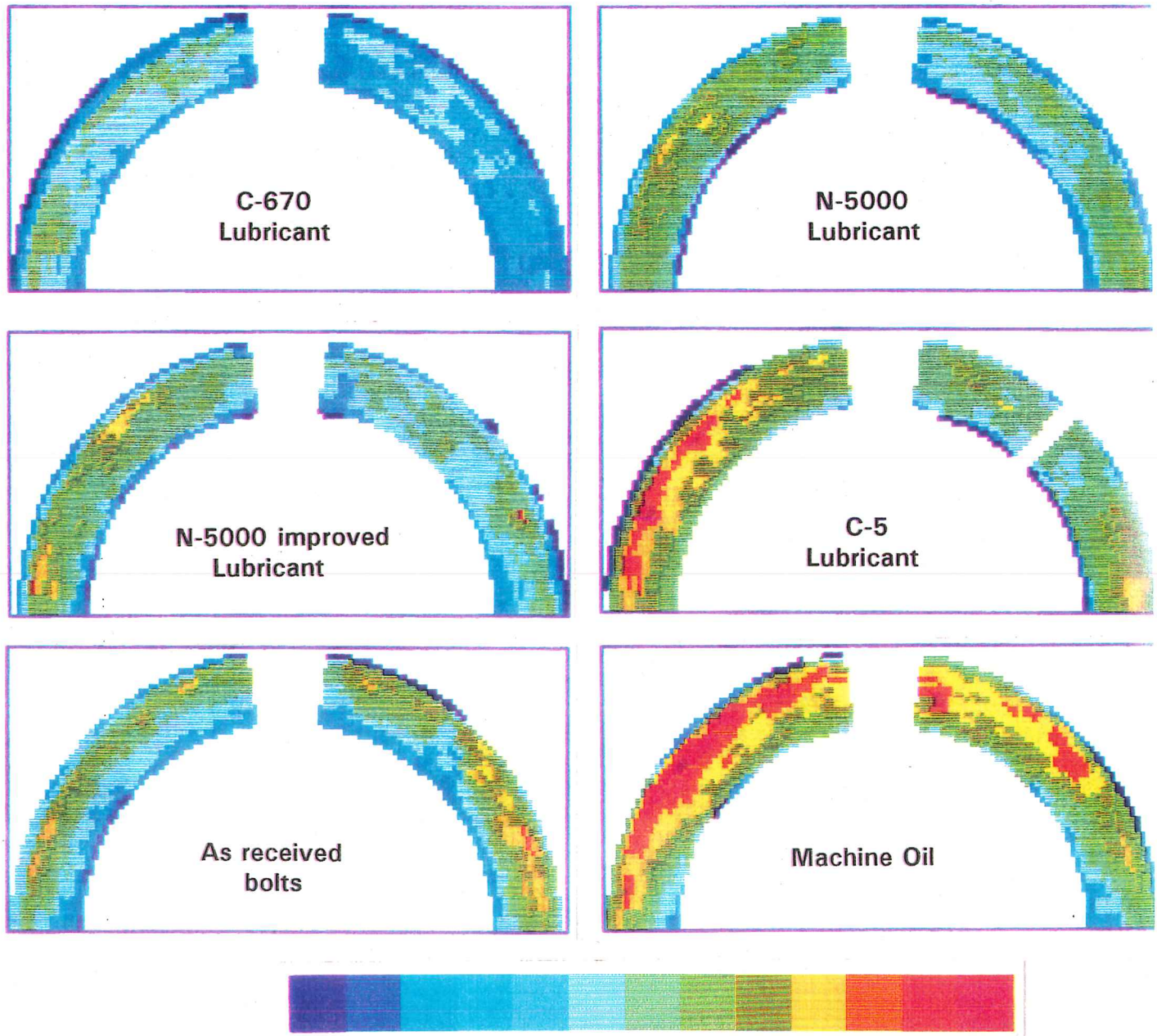

Linear Calibration ksi	0.3	1.5	2.7	3.8	5.0	6.0	7.2	8.3	9.5	10.5	11.7	12.8	14.0	15.0
Non-Linear Calibration, ksi	0.1	1.1	2.5	4.0	6.0	7.8	10.2	12.4	14.9	17.3	20.1	22.9	26.0	28.7

Figure 5.3 Gasket stress distribution at full torque

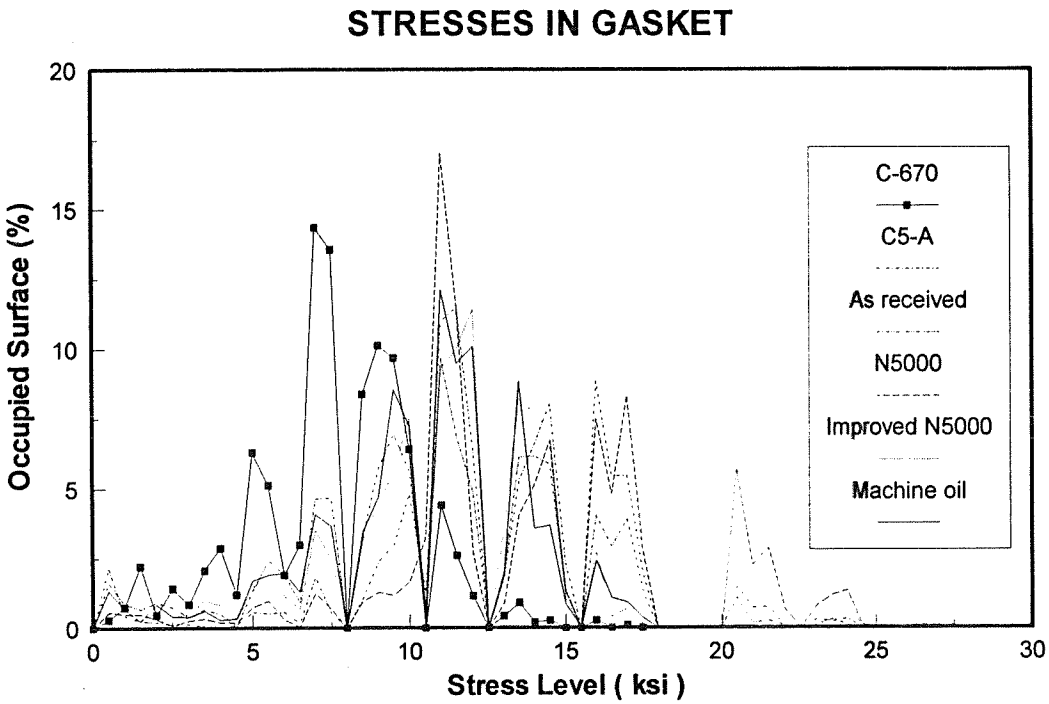

Figure 5.4 Percentage of gasket area vs stress level

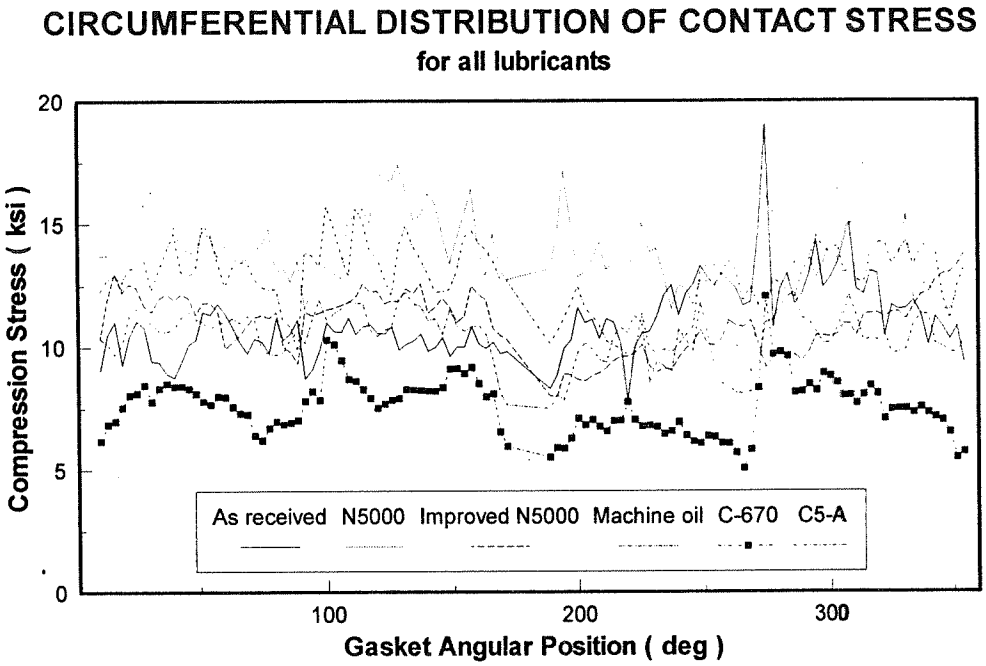

Figure 5.5 Sensor circumferential distribution of stress

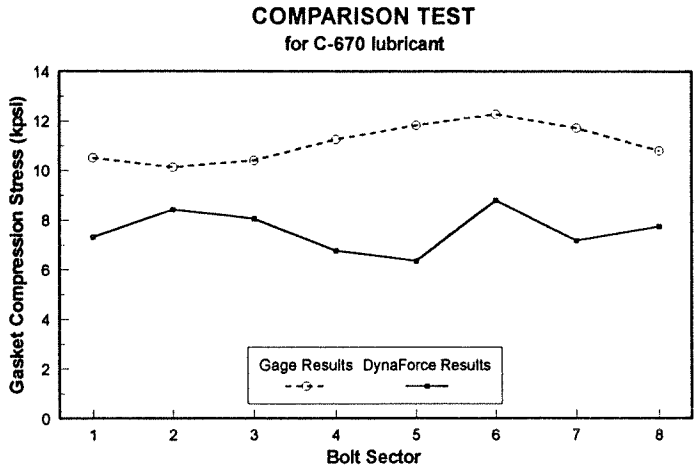

Figure 5.6a Comparison of stresses using C-650 lubricant

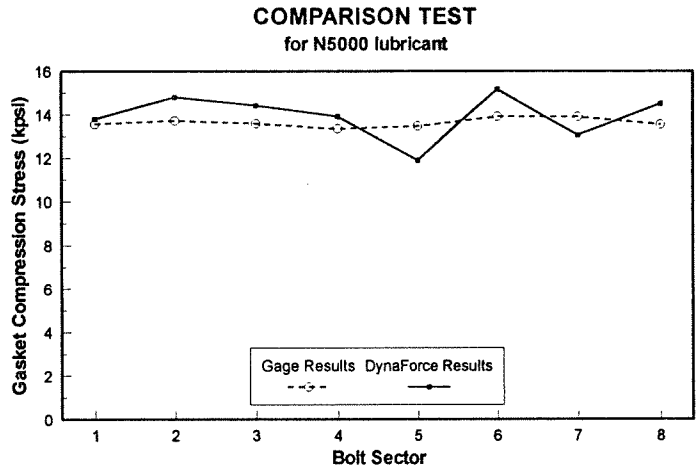

Figure 5.6b Comparison of stresses using N5000 lubricant

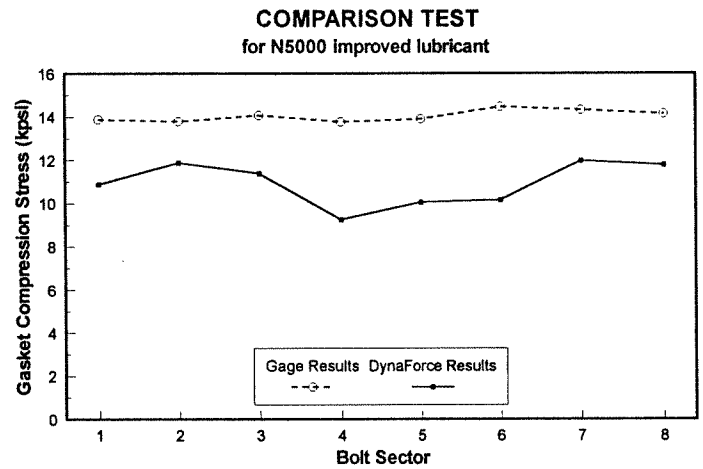

Figure 5.6c Comparison of stresses using Improved N5000 lubricant

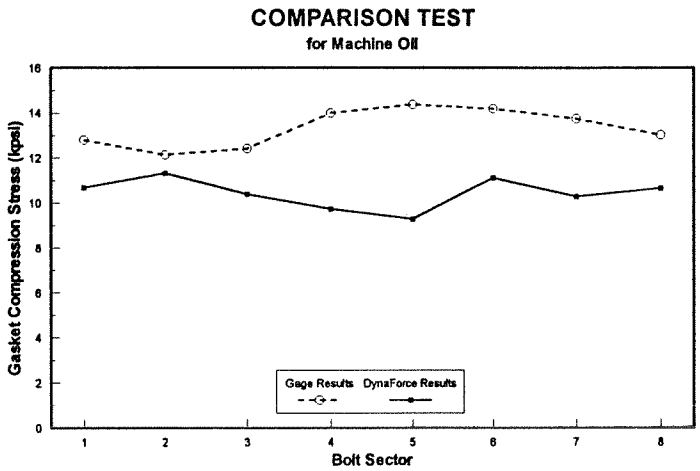

Figure 5.6d Comparison of stresses using Machine oil

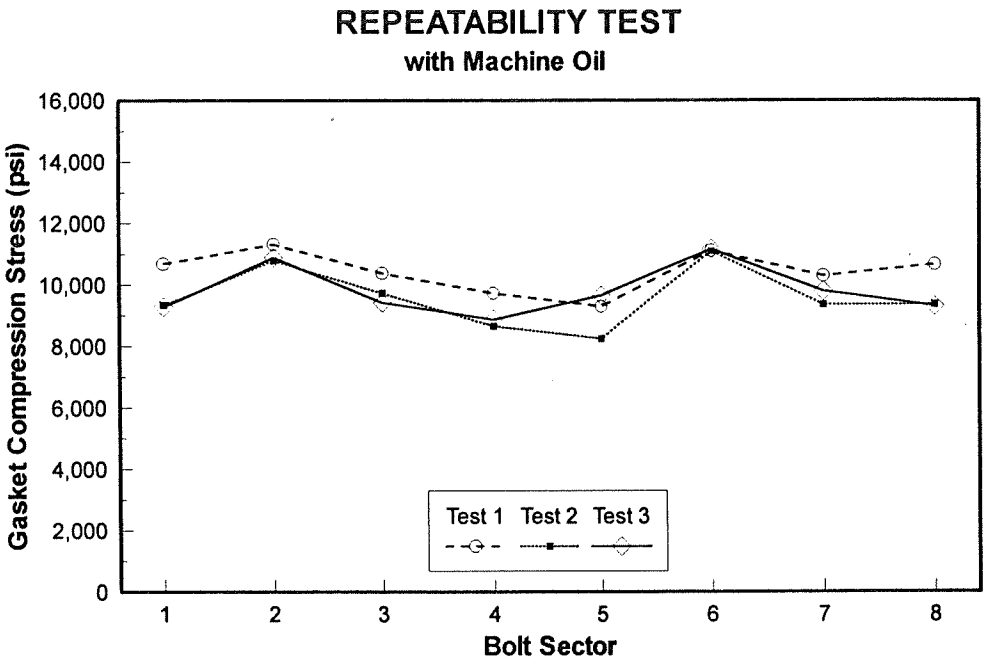

Figure 5.7 Sensor repeatability

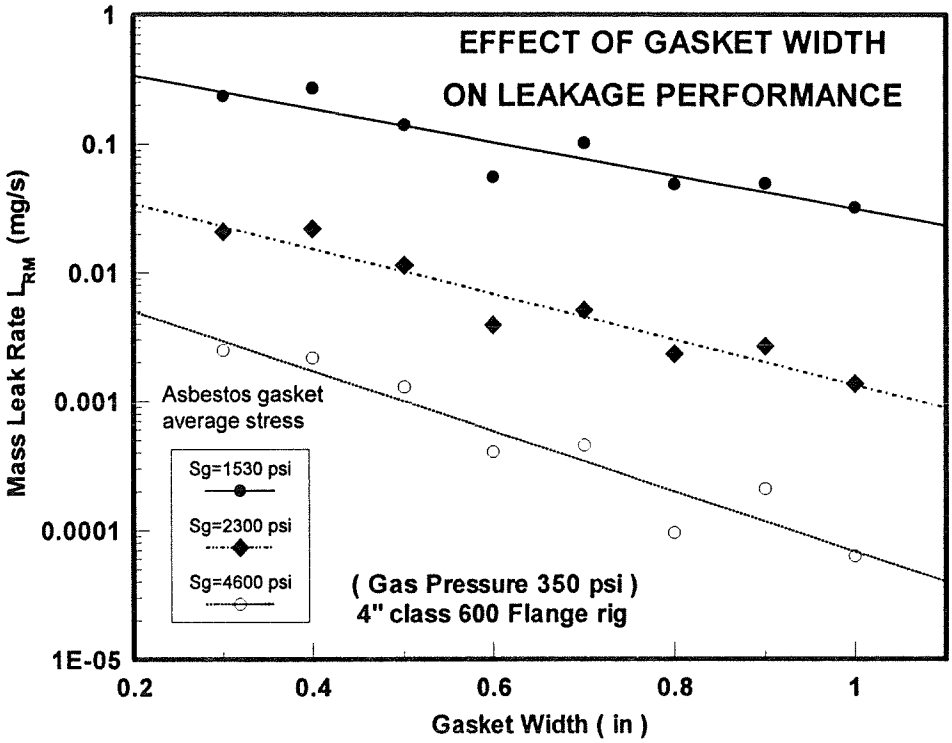

Figure 5.8 Effect of gasket width at constant gasket stress

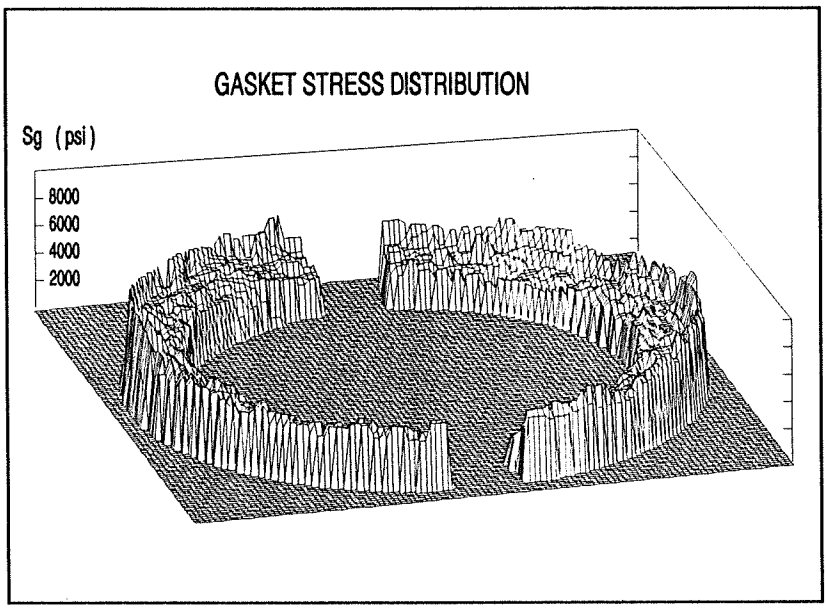

Figure 5.9 Dynaforce measured gasket stress distribution

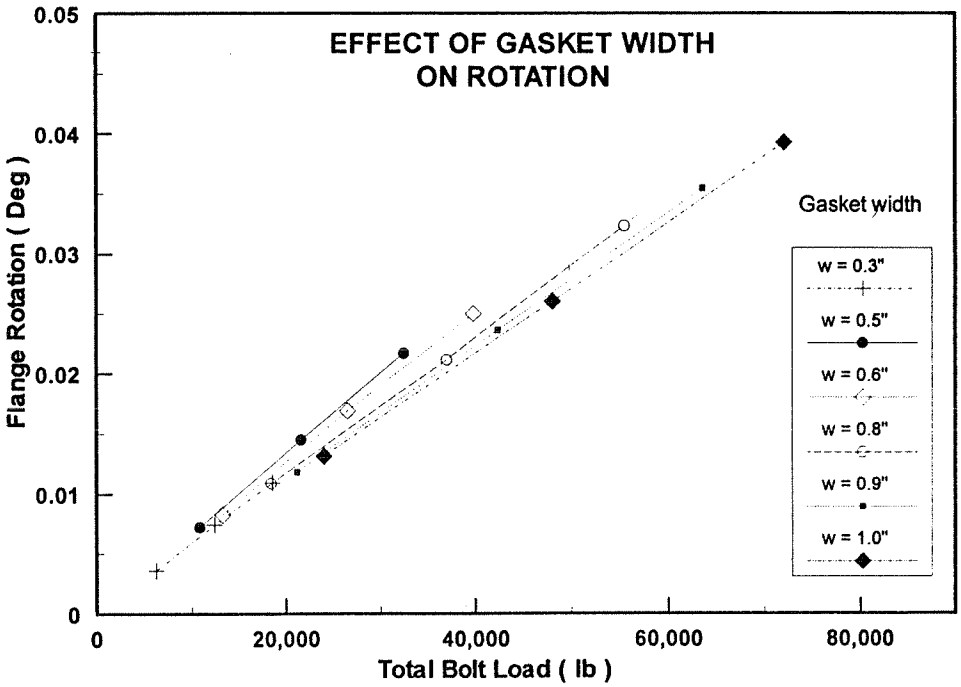

Figure 5.10 Experimentally determined effect of gasket width on rotation

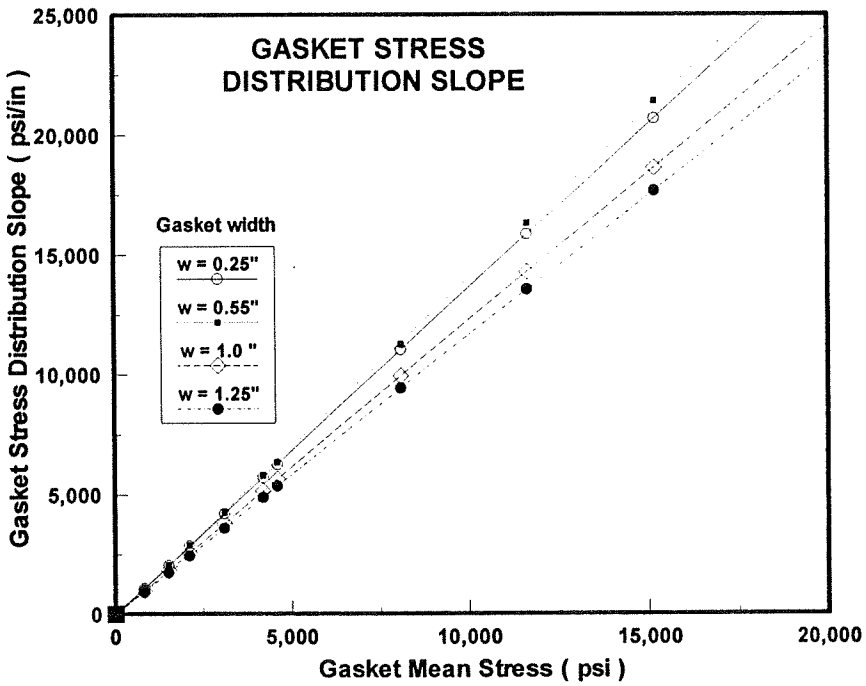

Figure 5.11 Gasket stress distribution slopes

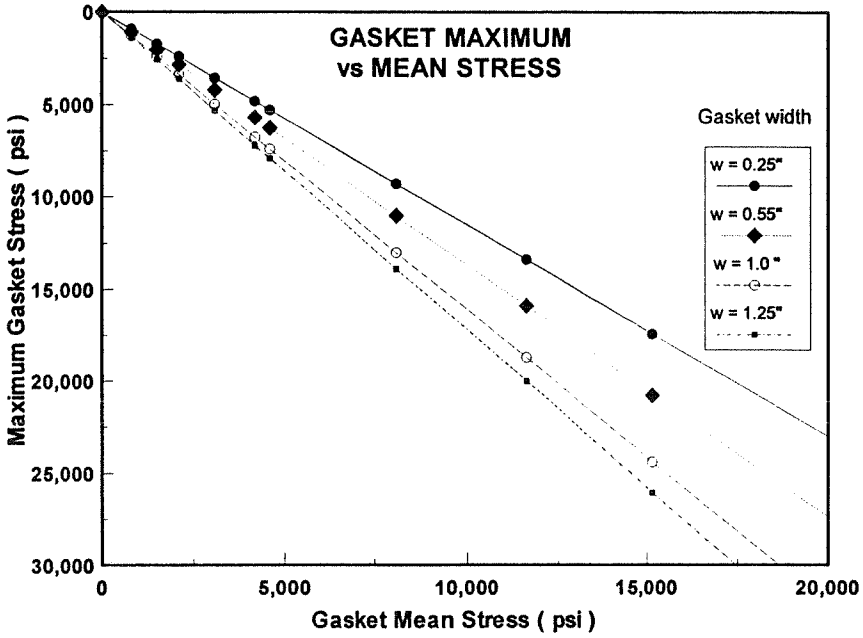

Figure 5.12 Gasket maximum and mean stresses relationship

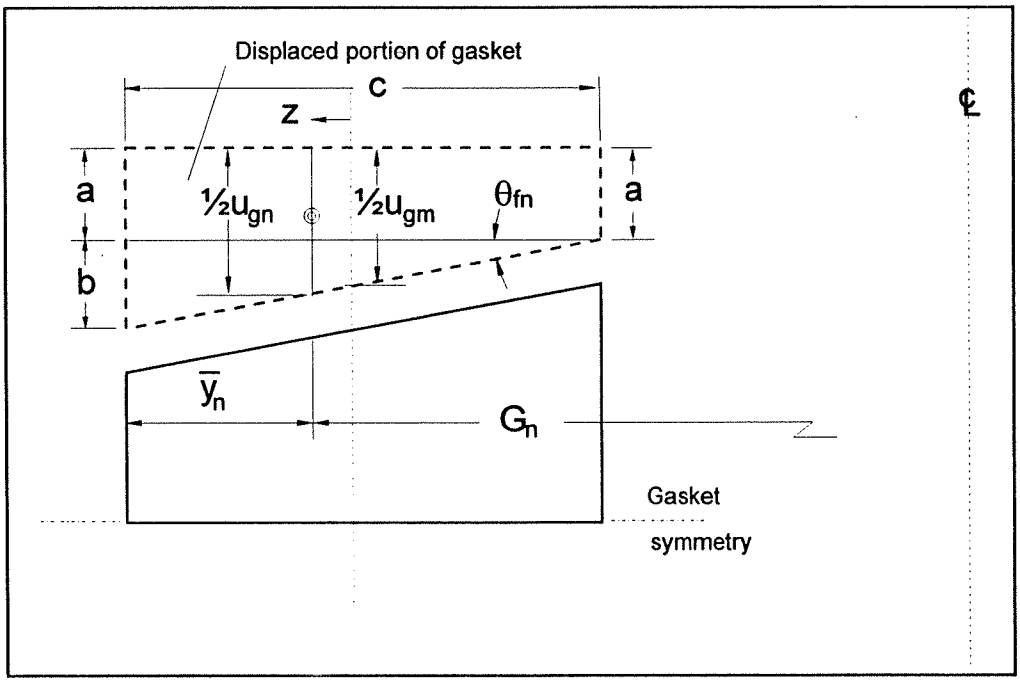

Figure 5.13 Gasket deformation due to flange rotation

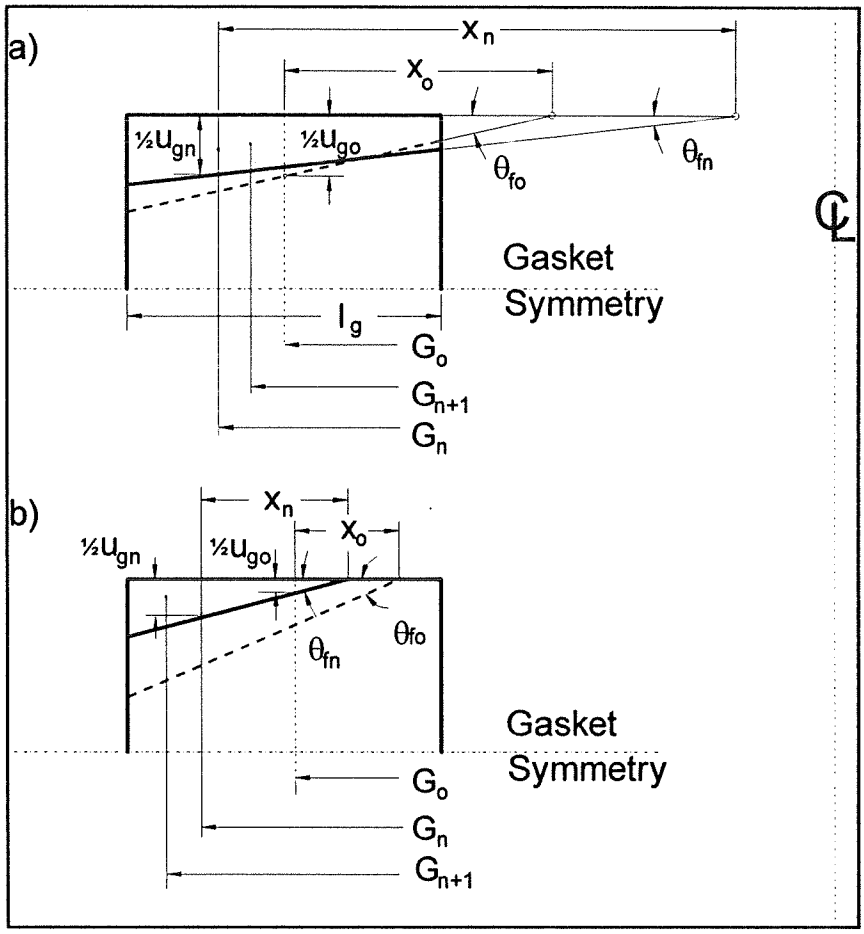

Figure 5.14 Gasket reaction location adjustment after n iterations

a) fully loaded, b) partially loaded

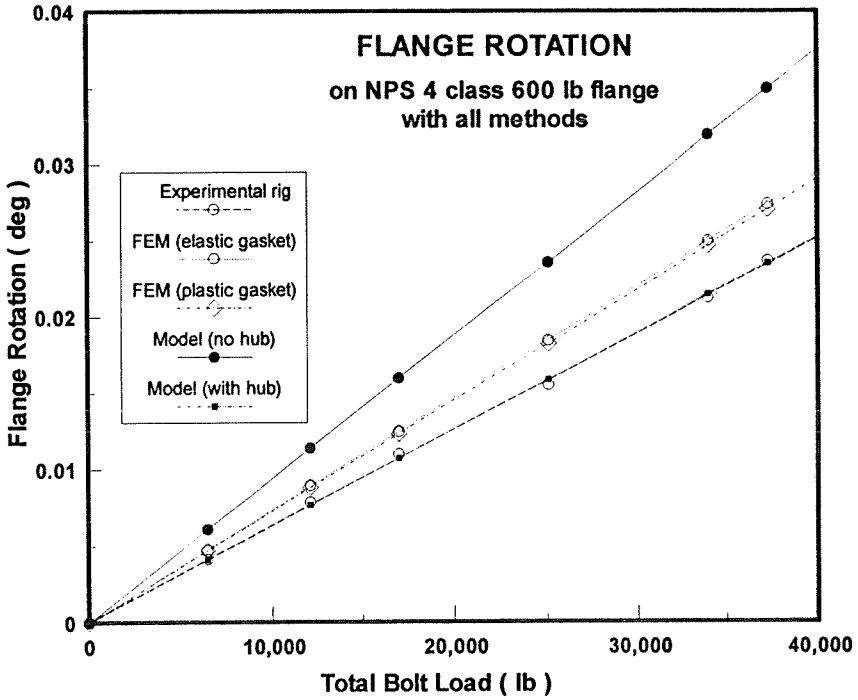

Figure 5.15 Comparison of flange rotations

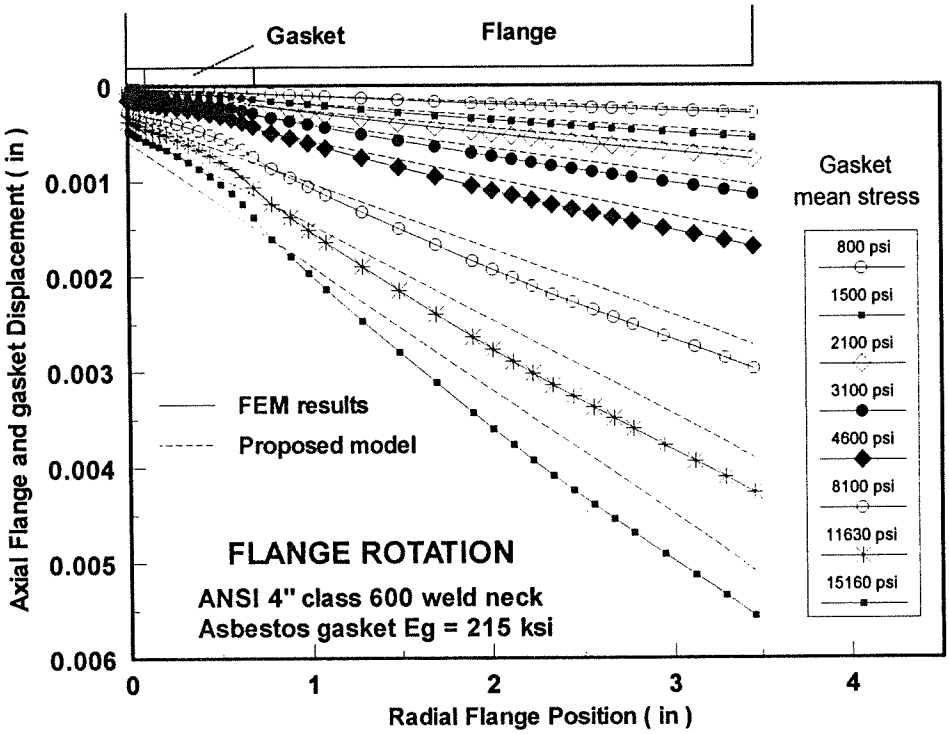

Figure 5.16 Comparison of flange and gasket displacements

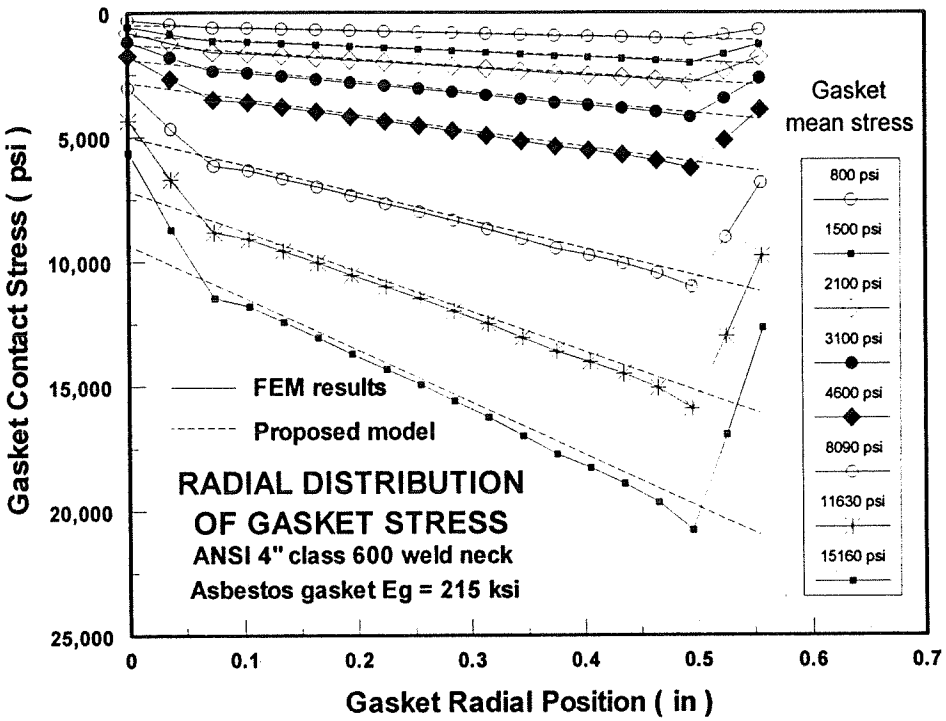

Figure 5.17 Estimating radial distributions of gasket contact stress

CHAPTER 6

A METHOD OF PREDICTING RELAXATION IN BOLTED FLANGED JOINT

6.1 INTRODUCTION

The loss of tightness of bolted flanged joints is primarily due to the relaxation of the joint caused by thermally induced effects. In particular, the clamping load is affected by the amount of relaxation that a gasket exhibits over time. Test methods are available for evaluating the ability of a gasket to maintain a given compressive stress. But in general, it is necessary to evaluate the response of the joint members to a small change in gasket thickness produced by the effects of the difference in thermal dilatation, the creep of the gasket and bolts and in some cases the thermal degradation of the gasket.

Several other factors have been reported to contribute to the relaxation in joints. Some of these factors are vibration, relative movement between flanges of the different mechanical components and pressure effects. Although the approach in considering any of these effects are similar in resolution as will be pointed out later, this chapter will explicitly include a detailed analytical evaluation of the effect of gasket creep relaxation on the remaining gasket stress taking into account the flexibility of all joint members, thus allowing a better evaluation of the required initial tightening load on the gasket. The

results obtained by this approach will be compared to those determined on an experimental rig made up of 4-inch class-600 lb pair of flanges. Axisymmetric finite element models of larger flange assemblies will also be used for comparison. Finally, we will show that the creep relaxation of gaskets has a major influence on the remaining compression load on the gasket.

Many bolted flanged joint calculation methods have been developed, but very few of them are sophisticated enough to take into account most of the parameters involved in long term leak safe design: i.e the influence of relaxation and the overall behavior of bolted flanged joints especially at high temperature. A new method of predicting relaxation produced by temperature induced effects will also be presented.

6.2 METHOD OF ANALYSIS OF THE RELAXATION IN FLANGED JOINTS

The flexibility of the bolts and gasket together with the rotation of the flange, the friction between the gasket and the flange and the effects of relaxation are known to have a strong influence on the final gasket compression stress (Wesstrom and al., 1951, Bouzid and Chaaban, 1993 and Chaaban et al.,1993).

As discussed in Chapter 2, it is currently being proposed to substitute the traditional m and y factors by constants G_b, a and G_s to better characterize gasket

performance so as to introduce leakage tightness considerations in the design of bolted flanged joints. For long term predictions, however, a design approach accounting for the gasket relaxation is necessary.

6.2.1 Analytical Approach

The proposed analytical approach takes into account the flexibility of all the flanged joint members. The model for evaluating the relaxed bolt and gasket loads and hence the gasket stresses is the same as that of Fig. 4.3. First it is necessary to find a relationship between the bolt initial seating load F_b^i or the bolt final operating load F_b^f and the bolt relaxed load F_b^r. This is achieved by looking at the axial geometrical compatibility condition as detailed in Chapter 4. As shown in Fig. 6.1, the displacement of the nut Δ_n at any time is the summation of the individual axial displacement of all joint members; i.e, at initial tightening "i", after final pressurisation "f", and at any given relaxed state, "r". Δ_n is given by the following relationships:

$$\Delta_n = \sum_{e=1}^{4} u_e^i = \sum_{e=1}^{4} u_e^f = \sum_{e=1}^{4} u_e^r = \text{Const.} \tag{6.1}$$

$$\text{i.e.,} \quad \begin{aligned} \Delta_n &= u_g^i + u_b^i + u_p^i + u_f^i \\ &= u_g^f + u_b^f + u_p^f + u_f^f \\ &= u_g^r + u_b^r + u_p^r + u_f^r \end{aligned} \tag{6.2}$$

$$\text{where} \qquad u_e = \frac{F_e}{K_e} \tag{6.3}$$

The expression for the nut displacement Δ_n involves the axial rigidity of all joint members as obtained by linear force-displacement relationships. Index "e" denotes the joint element under consideration and may be the bolt b, the gasket g, the flange f, or the blind cover p. F_e represents the resultant axial force on the joint element. For the symmetrical case of a pair of identical flanges, K_p is replaced by K_f in the analysis.

6.2.2 Gasket Deformation Analysis

Considering the relaxation of the gasket material as illustrated in Fig. 6.2, at a given relaxed position, the resultant gasket relaxation displacement e_r is to be added to the operating gasket displacement u_g^f to give the total relaxed gasket displacement u_g^r:

$$u_g^r = u_g^f + e_r \qquad \text{or} \qquad u_g^r = \frac{F_g^f}{K_g} + e_r \tag{6.4}$$

e_r is the total relaxed displacement due to the effect of difference in thermal dilatation e^t between the gasket, the bolts and the flanges, the creep relaxation e^c of the bolts and gasket and the thermal degradation e^d of the gasket if any, such that:

$$e_r = e^t + e^c + e^d \tag{6.5}$$

6.2.2.1 Deformation Due to Differential Thermal Expansion

The amount of displacement e^t is obtained by analysing the joint members thermal expansion in the axial direction. Due to the difference in their thermal expansion coefficients, the bolt expansion is different from the sum of the expansions of the flange thickness t_f, the gasket thickness t_g and the blind plate cover t_p, thus creating a change in bolt and gasket loads. The analysis is not straight forward because not only the temperature of each joint element is different but a gradient exists within the element itself. However, the analysis may be simplified by considering the bolt, the flange and the end cover subjected to average temperature differences ΔT_b, ΔT_g, ΔT_f and ΔT_p respectively, such that their axial expansions are:

$$
\begin{aligned}
u_g^r &= \frac{F_g^r}{K_g} - \alpha_g \, \Delta T_g \, t_g \\
u_b^r &= \frac{F_b^r}{K_b} + \alpha_b \, \Delta T_b \, l_b \\
u_f^r &= \left(\frac{C-G}{2}\right) \theta_f^r - \alpha_f \, \Delta T_f \, t_f \\
u_p^r &= u_p(F_g^r) - u_p(F_b^r) + u_p(p) - \alpha_p \, \Delta T_p \, t_p
\end{aligned}
\qquad (6.6)
$$

The displacement of the gasket due to the difference in thermal expansion may therefore be obtained from Eqs. (6.5) and (6.6) as:

$$
e^t = \alpha_b \, \Delta T_b \, l_b - (\alpha_g \, \Delta T_g \, t_g + \alpha_f \, \Delta T_f \, t_f + \alpha_p \, \Delta T_p \, t_p) \qquad (6.7)
$$

6.2.2.2 Deformation Due to Thermal Degradation

The change in gasket thickness e^d is that due to the degradation of the gasket material. The thermal exposure of certain types of gaskets (fibres reinforced elastomer based sheet materials, flexible graphite sheets) provoke an aging mechanism that results in a change in their physical properties. Marchand et al. (1992) have established a correlation of the weight loss for sheet gasket materials with time and temperature of exposure and have successfully combined the two effects in a single time-temperature equation using as reference a 48-hour exposure time:

$$w = -\left(\frac{t}{48}\right)^{d} \frac{m_w}{1/T_0 - 1/T} \tag{6.8}$$

m_w slope of curve w_{48} versus $1/T$

t is the exposure time, hr

T is the exposure absolute temperature, °K and

T_0 is the intercept temperature at $w=0$, °K

w is the fraction of the weight loss

Equation (6.8) leads conveniently to the definition of an aging parameter A_p based on the weight-loss correlation such that:

$$A_p \equiv \frac{w}{m_w\ (48^{0.6}/100)} \tag{6.9}$$

In his work, Marchand (1992) has measured the relaxation of the gasket due to aging in terms of the thickness change e^d and has found that the relationship with the aging parameter A_p is particular for every joint type. He also found that after a weight loss of about 15%, the gasket creep increases with the additional weight loss.

6.2.2.3 Deformation Due to Creep

In a real bolted gasketed joint, three phenomena occurs simultaneously: creep, relaxation and strain recovery. In fact, as the creep takes place the stress in the gasket drops instantaneously causing not only the gasket to relax but also some instantaneous strain recovery. Pure relaxation is also a time dependent phenomenon observed when the strain is held fixed, however the type of relaxation that is sometimes referred to in the literature on bolted joints is the drop of gasket stress that is caused by the creep only. In what follows only the relaxation due to creep will be considered and therefore both pure relaxation and strain recovery phenomena are not covered and will be ignored.

In a pure creep test, the relationship between gasket creep and time is of logarithmic nature as found by Bazergui, 1984. The gasket creep curve is strongly influenced by the compression stress and temperature as it is the case with metals. Even at constant ambient temperature, the influence of stress is quite important, particularly for PTFE-based material gaskets. The temperature has the effect of accelerating the creep phenomenon. Therefore, its influence at constant stress has a similar effect.

In a bolted joint, the displacement of the gasket e^c cannot be considered to be equivalent to the one obtained from either a pure creep nor a pure relaxation tests but rather from a combined test since it is a function of both. To demonstrate the merits of the developed method, the only resulting effect e_r that will be considered further is the combined effect of creep relaxation e^c. As in a pure creep situation, the relaxed displacement due to this effect is also a function of stress S_g, temperature T and time t:

$$e^c = f (S_g, t, T) \tag{6.10}$$

Therefore, after substitution of Eq. (6.4) into the expression of the nut displacement, Eq. (6.2) may be rearranged to give:

$$u_b^f + u_p^f + u_f^f = u_b^r + u_p^r + u_f^r + e_r \tag{6.11}$$

For the particular case of a pair of identical flanges, u_p is replaced by u_f in Eq. (6.11). The relative axial displacement of the flange u_f at the bolt circle diameter position may be found by considering rigid rotation of the flange such that :

$$u_f = \frac{(C-G)}{2} \theta_f \tag{6.12}$$

and $\therefore$ $$\frac{F_b^f}{K_b} + (C-G)\, \theta_f^f = \frac{F_b^r}{K_b} + (C-G)\, \theta_f^r + e_r \tag{6.13}$$

This states that, in a particular bolted joint, for a given amount of creep displacement e_r, the bolt and gasket residual loads are independent of the type of gasket used. However, the amount of creep displacement will depend on the gasket type, the temperature, the time and the gasket compression stress.

Equation (6.13) requires a proper evaluation of the flange rotation as it is a quantity that is directly related to the flange rigidity; its value greatly depends upon the type of flange used. For the case of a weld-neck type of flange, the hub which has the effect of stiffening the flange and not represented in Fig. 6.1, has a great influence on the final results as will be demonstrated. For the purpose of simplicity and understanding of the method used, a theoretical approach applicable to slip-on type flanges will be detailed further below. Nevertheless, the program "POLYFLG" which includes an accurate analysis of the hub, is capable of handling relaxation in weld-neck type flanges.

6.2.3 Simplified Method of Relaxation in Joints

Because of its variable thickness, the solution of the radial displacement of the hub must be found in terms of Bessel functions, and involves four constants of integration requiring four simultaneous equations. To reduce the amount of work involved necessary to solve the system of equation it is desirable to make some simplifying assumption so that the evaluation of the bolt loss due to relaxation does not become prohibitive.

6.2.3.1 Analysis of Ring Type Flanges

Considering the cylindrical part of the assembly, the shell end is subjected to the discontinuity edge moment M_0 and shear force P_0 per unit circumference. The radial displacement w_c and slope θ_c at the junction are given by the theory of a "beam on elastic foundation" (see Eqs. (4.7) and (4.8)):

$$w_c = \frac{6(1-\nu_c^2)P_0}{E_c t_c^3 \beta_c^3} - \frac{6(1-\nu_c^2)M_0}{E_c t_c^3 \beta_c^2} \tag{6.14}$$

and

$$\theta_c = \frac{12(1-\nu_c^2)M_0}{E_c t_c^3 \beta_c} - \frac{6(1-\nu_c^2)P_0}{E_c t_c^3 \beta_c^2} \tag{6.15}$$

The radial displacement at the cylinder to the flange junction w_c, may be considered to be zero as in the Taylor Forge analysis (Waters et al., 1979). Bearing in mind that for large diameter flanges, this may not necessarily be true (Murray and Stuart, 1961), the analysis is nevertheless simplified to give a direct relationship between the discontinuity edge moment M_0 and shear force P_0 such that:

$$M_0 = \frac{P_0}{\beta_c} \tag{6.16}$$

The flange rotation θ_f, which is equal to the cylinder rotation θ_c due to geometrical compatibility, may be obtained from the theory of a circular plate with a central hole subjected to an equivalent circumferential twisting couple M_f located at the inside and outside diameters of the flange (see Eq. (4.21)):

$$\theta_f = \frac{B\pi Y M_f}{E_f t_f^3} \tag{6.17}$$

Referring to Eq. (6.17), Y is the ASME Code factor that involves K and which may conveniently be simplified as 6 / π LnK by considering the ring bending theory (Eq. (6.4)). Also, the flange equivalent twisting couple M_f can be obtained from considering the equilibrium about the flange centroid such that:

$$M_f = -\frac{B}{D_0} M_0 - \frac{Bt_f}{2D_0} P_0 + \frac{(C-G)}{2\pi D_0} F_b \tag{6.18}$$

Finally, by combining Eqs. (6.15), (6.16), (6.17) and (6.18), an expression for the rotation of the flange θ_f may be obtained such that:

$$\theta_f = \frac{3\,(C-G)\,F_b}{\pi \left[E_f t_f^3\, LnK + \frac{E_c t_c^3\, B\, \beta_c}{1-\nu_c^2} \left(1 + \beta_c \frac{t_f}{2}\right) \right]} \tag{6.19}$$

Using Eqs. (6.12) and (6.19), the axial rigidity of the flange may be obtained:

$$K_f = \frac{F_b}{u_f} = \frac{2\,\pi}{3(C-G)^2} \left[E_f t_f^3\, LnK + \frac{E_c t_c^3\, B\, \beta_c}{1-\nu_c^2} \left(1 + \beta_c \frac{t_f}{2}\right) \right] \tag{6.20}$$

Using Eq. (6.12), and bearing in mind that the flange axial displacement u_f is related to the bolt force F_b by the axial flange rigidity K_f, then Eq. (6.13) may be rearranged to give the relaxed bolt load as:

$$F_b^r = F_b^f - \frac{e_r}{\left[\frac{1}{K_b} + \frac{2}{K_f}\right]} \qquad \text{or} \qquad F_b^r = F_b^f - K_j\, e_r \tag{6.21}$$

where K_j is the joint axial rigidity obtained by considering the combination in series of the pair of identical flanges and the bolts such that:

$$\frac{1}{K_j} = \frac{2}{K_f} + \frac{1}{K_b} \tag{6.22}$$

and for the bolts, the rigidity K_b is simply:

$$K_b = \frac{E_b\, A_b}{l_b} \tag{6.23}$$

Provided the pure creep displacement of the gasket e_r may be put into equation as proposed by Bazergui (1984), the bolt load and hence the gasket stress can be found. As a direct result, the evolution of leakage with time becomes a predictable parameter which is very useful for maintenance purposes. An interesting feature resulting from the analysis is that the force relaxation in the bolts is strongly related to the gasket relaxed displacement e_r. In fact, a linear relationship between the two quantities exists and the resulting slope is the rigidity of the flange including the bolts.

6.2.3.2 Analysis of Weld-Neck Type Flange

For weld-neck type flanges, it is suggested that the actual taper hub construction be replaced, for calculation purposes, by an equivalent shell of uniform thickness. As the bending moment and shearing forces, M_0 and P_0, have a minor effect at a distance of $\sqrt{0.5\ Bg_1}$ from the flange to hub junction, then the hub may be considered equivalent to a cylinder with an equivalent thickness (Lake and Boyd, 1957) such that:

$$t_e = t_c + \frac{x\ (g_1 - t_c)}{2\ \sqrt{0.5\ Bg_1}} \qquad \text{for hub lenth } x < \sqrt{0.5Bg_1} \tag{6.24}$$

$$t_e = 0.5\ (t_c + g_1) \qquad \text{for hub lenth } x > \sqrt{0.5Bg_1} \tag{6.25}$$

6.3 APPLICATION OF RELAXATION DUE TO CREEP OF GASKETS

6.3.1 Mathematical Modeling of Creep Relaxation of Gaskets

The formulation of the problem of creep relaxation of gaskets is not straight forward. Since every material has a its own creep behavior, it is not possible to come out with a creep model that can represent all types of gasket materials. Creep tests have to

be done on every material in order to be able to predict the relaxation of the gasket with time. In general the creep curves, as the ones shown in Fig. 6.3 suggest that the creep strain is a function of stress S_g, temperature T and time t:

$$\varepsilon_c = F (S_g, T, t) \tag{6.26}$$

Bazergui (1984), in his paper on short term creep of gaskets at room temperature showed that, for most types of non-metallic and metal composite gasket, a linear relationship exits between the displacement due to creep and the time in a semi-logarithmic plot. An adequate representation is therefore:

$$e_{cp} = a + b \, Ln \, t \tag{6.27}$$

where e_{cp} is the gasket thickness change that occurs during a period of time t where as a and b are coefficients that depend on the gasket stress level.

Starting from Eq. (6.27), we can assume that for a relatively small period of time the relaxation that takes place in a joint is due to a small amount of gasket creep e_{cp} produced under a constant gasket load. At the end of this small period of time, the gasket load is readjusted to be used for calculations of e_{cp} in the next time interval. By adding successive creep displacements obtained under different decreasing stresses, the appropriate amount of gasket creep relaxation displacement is obtained for the time considered. The whole process is referred to in Fig. 6.4.

Starting with a stress S_{g1} on the gasket, after a small period of time, the corresponding creep due to this assumed constant stress, is $e_{cp1} = e_c = e_r$. With this relaxed displacement e_r, the new gasket stress S_{g2} is calculated for evaluating the new creep displacement e_{cp2} obtained after another small period of time. The new total relaxed displacement $e_r = e_{cp1} + e_{cp2}$ is then used to recalculate the new gasket stress S_{g3} and so forth. This algorithm is coded into a subroutine of the POLYFLG program and the detailed flow chart is given in Appendix III.

6.4 RESULTS AND DISCUSSION

From the creep relaxation displacements curves of Fig. 6.5 obtained experimentally on the NPS 4 class-600-lb rig, it appears that the general trend of the relaxation behavior of the gaskets tested on a real bolted joint is similar to the pure creep situation and, a logarithmic time dependency is also observed. The creep relaxation equation can therefore be written as:

$$e_r = e_c = a' + b' \text{ Ln } t \tag{6.28}$$

where e_r is the gasket relaxed deflection; in.

e_c is the gasket relaxed deflection due to creep only; in.

a' and b' are coefficients as function of stress level and gasket material and

t is the time in sec.

Figure 6.6 shows the relaxation of the gasket load for different types of gaskets as obtained from the bolted flange rig and the analytical model. Although, the initial tightening load is different in some cases, it can be seen that the relaxation is function of the gasket material and thickness. For material 'A' 1/8" (3.2 mm) thick, more than 30% of the gasket initial load is relaxed in less than four hours. The gasket load variation with time as obtained from the experimental results compare quite well with the ones obtained with the proposed model. As an example, for material 'A' 1/8" (3.2 mm) thick gasket, the computed relaxation load curve is very close to the experimental curve, i.e. less that 2% error; and thus, an accurate prediction of the load with time is demonstrated.

Table 6.1 contains a summary of the results of rigidity calculations some of which are derived from the slopes of Figs. 6.7 and 6.8. Three types of flanges are considered, two of which are ANSI B16.5 types of flanges, namely NPS 3 class-150 lb and NPS 4 class-600 lb, while the last flange is an example of a large diameter type, same as in Waters et al. (1937). The results show that a good agreement exists between the different methods. The rather high rigidities obtained by FEM is due to the fact that gasket load is obtained from the calculated average nodal gasket stresses rather than the nodal gasket forces which are not available with the creep option in the ABAQUS program. From Fig. 6.7, it can be shown that the slopes of the curves which represent the axial joint rigidity, have all the same value and are neither dependent of the gasket material nor of the amount of bolt initial load. Therefore, there is a good agreement between the three values

obtained experimentally, by FEM and by the analytical approach.

Figure 6.9 shows the variation of the flange rotation as the gasket relaxes. This is an indirect representation of the uniaxial flange rigidity provided the flange rotation with load is known. The computed values of rotations are somewhat higher because the point of application of the gasket load was assumed to act at the mid-gasket location. However, as pointed out previously, flange rotation causes a non-uniform gasket stress distribution which shifts the location of the gasket reaction.

The stiffness of joints has long been suspected as playing a major role in creep relaxation behavior of gaskets. In fact, the joint stiffness which depends mainly on the flanges and bolts rigidities has a great influence on the relaxation of the bolt and gasket loads. Fig. 6.10 shows the tests performed on a UGR rig which can be adjusted to the required stiffness value so as to simulate the behavior of a specific joint. As an example, tests simulating a NPS 4 slip-on and welding-neck flanges of the same 150 class show this strong influence clearly. The joint stiffness dependence has been demonstrated analytically in Eq. (6.21) which shows the linear interdependency between the bolt load and the joint stiffness K_j. Therefore, increasing joint flexibility by extending the bolts, introducing "Belleville" washers or making the flanges lighter is one way of reducing the effect of relaxation. An alternative solution is, however, the introduction of a metallic spacer which controls the gasket displacement due to creep. Also, from the same Fig. 6.10, good agreement between the results obtained by the analytical model and the

simulating joint rig, is demonstrated.

Experience in the field of pressure vessels still shows that some bolted gasketed joints are difficult to seal, and that leakage appears some time after start-up. The approach to relaxation presented in this chapter has produced results which compare reasonably well with actual tests carried out on a real bolted flange joint. The evolution of the residual bolt and gasket loads with time together with the resulting deflections and rotations can therefore be predicted. The proposed model has potential for becoming a design tool for leakage prediction.

Table 6.1 Flange axial rigidities

	NPS 3 class 150	NPS 4 class 600	Large Flange A=127 B=120¼
Experimental results (lb/in)	$4.65\ 10^6$	$9.51\ 10^6$	N/A
FEM method (lb/in)	N/A	$11.5\ 10^6$	$878.47\ 10^6$
Equation (6.20), (lb/in)	$4.71\ 10^6$	$9.14\ 10^6$	$600.8\ 10^6$
POLYFLG, (lb/in)	$4.63\ 10^6$	$10.3\ 10^6$	$703.8\ 10^6$

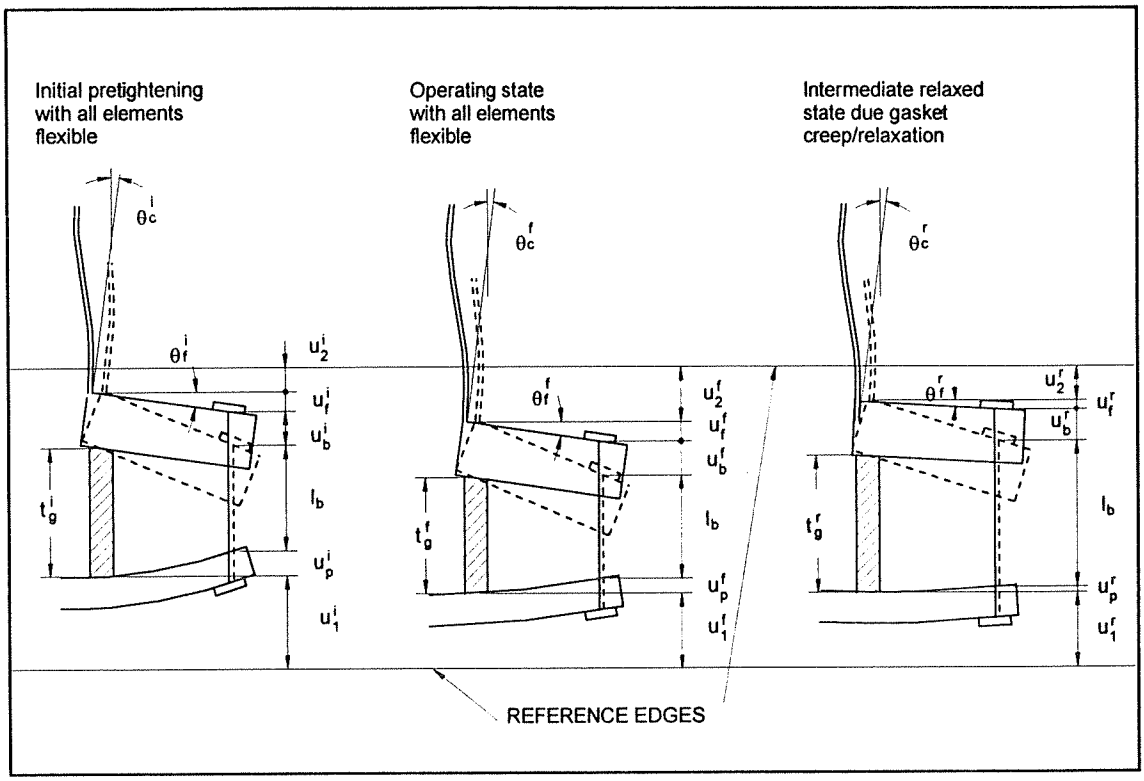

$$l_b + \Delta_e = l_b + u_b^i + u_1^i + u_2^i + u_f^i + u_p^i = l_b + u_b^r + u_1^r + u_2^r + u_f^r + u_p^r$$

$$\text{or} \quad u_1^i + u_2^i = u_g^i \quad \text{and} \quad u_1^r + u_2^r = u_g^r$$

$$\text{then} \quad \Delta_n = u_b^i + u_g^i + u_f^i + u_p^i = u_b^r + u_g^r + u_f^r + u_p^r$$

Figure 6.1 Modeling of the joint relaxation

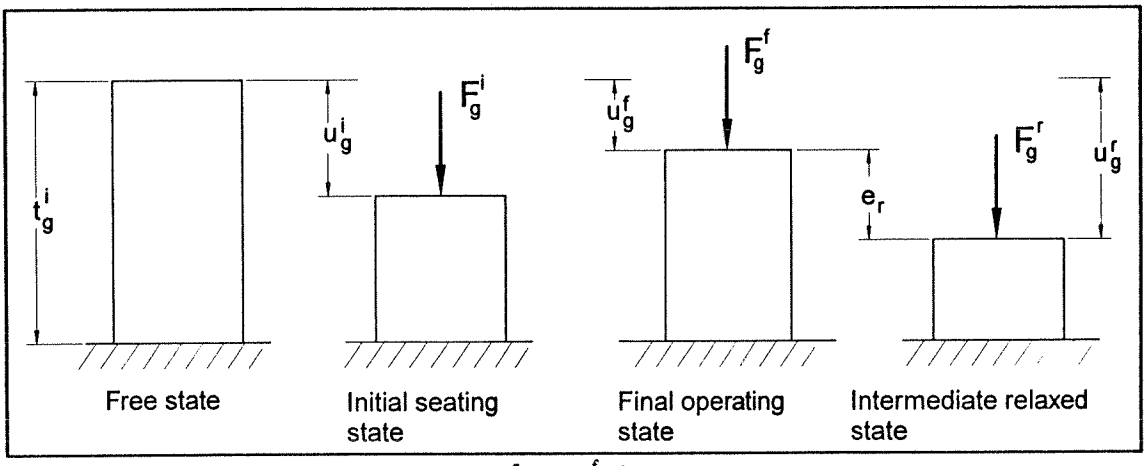

$$u_g^r = u_g^f + e_r$$

Figure 6.2 Different stages of gasket displacement

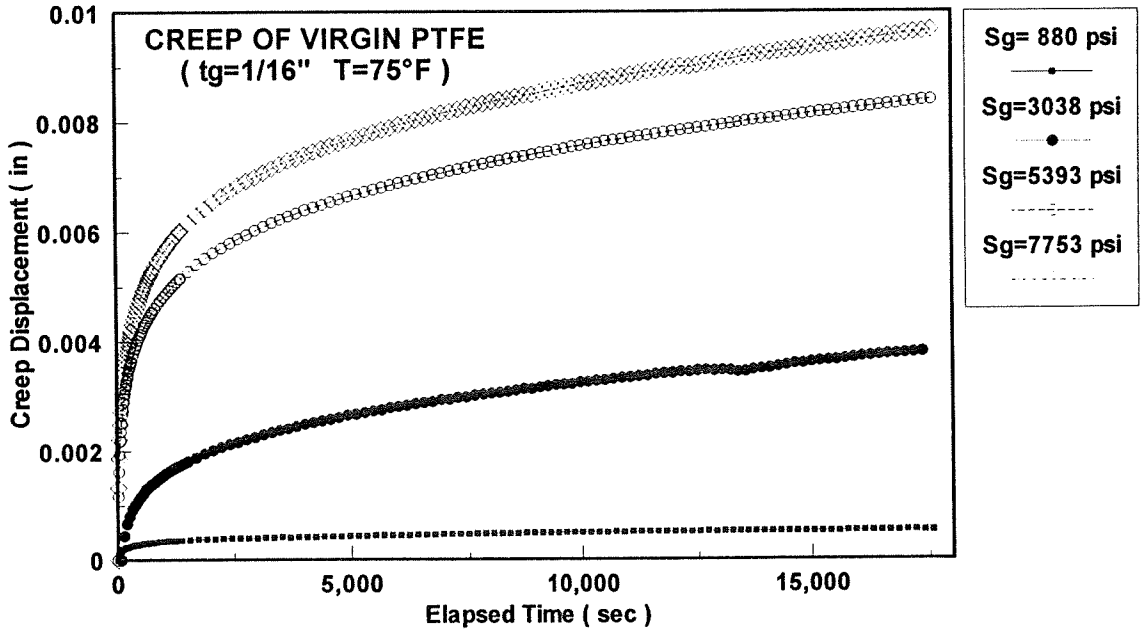

Figure 6.3 Pure creep of PTFE virgin gasket type material

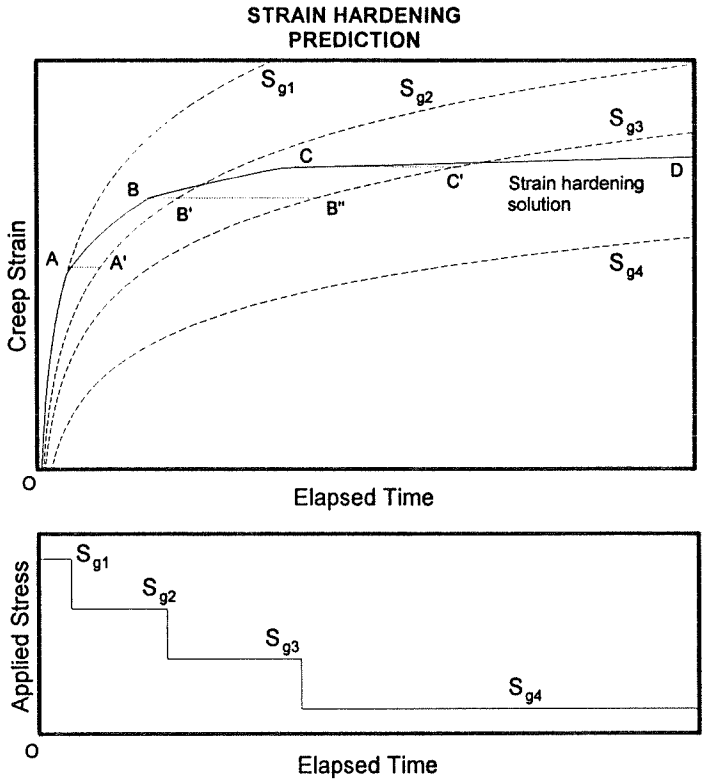

Figure 6.4 Modeling of creep relaxation

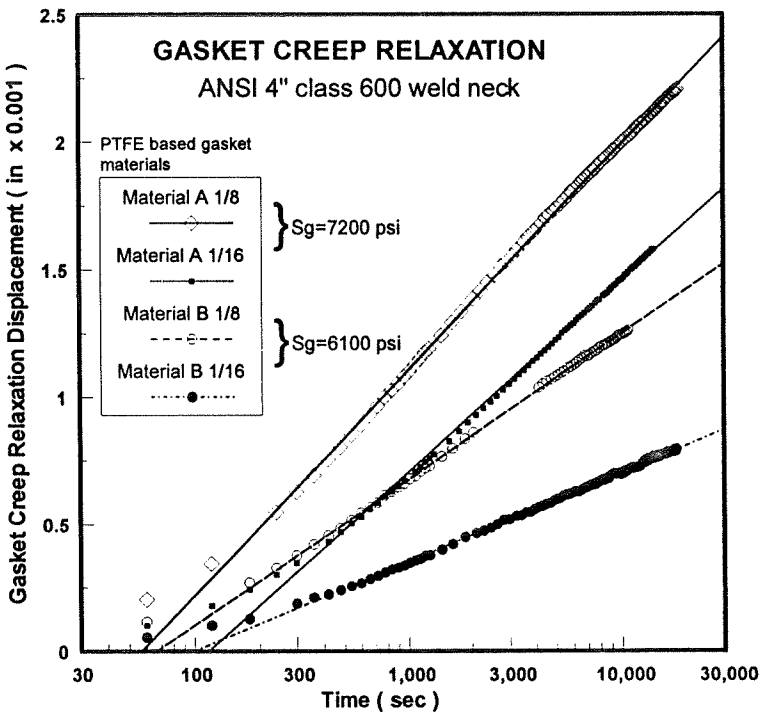

Figure 6.5 Gasket creep relaxation

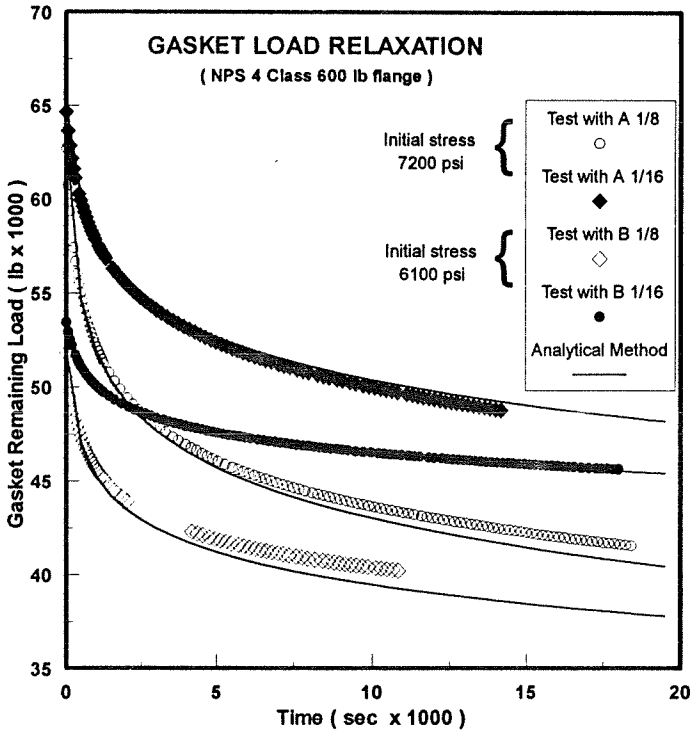

Figure 6.6 Gasket load relaxation with time

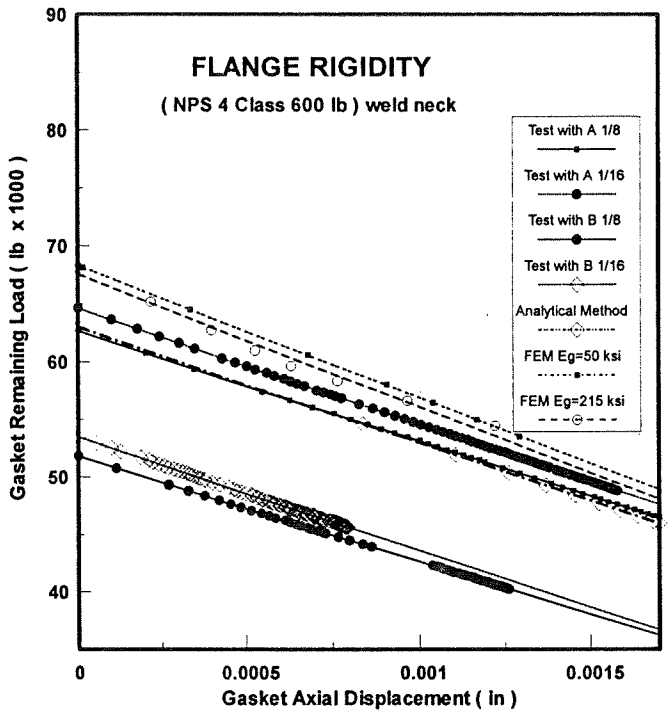

Figure 6.7 Joint gasket load-displacement relation

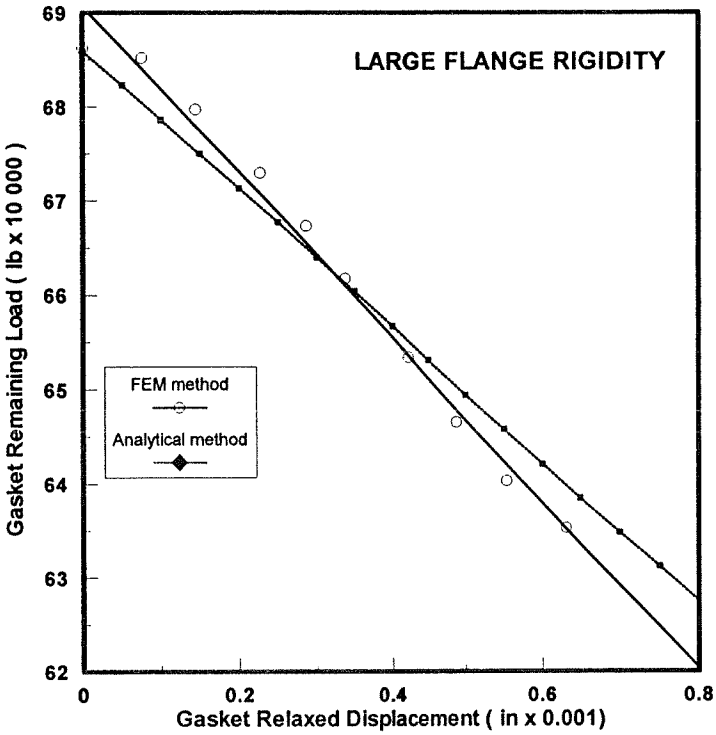

Figure 6.8 Case of large flange
A=127", B=120 ¼", t_c=⅝", t_f=$^{15}/_{16}$", g_1=1⅛" and x=3⅛"

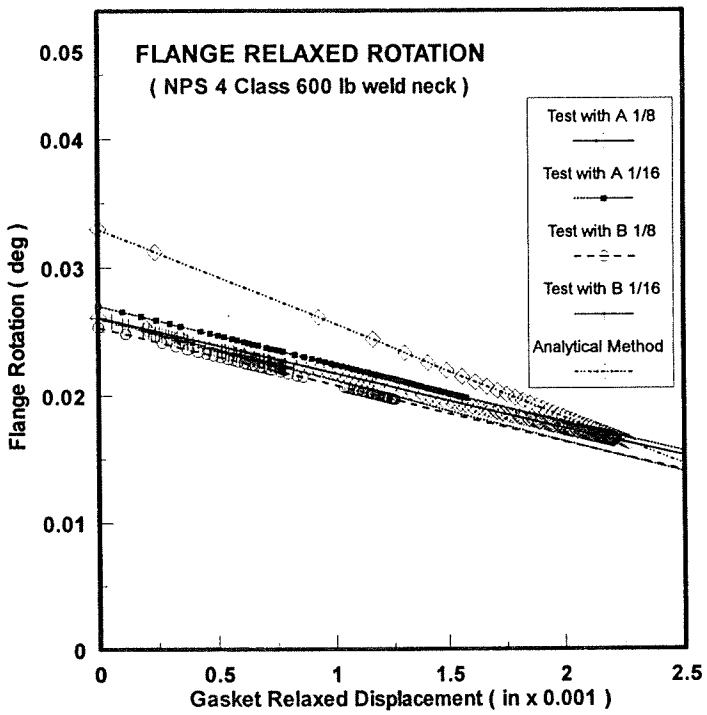

Figure 6.9 Flage rotation due to relaxation

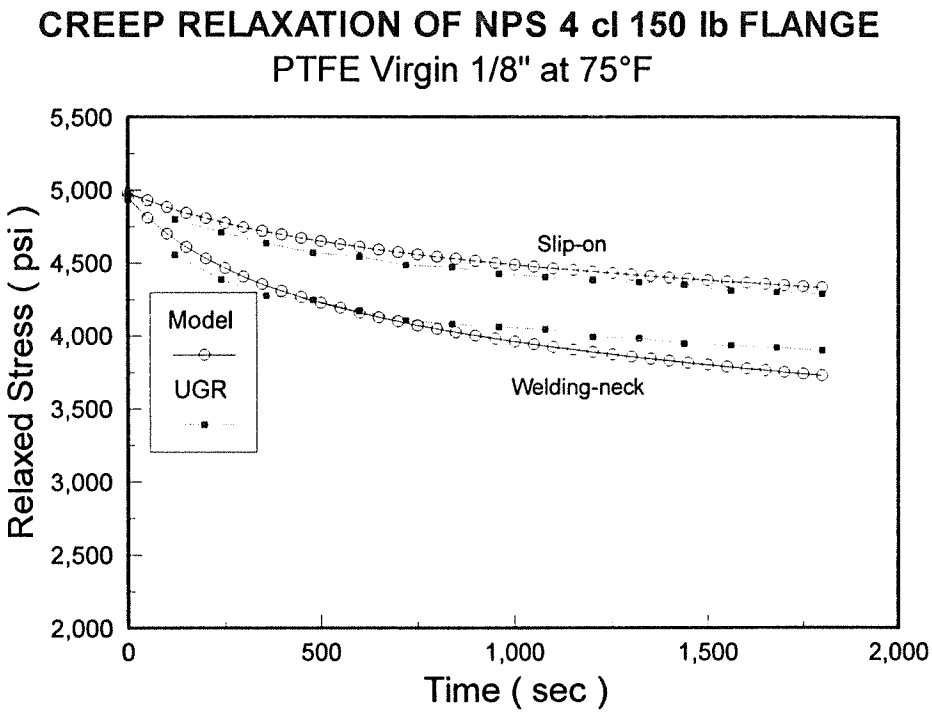

Figure 6.10 Effect of flange rigidity

CHAPTER 7

CONCLUSIONS AND RECOMMENDATIONS

7.1 GENERAL FINDINGS

An accurate approach to the design of bolted flanged gasketed joint has been developed. This approach considers an analytical joint model that includes the flexibility of all joint members in both the axial and radial directions and is based on the elastic interaction between them. The proposed method is capable of examining joint structural integrity, as well as leak tightness and their evolution with time. Numerical results have been presented which show the effect of gasket pre-strain, and flange and bolt flexibilities on the final configuration. A simplified approach of gasket modeling has led us to establish the radial distribution of gasket contact stress. A method is proposed for simulating relaxation in gasketed joints due to thermally induced effects as well as relaxation caused by gasket creep. The influence of joint rigidity on the gasket and bolt relaxations observed experimentally is demonstrated by the simple analytical model using a time hardening law to evaluate the gasket creep occurring in a joint.

The method presented in this thesis provides a formulation consistent with the general philosophy of the ASME Code, allowing an accurate and comprehensive design and evaluation of bolted flanged joints having a raised face configuration. The proposed

analytical approach to flange design holds promise of reliable leakage control compared with the conventional design methods. This is by considering the flexibility of both the gasket and the bolts, the flange ring rotation and the interdependence between the initial seating and final operating loads. The bolt load which is assumed in the rigid flange approach to always increase with higher pressure, is shown to remain unchanged and even decreased in some flange cases, as observed experimentally. Thus, the analytical model, based on the elastic interaction of all joint members, successfully reproduces the real behavior of joints.

Using this model, it could be possible to apply lower assembly loads with an adequate safety margin while providing the required clamping force to maintain a tight joint during operation. Therefore, it can be conceived that gasket overload and excessive flange rotation may also be avoided. In addition, the joint may further be lightened by reducing flange thickness and bolting which is not only beneficial in term of material saving and cost, but also, advantageous for application where gasket creep relaxation is important.

A tight joint is achieved by the combined action of the gasket mechanical properties and the flange assembly and external forces. The most important factor which determines the ability of a flange to seal is the gasket stress, the amount of pressure applied to the gasket via the flange face. As a rule, the higher the gasket stress, the tighter the gasket seal. However, due to flange rotation a radial variation in gasket

compression is present and is known to affects the leakage performance of the joint when it becomes excessive.

As a result, a method was developed for evaluating the radial distribution of gasket compressive stress based on the flange rotation and the readjustment of the gasket reaction or the gasket single spring location. From the results obtained by both the experimental and numerical FEM analysis, the model has proved to be efficient in predicting rotation, gasket radial displacement and stress distribution. It was hoped that the DynaForce sensing device would provide a means to measure the actual gasket stress distribution with reasonable accuracy. Unfortunately, due to its highly nonlinear behavior coupled with a large hysteresis effect, the sensor cannot be used yet as a reliable measuring device. Unless improvements are made to the sensor itself and the method of calibration, only qualitative measurements are obtained. An interesting result was the confirmation of the general trend of the radial distribution of stress by the DynaForce sensor.

The model presented in Chapter 6 is capable of predicting relaxation due to room temperature creep of the gasket with reasonable accuracy. The prediction and the evolution of tightness with time is now possible. Up to 30% of the gasket initial load is relaxed in less than four hours for some of the gasket materials tested. The thicker the gasket, the higher the relaxation is. The model may be extended to include gasket relaxation at elevated temperature which has simply the effect of accelerating this

phenomenon.

The initial bolt load plays a major role in the performance of the bolted joint and this should be given careful consideration. Over-tightening of bolts, for example, is often a source of gasket failures. The maximum allowable gasket preload is limited by flange stresses, flange rotation, bolt stress, or gasket crush so, simply increasing the flange thickness may not be beneficial since this would result in an increase in joint stiffness which may not help the effect of relaxation due to creep. Extended bolts adds flexibility and "Belleville" washers achieve the same effect. One way to overcome joint relaxation is, however, by having a gasket which is a combination of a soft material with metallic rings. With this configuration, while the soft gasket material provides tightness the rings prevents gasket thickness changes and radial expansion that causes the drop in bolt load.

7.2 RECOMMENDATIONS FOR FUTURE WORK

The state of the art of bolted gasketed joints involves a large number of variables that are difficult to predict and control. A few of these variables are pressure, gasket behavior, external moments and forces, differences in bolt-flange service temperatures and materials, relaxation due pressure and temperature transitions. The proposed analytical model is believed to be capable of predicting with reasonable accuracy the effect of some parameters such as pressure and gasket creep. Additional parameters such

as temperature could be readily incorporated in this model.

It is well established that the leakage behavior of joints is conditioned by the amount of contact pressure on the gasket. Therefore, the radial distribution of gasket stress needs to be investigated in more details so as to relate it to tightness performance. The DynaForce sensing system has potential in becoming a powerful experimental tool if its nonlinearity and hysteresis could be controlled and a more appropriate calibration method could be developed.

The effect of the gasket width and the influence of flange rotation on the tightness performance need also to be further examined. The new gasket constants obtained from the current room temperature tests and performed with rigid platens need to account for real flange conditions. Of interest, in particular, is a further study on the influence of external bending loads which could be conducted using the DynaForce sensor.

Another major concern of bolted flange users is the elevated temperature behavior of joint and the influence of temperature on the leakage characteristics of gaskets. The importance of the short term relaxation of gasket has been demonstrated, but the model could easily modified to incorporate the long term gasket creep behavior and, in particular, the effect of bolt creep.

The effect of differential expansion between the bolts and flanges, due to temperature gradients or the use of materials having different coefficients of thermal expansion has not been investigated deeply although an attempt was made in Chapter 6 to tackle such a problem by laying the basic formulation. It may be possible to adapt these formulas to make proper assessments of the thermal transients and the response of the joint to temperature changes, but the proper method of doing this needs further development. Transient thermal differences between the flange, the bolts and the gasket can increase gasket stress. This type of study should take full advantage of advanced finite element methods and modeling techniques. However, more experimental test results would be more than necessary in order to validate any new analytical development.

BIBLIOGRAPHY

ABAQUS, 1988, Hibbitt, Karlson and Sorenson Inc.

ALVARO,M.A., 1990, "A Simplified Procedure for the Design of Bolted Gasketed Flanges," M.Sc.A. thesis submitted at the Ecole Polytechnique, Montreal, Quebec, Canada.

American Society for Testing Material, 1993, ASTM F36,F37 and F38, Philadelphia, PA.

Anonymous, 1905, "The Flanged Mouth-piece Rings of Vulcanizers and Similar Vessels," *The Locomotive*, Vol. 25, No. 7, pp. 177-203.

Anonymous, 1967, "DIN 2505 - Calculation of Flanged connections," British Standard Institute Document No. 67 (22328).

ASME/ANSI, 1988, "Pipe Flanges and Flanged Fittings," *ASME/ANSI B-16.5*, 1988, The American Society of Mechanical Engineers, New York.

ASME Boiler and Pressure Vessel Code, Section VIII, Division 1, Pressure Vessels, 1992, the American Society of Mechanical Engineers, New York.

BACH,C., 1896, "Mashinelemente," Verlag Cotta, Stuttgart, Germany, 5th ed., pp. 611-617.

BACH,C., 1891, "Versuche über die Widerstandfähigkeit ebener Platten," Springer Verlag, Berlin, Germany.

BAILEY,R.W., 1937, "Flanged Pipe Joints for High Pressures and High Temperatures," *Engineering*, Vol. 144, pp. 364-365, 419-421, 490-492, 538-539, 615-617, 674-676.

BAZERGUI,A. and PAYNE,J.R., 1984, "Progress in Gasket testing - Milestone Results," *ASME journal of Pressure vessel technology*, Vol. 106, pp. 93-103.

BAZERGUI,A. and MARCHAND L., 1984, "PVRC Milestone Gasket tests - First Results," *Welding Research Council Bulletin No. 292.*

BAZERGUI,A., 1984, "Short Term Creep Relaxation Behaviour of Gaskets," *Welding Research Council Bulletin No. 294*, pp. 9-22.

BAZERGUI,A., MARCHAND,L. and RAUT,H.D., 1985, "Development of a Production Test Procedure for Gaskets," *Welding Research Council Bulletin No. 309*, pp. 1-39.

BAZERGUI,A., MARCHAND,L. and PAYNE,J.R., 1989, "The Aged Hot Tightness Test for Gaskets," *ASTM-SAE International Congress and Exposition-Gasket Symposium*, Paper No. 890273, Detroit, Michigan.

BICKFORD,J.H., HAYASHI,K., CHANG,A.T. and WINTER,J.R., 1989, "A Preliminary Evaluation of Elevated Temperature Behavior of a Bolted Flanged Connection," *Welding Research Council Bulletin No. 341*, pp. 1-24.

BICKFORD,J.F., 1990, An Introduction to the Design and Behaviour of Bolted Joints, 2nd ed., rev. and expanded, Marcel Dekker Inc., New York.

BLACH,A.E., 1983, Bolted Flanged Connections with Full Face Gaskets, Ph.D Dissertation, Ecole Polytechnique, Montreal, Quebec, Canada.

BLACH,A.E., BAZERGUI,A. and BALDUR,R., 1986, "Bolted Flanged Connections with Full Face Gaskets," *Welding Research Council Bulletin No. 314*, pp. 1-13.

BLACH, A.E. and BAZERGUI, 1981, "Methods of Analysis of Bolted Flanged Connections - A Review," *Welding Research Council Bulletin No. 271*, pp. 1-15.

BONEH,B., AYRAULT,D. and BOILLOT,L., 1986, "Amelioration d'une Methode d'Analyse des Brides Circulaires Boulonnées," International Symp. on Fluid Sealing, Application to Bolted Flanged Connections, Nantes, pp. 107-119.

BOON,E.F. and LOK,H.H., 1958, "Untersuchungen an Flanschen und Dichtungen," *Ver. Dtsch. Ing. Z.*, Vol. 100, pp. 1613-1624.

BOUZID,A. and CHAABAN,A., 1993, "Flanged Joint Analysis: A Simplified Method Based on Elastic Interaction," CSME *Transactions*, Vol. 17, N°2, pp. 181-196.

BOUZID,A., CHAABAN,A. and BAZERGUI,A., 1994a, "The Effect of Creep Relaxation on the Leakage Tightness of Bolted Flanged Joints," *Proc. ASME/PVP Conference*, Minneapolis, PVP-Vol. 286, Changing Properties of Codes and Standards: Failure, Fatigue and Creep, pp. 155-163.

BOUZID,A., CHAABAN,A. and BAZERGUI,A., 1994b, "The Influence of the Flange Rotation on the Leakage Performance of Bolted Flanged Joints," *Proc. CSME Forum*, Montreal, Vol. I, pp. 184-194.

British Standard, BS 1500, "Fusion Welded Pressure Vessels for General Purpose,"

CASCALES,D.H., MILITELLO,C. and MIHALL,W.J., 1987, "Bolted Flanged Joint Analysis with Non-linear Gasket Behavior," *Int. J. of PVP*, Vol. 30, pp. 205-215.

CASCALES,D.H. and MILITELLO,C., 1987, "An Accurate Simple model to Evaluate Integral Flange Rotation," *Int. J. of PVP*, Vol. 30, pp. 151-159.

CHAABAN,A., BOUZID,A., DERENNE,A. and SCHEIFER,W., 1993, "Evaluation of Torque Coefficients and Gasket Stress Distributions in Bolted Flanged Joint Using Different Type of Lubricants," *3rd International Symposium on Fluid Sealing of Static Gasketed Joints*, Biarritz-France.

CHIVERS,T.C. and HUNT,R.P., 1978, "Scaling of Gas Leakage from Static Seals," *Proc. 8th Fluid Sealing Conference*, Durham, England, BHRA, Paper G3.

CZERNIK,D.E. and MISZCZAK,F.L., 1991, "A New Technique to Measure Real-Time Static and Dynamic Gasket Stresses," *SAE Transaction*, Section 3, Technical Paper No. 910205.

DERENNE,M., MARCHAND,L., PAYNE,J.,R. and Bazergui,A., 1994, "Elevated Temperature Testing of Gaskets for Bolted Flanged Connections," *Welding Research Council Bulletin No. 391*, pp. 1-37.

Design Division Problem No. XIII, 1984, "Re-evaluation of Gasket Factors Used in Flange Design," Long Range Plan for Pressure Vessel Research, 7th edition, *Welding Research Council Bulletin No. 298.*

DIN Standard 2505, 1961, Berechung von Flanschverbindungen, (Stress Calculation of Bolted Flanged Connections), Beuth Verlag, Berlin, Tentative 1964 Final.

DONALD,M.B. and SALOMON,J.M., 1957, "Behaviour of Compressed Asbestos-Fibre Gaskets in Narrow-Faced, Bolted, Flanged Joints," *Inst. of Mech. Eng.-Proc.*, Vol. 171, pp. 829-833.

Fel-Pro, Manufacturing firm, Gasket, Sealing products, Lubricants; Skokie, U.S.A.

FARNAM,R.G., 1951, "Studies of Relaxation Characteristics of Nonmetalic Gasket Material," *India Rubber World*, Vol. 123, No. 6, pp. 679-682.

FESSLER,H. and SWANNELL,J.H., 1974, "Prediction of the Creep Behaviour of a flanged Joint," *Proc. Conference on Creep Behaviour of Piping*, Inst. of Mechanical Engineers, pp. 39-49.

FLUGGE,W., 1973, Stresses in Shells, 2nd ed., Springer-Valeg New York Heidelberg Berlin.

G&W Taylor-Bonney Division, 1978, "Modern Flange Design," Bulletin 502, Edition VII, Southfield, Michigan.

GARN,D., 1965, Thermoanalytical Methods of Investigation, Academic Press Inc, pp. 208-209.

GILL,S.S., 1970, Stress Analysis of Pressure Vessels and Pressure Vessel Components, chap. 6 ("Flanges", by R.T. Rose), Pergamon, NY, pp. 267-315.

HARVEY,J.F., 1980, Pressure Component Construction, Van Nostrand, NY.

HAYES,J.K. and ROBERTS,B., 1970, "Measurement of Stresses Under Elastic-Plastic Strain Conditions at Elevated Temperatures (550°C Maximum)," *Experimental Mechanics*, pp. 440-448.

HSU,K.H., PAYNE,J.R. and WINTER,J.R., 1994, "PVRC Bolted Flanged Connection Reseach Program and 5-Year Plan," *Proc. ASME/PVP Conference*, Minneapolis, PVP-Vol. 274, Advanced Computer Applications, pp. 53-62.

KOHMURA,S., 1985, "The design of Aluminium Bolted Flange Connections, Part I Relationship between Leak Properties and Gasket Loads in Integral Hub Flanges," *Bulletin of JSME*, Vol. 28, No. 243, pp. 2181-2187.

KOMANO,H., SAWA,T., HIROSE,T. and NAKAGO,Y., 1993, "The Characteristics of a Bolted Joint under Thermal Changes," *3rd Intern. Symp. on Fluid Sealing of Static Gasketed Joints*, Biarritz-France, pp. 101-109.

KRAUS,H., 1980a, "Interpretive Report on Gasket Leakage Testing," *Welding Research Council Bulletin No. 262*, pp. 17-33.

KRAUS,H., 1980b, Creep Analysis, John Wiley & Sons, New York.

KRAUS,H., and ROSENKRANS,W., 1984, "Creep of bolted Flanged Connections," *Welding Research Bulletin No. 294*, pp. 2-8.

LAKE,G.F. and BOYD,G., 1957, "Design of Bolted flanged Joint of Pressure Vessels," *Proc. Inst. of Mechanical Engineers*, Vol. 171, pp. 843.

MARCHAND,L., 1982, "Effet de la Rotation des Brides sur l'Etancheité des Garnitures à Enroulement Spiral," M.Sc.A. Thesis submitted at the Ecole

Polytechnique, Montreal, Canada.

MARCHAND,L, DERENNE,M. and BAZERGUI,A., 1990a, "Weight Loss Correlation for Sheet Gasket Materials," *The 1990 Pressure Vessel and Piping Conference*, Nashville, Tennesse, pp. 77-84.

MARCHAND,L, DERENNE,M. and BAZERGUI,A., 1990b, "The Influence of Thermal Degradation on Sealing Performance of Compressed Sheet Gasket Materials with Elastomer Binder Part I: Experimental Methods," *2nd Internat. Symp. on Fluid Sealing of Static Gasketed Joints*, La Baule, France, pp. 243-254.

MARCHAND,L, DERENNE,M. and BAZERGUI,A., 1990c, "The Influence of Thermal Degradation on Sealing Performance of Compressed Sheet Gasket Materials with Elastomer Binder Part II: Analysis," *2rd International Symposium on Fluid Sealing of Static Gasketed Joints*, La Baule, France, pp. 255-266.

MARCHAND,L, 1991, "Effet du vieillissement à haute température sur le comportement des joints d'étancheité de brides boulonnées," Ph.D Thesis submitted at the Ecole Polytechnique, Montreal, Canada.

MARCHAND,L., DERENNE,M. and BAZERGUI,A., 1992, "Weight Loss Correlation for Sheet Gasket Materials," *ASME Journal of Pressure Vessel Technology*, Vol. 114, pp. 1-7.

MARCHAND,L., BAZERGUI,A., HAHN,A. and KOCKELMANN,H., 1993, "The Influence of the Stiffness of Flanges and Bolts on the Creep-Relaxation Behaviour of Gaskets," *3rd Intern. Symp. on Fluid Sealing of Static Gasketed Joints*, Biarritz-France, pp. 31-42.

MARINE,J., 1938, "Stress and Deformation in Pipe Flanges Subjected to Creep at high Temperatures," *Franklin Inst. J.*, Vol. 226, n 5, pp. 645-657.

MARR,J.W., 1968, Leakage Testing Handbook, NASA-CR-952, April.

Modern Flange Design, 1979, Taylor Forge and pipe works, Chicago.

MURRAY,N.W. and STUART,D.G., 1961, "Behaviour of Large Taper Hub Flanges," *Proc. Symp. Pressure Vessel Research Towards Better Design*, Inst. Mech. Eng., pp. 133-147.

PAYNE J.R., 1985, "PVRC Flanged Joint Survey," *Welding Research Council Bulletin No. 306*, pp. 1-39.

PAYNE,J.R., BAZERGUI,A. and LEON,G.F., 1985, "New Gasket Factors- A Proposed procedure," *Proc. ASME-PVP conference*, New Orleans, Vol. 98-2, Pressure vessel components and analysis, pp. 85-93.

PAYNE,J.R., BAZERGUI,A. and LEON,G.F., 1988, "Getting New Gasket Design Constants from Gasket Tightness Data," Special Supplement, *Experimental Techniques*, pp. 22-27.

PAYNE,J.R., MUELLER,R.T. and BAZERGUI,A., 1989a, "A Gasket Test Scheme for Petrochemical Plants, Part I: Test Methods and Application Results Part II: Quality Criteria and Evaluation Scheme," *Proc. ASME/JSME Pressure Vessel & Piping Conf.*, Hawaii.

PAYNE,J.R., MARCHAND,L. and BAZERGUI,A., 1989b, " Estimating Elevated Temperature Gasket Performence with ATRS Tests," *ASTM-SAE International*

Congress and Exposition-Gasket Symposium, Paper No. 890277, Detroit, Michigan.

PAYNE,J.R. and BAZERGUI,A., 1990, "Evaluation of Test Methods for Asbestos Replacement Gasket Materials," MTI Project No. 47, Final Report, *Materials Technology Institute of Chem. Process Industries*, Publication No. 36.

Pressure Vessel Research Committee, 1975, "Long-Range Plan for Pressure Vessel Research -Fourth Edition," *Welding Research Council Bulletin No. 209*, pp. 1-29.

PORDHORSKY,M. and VU,T., 1984, "Vorschlag Eines Berechnungsverfahrens fûr die Flanschdimensionierung," *VGB Kraftwerkstechnik*, N° 7, pp. 655-686.

RATHBURN,F.O.,Jr., 1964a, Design Criteria for Zero Leakage Connectors for Launch Vehicules, NASA-CR-56571.

RATHBURN,F.O.,Jr., 1964b, Leakage Rate Experiments, Conference on Design of Leak-tight Separable Fluid Connectors, Marshall Space Flight Center, Huntsville, AL.

RAUT,H.D. and LEON,G.F., 1977, "Report of Gasket Factor Tests," *Welding Research Council Bulletin No. 233*, pp. 1-23.

REUTER,R., 1973, "Leak Rates of Flanged Joints with Flat Gaskets," *Wasser, Luft Betr.*, Vol. 17, pp. 169-175.

ROARK,R.J. and YOUNG,W.C., 1988, Formulae for Stress and Strain, Mc Graw Hill, NY.

ROBERTS,I., 1950, "Gaskets and Bolted Joints," *J. applied Mech.*, Vol. 17, No. 2, pp. 169-179.

ROSSHEIM,D.B. and MARKL,A.R., 1943, "Gasket Loading Constants," *Mechanical Engineering*, Vol. 65, pp. 647.

SAUTER,E.M., 1982, "Current and Future Gasket Materials; Methods of Evaluating Some of their Functional Properties," Research laboratories for the Klinger group of companies, Switzerland, (U.S branch: SIDNEY,OHIO).

SAWA,T., KUMANO,H., HIROSE,T. and NAKAGOMI,Y., 1994, "Behavior of a Taper Hub Flange with a Bolted Flat Cover in Trasient Temperature Field: The Case where Tap Bolts are Used," *Proc. ASME/PVP Conference*, Minneapolis, PVP-Vol. 274, Advanced Computer Applications 1994, pp. 83-90.

SAWA,T., HIGURASHI,N. and AKAGAWA,H., 1991, "A Stress Analysis of Pipe Flange Connections," *ASME Journal of Pressure Vessel Technology*, Vol. 113, pp. 497-503.

SCHWAIGERER,S., 1951, "Die Berechung von Flanschverbindungen fur Heissdamplfrohrleitungen," (Design Calculation for Flanges in High Temperature Steam Piping), *VGB-Merkblatter*, No. 4.

SCHWAIGERER,S. and SEUFERT,W., 1951, "Untersuchungen Uber das Dichtvermogen von Dichtleisten," *Brennstoff-Warme-Kraft*, Vol. 3.

SCHWAIGERER,S., 1954, "Die Berechung der Flanschverbindungen Behalter und Rohrleitungsbau," (Design Calculation of Flanged Joint for Pressure vessels and Piping), *Ver. Dtsch. Ing. Z.*, Vol. 96, pp. 7-12.

SCHWAIGERER,S., 1961, "Festigkeitsberechnung von Bauelementen des Dampfkessel Behalter und Rohrleitungsbaues," Spinger-Verlag, Berlin.

SCHNEIDER,R.W., 1968, "Flat Face Flanges with Metal-to-Metal Contact Beyond the Bolt Circle," *Trans. ASME, Journal of Engineering for Power*, Series A, Vol. 90, No. 1, pp. 82-88.

SCHNEIDER,R.W. and WATERS,E.O., 1969, "Axisymmetric Non-identical, Flat Face Flanges with Metal-to-Metal contact Beyond the Bolt Circle," *Trans. ASME, Journal of Engineering for Industry*, Series B, Vol. 91, No. 3, pp. 615-622.

SCHNEIDER,R.W. and WATERS,E.O., 1978, "The Background of ASME Code Case 1828: A Simplified Method of Analyzing Part B Flanges," Trans. ASME, *Journal of Pressure Vessel Technology*, Vol. 100, No. 2, pp. 215-219.

SCHNEIDER,R.W. and WATERS,E.O., 1979, "The Application of ASME Code Case 1828," Trans. ASME, *Journal of Pressure Vessel Technology*, Vol. 101, No. 1, pp. 87-94.

SCHNEIDER,R.W. and RODABOUGH,E.C., 1982, "Flanges, Gaskets and Closure Systems," *Pressure Vessel and Piping: Design Technology-1982*, A decade of Progress, ASME, New York.

SHORT II,W.E., 1992, " A Parametric Study of Class 150 Flanges with Spiral Wound Gaskets," *Pressure Vessel and Piping*, Vol. 235, Design and Analysis of Pressure Vessels, Piping, and Components, ASME.

SIEBEL,E. and WELLINGER,K., 1942, "Experiments with Soft Sealing Materials," *Die Chemische Techni.* .

SINGH,K.P. and HOLTZ,M., 1979, "Analysis of Temperature Induced Stress in the Body Bolts of Single Pass Heat Exchangers," ASME Paper 79-WA/NE-7, pp 1-9.

SINGH,K.P. and SOLER,A.I., 1984, Mechanical Design of Heat Exchangers and Pressure Vessel Components, Arcturus Publishers, New Jersey.

SMOLEY,E.,M., KESSLER,F.J., KOTTMEYER,R.E. and TWEED,R. G., 1963, "The Creep Relaxation Properties of a Flat Face Gasketed Joint Assembly," *SAE Paper S 361.*

SOLER,A.I., 1980, "Analysis of Bolted Joints with Nonlinear Gasket Behavior," Trans. ASME, *Journal of Pressure Vessel Technology*, Vol. 102, pp. 249-256.

SZILARD,R., 1984, Theory and Analysis of Plates, Classical and Numerical Methods, Prentice-hall, New Jersey.

TAPSELL,H.J., 1939, "Second Report on the Pipe Flanges Research Committee," *Institution of Mechanical Engineers - Proc.*, Vol. 141, No. 5, pp. 433-458.

TGL, 1991, Main Features and Advantage of the Draft " Design Rules for Flange Connections," Doc n 34-91.

TIMOSHENKO,S., 1930, Strength of Material Part II, Van Nostrand, Princeton, NY.

TIMOSHENKO,S. and WOINOWSKI-KRIEGER,S., 1959, Theory of Plates Shells, McGraw-Hill, New York.

Tightness Testing ans Research Laboratory, 1993, "PTFE Gasket Qualification Project," Progress report No. 2, Ecole Polytechnique of Montreal.

THOMSON,G., 1987, "Strength and Flexibility of Pressurised Taper Hub Flanged Joints," *Applied Solid Mechanics Conf.*, Univ. of Strathclyde, Glasgow.

THORN,F.C., 1942, "Stress Decay in Rubber Gaskets," *Mech World*, Vol. 111, No. 2873, pp. 80-81.

THORN,F.C., 1949, "Creep and Relaxation in Compressed Asbestos Gaskets," *ASTM Bul.*, No. 160, pp. 58-61.

THORN,F.C., 1955, "Sealability of Gasketing Materials on Smooth and Wavy Flanges," *ASTM-Bul. No. 210*, pp. 43-44.

VIGNAUD,J.C., MOINEREAU,D., NOWAK,H. and DIGAT,P., 1986, "Comportement Mécanique des Joints Spiralés; Compression et Relaxation du Joint," *International Symposium on Fluid Sealing; application to Bolted Flanged Connections*, Nantes, France.

WATERS,E.O. and TAYLOR,J.H., 1927, "The Strength of Pipe Flanges," *Mechanical Engineering*, Vol. 49, pp. 531-542.

WATERS,E.O., ROSSHEIN,D.B., WESSTROM, D.B. and WILLIAMS, F.S.G., 1937, "Formulas for Stresses in Bolted Flanged Connections," *Transaction of the* ASME, Vol. 59, pp. 161-169.

WATERS,E.O., 1938, "Analysis of Bolted Joints at High Temperatures," *Transaction of the* ASME, Vol. 60, pp. 83-86.

WATERS,E.O., ROSSHEIN,D.B., WESSTROM,D.B. and WILLIAMS,F.S.G., 1949, "Development of General Formulas for Bolted Flanges," Taylor Forge and Pipe Works, Chicago, Illinois.

WATERS, E.O., 1971, "Derivation of Code Formulas for Part B Flanges," *Welding Research Council Bulletin No. 166*, pp. 27-37.

WATERS,E.O. and SCHNEIDER,R.W., 1980, "Derivation of ASME Code Formulas for the Design of Reverse Flange," *Welding Research Council Bulletin No. 262*, pp. 2-9.

WERKENTHIN,T.A., SWENSON,A.D., CHATTEN,C.K. and MORRIS,R.E., 1945, "Sealing and Seal-Aging Properties of Rubber Gaskets," *Rubber Age*, Vol. 56, No. 4, pp. 389-396.

WESSTROM,D.B. and BERGH,S.E., 1951, "Effects of Internal Pressure on Stresses and Strains in Bolted Flanged Connections," *Transaction of the* ASME, Vol. 73, N° 5, pp. 508-568.

WESTPHAL,M., 1897, "Berechung der Festigkeit loser und fester Flansche," *Ver. Dtsch. Ing. Z.*, Vol. 41, No. 36, pp. 1036-1042.

APPENDIX I

Functions involved in the tapered hub solution

The solution of the differential equation of the tapered hub involves the resolution of two new second order equations. Their solutions are complex value functions of x and conjugate complex to them which are linearly interdependent and form a complete system of four independent solutions. The complete solution to this problem is given in various textbooks on cylindrical shells including the two used references by Timoshenko (1959) and Flugge (1973).

The S coefficients used in the tapered hub solution are combination of Schleider functions and their derivatives and are given by the following;

$$S_1 = \varepsilon\, \psi_2(\varepsilon) - 2\psi_1'(\varepsilon)$$

$$S_2 = \varepsilon\, \psi_1(\varepsilon) + 2\psi_2'(\varepsilon)$$

$$S_3 = \varepsilon\, \psi_4(\varepsilon) - 2\psi_3'(\varepsilon)$$

$$S_4 = \varepsilon\, \psi_3(\varepsilon) + 2\psi_4'(\varepsilon)$$

$$S_5 = \varepsilon^2\, \psi_2'(\varepsilon) - 4\varepsilon\, \psi_2(\varepsilon) + 8\psi_1'(\varepsilon)$$

$$S_6 = \varepsilon^2\, \psi_1'(\varepsilon) - 4\varepsilon\, \psi_1(\varepsilon) - 8\psi_2'(\varepsilon)$$

$$S_7 = \varepsilon^2\, \psi_4'(\varepsilon) - 4\varepsilon\, \psi_4(\varepsilon) + 8\psi_3'(\varepsilon)$$

$$S_8 = \varepsilon^2\, \psi_3'(\varepsilon) - 4\varepsilon\, \psi_3(\varepsilon) - 8\psi_4'(\varepsilon)$$

The functions ψ' are the first derivatives of the functions ψ given below with respect to the argument ε. A graphical representation of the functions ψ' are given in Figure A.1.1. It is seen that the values of these functions increase or decrease rapidly as

the distance from the end increases. This indicates that in calculating the constants of integration C_1 to C_4, we can very often proceed by considering the cylinder as an infinitely long one and using at each edge only two of the four constants in the solution of the radial displacement w_h of Equation (4.10)

$$\psi_1(\varepsilon) = 1 - \frac{\varepsilon^4}{(2.4)^2} + \frac{\varepsilon^8}{(2.4.6.8)^2} - \cdots$$

$$\psi_2(\varepsilon) = -\frac{\varepsilon^2}{2^2} + \frac{\varepsilon^6}{(2.4.6)^2} - \frac{\varepsilon^{10}}{(2.4.6.8.10)^2} + \cdots$$

$$\psi_3(\varepsilon) = \frac{1}{2}\psi_1(\varepsilon) - \frac{2}{\pi}\left[R_1 + \mathrm{Ln}\frac{\beta.\varepsilon}{2}.\psi_2(\varepsilon)\right]$$

$$\psi_4(\varepsilon) = \frac{1}{2}\psi_2(\varepsilon) + \frac{2}{\pi}\left[R_2 + \mathrm{Ln}\frac{\beta.\varepsilon}{2}.\psi_1(\varepsilon)\right]$$

where the quantities appearing between the square brackets in the last two equations have the form

$$R_1 = \left[\frac{\varepsilon}{2}\right]^2 - \frac{C_{(3)}}{(3.2)^2}\left[\frac{\varepsilon}{2}\right]^6 + \frac{C_{(5)}}{(5.4.3.2)^2}\left[\frac{\varepsilon}{2}\right]^{10} - \cdots$$

$$R_2 = \frac{C_{(2)}}{2^2}\left[\frac{\varepsilon}{2}\right]^4 - \frac{C_{(4)}}{(4.3.2)^2}\left[\frac{\varepsilon}{2}\right]^8 + \frac{C_{(6)}}{(6.5.4.3.2)^2}\left[\frac{\varepsilon}{2}\right]^{12} - \cdots$$

The constants $C_{(n)}$ and are given by

$$C_{(n)} = 1 + \frac{1}{2} + \frac{1}{3} + \frac{1}{4} + \cdots + \frac{1}{n} \qquad \text{and} \qquad \ln\beta = 0.57722$$

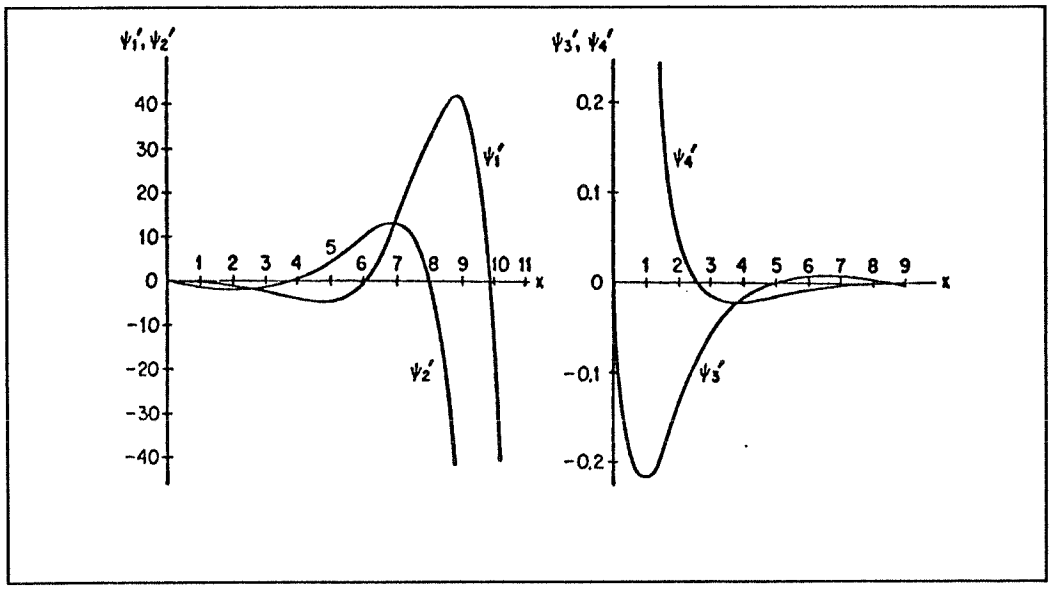

Figure I.1

The above derivative functions ψ' plotted in Figure A.1.1 with respect to the argument x are given for values between 0 and 10. However, for larger argument values, these functions can be described with sufficient accuracy by the following expressions:

$$\psi_1(\varepsilon) = \frac{1}{\sqrt{2\pi\varepsilon}}\, e^{\varepsilon/\sqrt{2}} \cos\left[\frac{\varepsilon}{\sqrt{2}} - \frac{\pi}{8}\right]$$

$$\psi_2(\varepsilon) = -\frac{1}{\sqrt{2\pi\varepsilon}}\, e^{\varepsilon/\sqrt{2}} \sin\left[\frac{\varepsilon}{\sqrt{2}} - \frac{\pi}{8}\right]$$

$$\psi_3(\varepsilon) = \sqrt{\frac{2}{\pi\varepsilon}}\, e^{-\varepsilon/\sqrt{2}} \sin\left[\frac{\varepsilon}{\sqrt{2}} + \frac{\pi}{8}\right]$$

$$\psi_4(\varepsilon) = -\sqrt{\frac{2}{\pi\varepsilon}}\, e^{-\varepsilon/\sqrt{2}} \cos\left[\frac{\varepsilon}{\sqrt{2}} + \frac{\pi}{8}\right]$$

$$\psi_1'(\varepsilon) = \frac{1}{\sqrt{2\pi\varepsilon}}\, e^{\varepsilon/\sqrt{2}} \cos\left[\frac{\varepsilon}{\sqrt{2}} + \frac{\pi}{8}\right]$$

$$\psi_2'(\varepsilon) = -\frac{1}{\sqrt{2\pi\varepsilon}}\, e^{\varepsilon/\sqrt{2}} \sin\left[\frac{\varepsilon}{\sqrt{2}} + \frac{\pi}{8}\right]$$

$$\psi_3'(\varepsilon) = -\sqrt{\frac{2}{\pi\varepsilon}}\, e^{-\varepsilon/\sqrt{2}} \sin\left[\frac{\varepsilon}{\sqrt{2}} - \frac{\pi}{8}\right]$$

$$\psi_4'(\varepsilon) = \sqrt{\frac{2}{\pi\varepsilon}}\, e^{-\varepsilon/\sqrt{2}} \cos\left[\frac{\varepsilon}{\sqrt{2}} - \frac{\pi}{8}\right]$$

APPENDIX II

System of equations obtained for flange types considered

Depending on the type of flange considered, five or eleven algebraic equations are assembled to solve for the unknows. These equations can be written in the matrix form and are give hereafter.

Ring Type Flanges

The system of equations in the edge loads M_0 P_0, flange rotation θ_f, frictional force V_g and bolt load F_b in relation to ring type flanges are given for the two cases considered in Figure 4.4:

a- Ring type flange used in pair

$$\begin{bmatrix} -\frac{6(1-\nu_c^2)}{E_c t_c^3 \beta_c^2} & \frac{6(1-\nu_c^2)}{E_c t_c^3 \beta_c^3}+\frac{B\gamma}{2t_f E_f} & -\frac{t_f}{2} & -\frac{\gamma}{2\pi G E_f t_f} & 0 \\ -\frac{12(1-\nu_c^2)}{E_c t_c^3 \beta_c} & \frac{6(1-\nu_c^2)}{E_c t_c^3 \beta_c^2} & 1 & 0 & 0 \\ -\frac{B}{D_0} & -\frac{Bt_f}{2D_0} & -\frac{E_f t_f^3}{B\pi Y} & -\frac{t_f}{2\pi D_0} & \frac{C-G}{2\pi D_0} \\ 0 & \frac{G\eta_f}{2E_f t_f} & \frac{t_f}{2} & -\frac{\eta_f}{2\pi E_f t_f}+\frac{\eta_g}{\pi E_g t_g} & \frac{\nu_g}{2\pi E_g l_g} \\ 0 & 0 & C-G & 0 & \frac{1}{K_g}+\frac{1}{K_b} \end{bmatrix} \begin{bmatrix} M_0 \\ P_0 \\ \theta_f \\ V_g \\ F_b^f \end{bmatrix} = \begin{bmatrix} \left(\frac{B\gamma}{2E_f}-\frac{(2-\nu_c)B^2}{8E_c t_c}\right)p \\ 0 \\ \frac{(G-B)(G^2+B^2)}{16\,D_0}p \\ \left(-\frac{\eta_g G}{2E_g}+\frac{\nu_g A_p}{2\pi E_g l_g}+\frac{\eta_f G}{2E_f}\right)p \\ \left[\left(\frac{1}{K_g}+\frac{1}{K_b}\right)F_b^i+(C-G)\theta_f^i+\frac{A_p}{K_g}\right]p \end{bmatrix}$$

b- Ring type flange used with blind cover

$$\begin{bmatrix} -\frac{6(1-\nu_c^2)}{E_c t_c^3 \beta_c^2} & \frac{6(1-\nu_c^2)}{E_c t_c^3 \beta_c^3}+\frac{B\gamma}{2t_f E_f} & -\frac{t_f}{2} & -\frac{\gamma}{2\pi G E_f t_f} & 0 \\ -\frac{12(1-\nu_c^2)}{E_c t_c^3 \beta_c} & \frac{6(1-\nu_c^2)}{E_c t_c^3 \beta_c^2} & 1 & 0 & 0 \\ -\frac{B}{D_0} & -\frac{Bt_f}{2D_0} & -\frac{E_f t_f^3}{B\pi Y} & -\frac{t_f}{2\pi D_0} & \frac{C-G}{2\pi D_0} \\ 0 & \frac{G\eta_f}{4E_f t_f} & \frac{t_f}{4} & -\frac{\eta_f}{4\pi E_f t_f}+\frac{\eta_g}{\pi E_g t_g}-\frac{\eta_p}{\pi E_p t_p} & \frac{\nu_g}{2\pi E_g l_g} \\ 0 & 0 & \frac{C-G}{2} & 0 & \frac{1}{K_g}+\frac{1}{K_b}+\frac{1}{K_p'}-\frac{1}{K_p''} \end{bmatrix} \begin{bmatrix} M_0 \\ P_0 \\ \theta_f \\ V_g \\ F_b^f \end{bmatrix} = \begin{bmatrix} \left(\frac{B\gamma}{2E_f}-\frac{(2-\nu_c)B^2}{8E_c t_c}\right)p \\ 0 \\ \frac{(G-B)(G^2+B^2)}{16\ D_0}p \\ \left(-\frac{\eta_g G}{2E_g}+\frac{\nu_g A_p}{2\pi E_g l_g}+\frac{\eta_f G}{4E_f}\right)p \\ \left(\frac{1}{K_g}+\frac{1}{K_b}+\frac{1}{K_p'}-\frac{1}{K_p''}\right)F_b^i+\frac{(C-G)}{2}\theta_f^i+\left(\frac{A_p}{K_g}+\frac{A_p}{K_p'}-a_0\right)p \end{bmatrix}$$

Weld Neck Type Flanges

The system of equations in the edge loads M_1, P_1, M_2 and P_2, hub constants C_1, C_2, C_3 and C_4, flange rotation θ_f, frictional force V_g and bolt load F_b in relation to welding neck type flanges are given for the two cases considered in Figure 4.4:

a- Welding neck type flange used in pair

$$[\,m\,] \cdot \begin{bmatrix} M_1 \\ P_1 \\ M_2 \\ P_2 \\ C_1 \\ C_2 \\ C_3 \\ C_4 \\ \theta_f \\ V_g \\ F_b^f \end{bmatrix} = \begin{bmatrix} \left[\frac{(2-\nu_h)a^2}{2E_h\alpha x_1} - \frac{(2-\nu_c)(B+t_c)^2}{8E_c t_c}\right] p \\ \frac{(2-\nu_h)a^2}{2E_h\alpha x_1^2}\, p \\ \left[\frac{(2-\nu_h)a^2}{2E_h\alpha x_2} - \frac{B\gamma}{2E_f}\right] p \\ \frac{(G-B)(G^2+B^2)}{16\, D_0}\, p \\ \frac{(2-\nu_h)a^2}{2E_h\alpha x_2^2}\, p \\ -4\ (2-\nu_h)a^2\alpha^2\, p \\ 0 \\ 4\ (2-\nu_h)a^2\alpha^2\, p \\ 0 \\ \left[-\frac{\eta_g G}{2E_g} + \frac{\nu_g A_p}{2\pi E_g I_g} + \frac{\eta_f G}{2E_f}\right] p \\ (\frac{1}{K_g}+\frac{1}{K_b})F_b^i + (C-G)\theta_f^i + \frac{A_p}{K_g} p \end{bmatrix}$$

$$
[m] = \begin{bmatrix}
-\frac{6(1-\nu_c^2)}{E_c t_c^3 \beta_c^2} & \frac{6(1-\nu_c^2)}{E_c t_c^3 \beta_c^3} & 0 & 0 & x_1^{1/2}\psi_1'(\epsilon_1) & x_1^{1/2}\psi_2'(\epsilon_1) & x_1^{1/2}\psi_3'(\epsilon_1) & x_1^{1/2}\psi_4'(\epsilon_1) & 0 & 0 & 0 \\
-\frac{12(1-\nu_c^2)}{E_c t_c^3 \beta_c} & \frac{6(1-\nu_c^2)}{E_c t_c^3 \beta_c^2} & 0 & 0 & \frac{x_1^{3/2}}{2}S_1(\epsilon_1) & -\frac{x_1^{3/2}}{2}S_2(\epsilon_1) & \frac{x_1^{3/2}}{2}S_3(\epsilon_1) & -\frac{x_1^{3/2}}{2}S_4(\epsilon_1) & 0 & 0 & 0 \\
0 & 0 & 0 & -\frac{B\gamma}{2t_f E_f} & x_2^{1/2}\psi_1'(\epsilon_2) & x_2^{1/2}\psi_2'(\epsilon_2) & x_2^{1/2}\psi_3'(\epsilon_2) & x_2^{1/2}\psi_4'(\epsilon_2) & \frac{t_f}{2} & \frac{\gamma}{2\pi G E_f t_f} & 0 \\
0 & 0 & -\frac{B+g_1}{D_0} & -\frac{Bt_f}{2D_0} & 0 & 0 & 0 & 0 & -\frac{E_f t_f^3}{B\pi Y} & -\frac{t_f}{2\pi D_0} & \frac{C-G}{2\pi D_0} \\
0 & 0 & 0 & 0 & \frac{x_2^{3/2}}{2}S_1(\epsilon_2) & -\frac{x_2^{3/2}}{2}S_2(\epsilon_2) & \frac{x_2^{3/2}}{2}S_3(\epsilon_2) & -\frac{x_2^{3/2}}{2}S_4(\epsilon_2) & -1 & 0 & 0 \\
-48(1-\nu_h^2) & 0 & 0 & 0 & E_h\alpha^3 x_1^{1/2}S_5(\epsilon_1) & -E_h\alpha^3 x_1^{1/2}S_6(\epsilon_1) & E_h\alpha^3 x_1^{1/2}S_7(\epsilon_1) & -E_h\alpha^3 x_1^{1/2}S_8(\epsilon_1) & 0 & 0 & 0 \\
0 & \frac{24(1-\nu_h^2)}{E_h\alpha^3\rho^2 x_1^{1/2}} & 0 & 0 & S_2(\epsilon_1) & S_1(\epsilon_1) & S_4(\epsilon_1) & S_3(\epsilon_1) & 0 & 0 & 0 \\
0 & 0 & -48(1-\nu_h^2) & 0 & E_h\alpha^3 x_2^{1/2}S_5(\epsilon_2) & -E_h\alpha^3 x_2^{1/2}S_6(\epsilon_2) & E_h\alpha^3 x_2^{1/2}S_7(\epsilon_2) & -E_h\alpha^3 x_2^{1/2}S_8(\epsilon_2) & 0 & 0 & 0 \\
0 & 0 & 0 & \frac{24(1-\nu_h^2)}{E_h\alpha^3\rho^2 x_2^{1/2}} & S_2(\epsilon_2) & S_1(\epsilon_2) & S_4(\epsilon_2) & S_3(\epsilon_2) & 0 & 0 & 0 \\
0 & 0 & 0 & \frac{G\eta_f}{2E_f t_f} & 0 & 0 & 0 & 0 & \frac{t_f}{2} & -\frac{\eta_f}{2\pi E_f t_f}+\frac{\eta_g}{\pi E_g t_g} & \frac{\nu_g}{2\pi E_g l_g} \\
0 & 0 & 0 & 0 & 0 & 0 & 0 & 0 & C-G & 0 & \frac{1}{K_g}+\frac{1}{K_b}
\end{bmatrix}
$$

b- Welding neck type flange used with blind cover

$$
[\,m\,]\;.\;\begin{bmatrix} M_1 \\ P_1 \\ M_2 \\ P_2 \\ C_1 \\ C_2 \\ C_3 \\ C_4 \\ \theta_f \\ V_g \\ F_b^f \end{bmatrix} = \begin{bmatrix} \left[\frac{(2-\nu_h)a^2}{2E_h\alpha x_1} - \frac{(2-\nu_c)(B+t_c)^2}{8E_c t_c}\right] p \\ \frac{(2-\nu_h)a^2}{2E_h\alpha x_1^2}\, p \\ \left[\frac{(2-\nu_h)a^2}{2E_h\alpha x_2} - \frac{B\gamma}{2E_f}\right] p \\ \frac{(G-B)(G^2+B^2)}{16\, D_0}\, p \\ \frac{(2-\nu_h)a^2}{2E_h\alpha x_2^2}\, p \\ (2-\nu_h)a^2\alpha^2\, p \\ 0 \\ (2-\nu_h)a^2\alpha^2\, p \\ 0 \\ \left[-\frac{\eta_g G}{2E_g} + \frac{\nu_g A_p}{2\pi E_g l_g} + \frac{\eta_f G}{4E_f}\right] p \\ \left(\frac{1}{K_g} + \frac{1}{K_b} + \frac{1}{K_p'} - \frac{1}{K_p''}\right)F_b^i + (C-G)\theta_f^i + \left(\frac{A_p}{K_g} + \frac{A_p}{K_p'} - a_0\right)p \end{bmatrix}
$$

$$
[m] = \begin{bmatrix}
-\frac{6(1-\nu_c^2)}{E_c t_c^3 \beta_c^2} & \frac{6(1-\nu_c^2)}{E_c t_c^3 \beta_c^3} & 0 & 0 & x_1^{1/2}\psi_1'(\epsilon_1) & x_1^{1/2}\psi_2'(\epsilon_1) & x_1^{1/2}\psi_3'(\epsilon_1) & x_1^{1/2}\psi_4'(\epsilon_1) & 0 & 0 & 0 \\
-\frac{12(1-\nu_c^2)}{E_c t_c^3 \beta_c} & \frac{6(1-\nu_c^2)}{E_c t_c^3 \beta_c^2} & 0 & 0 & \frac{x_1^{3/2}}{2}S_1(\epsilon_1) & -\frac{x_1^{3/2}}{2}S_2(\epsilon_1) & \frac{x_1^{3/2}}{2}S_3(\epsilon_1) & -\frac{x_1^{3/2}}{2}S_4(\epsilon_1) & 0 & 0 & 0 \\
0 & 0 & 0 & -\frac{B\gamma}{2t_f E_f} & x_2^{1/2}\psi_1'(\epsilon_2) & x_2^{1/2}\psi_2'(\epsilon_2) & x_2^{1/2}\psi_3'(\epsilon_2) & x_2^{1/2}\psi_4'(\epsilon_2) & \frac{t_f}{2} & \frac{\gamma}{2\pi G E_f t_f} & 0 \\
0 & 0 & -\frac{B+g_1}{D_0} & -\frac{Bt_f}{2D_0} & 0 & 0 & 0 & 0 & -\frac{E_f t_f^3}{B\pi Y} & -\frac{t_f}{2\pi D_0} & \frac{C-G}{2\pi D_0} \\
0 & 0 & 0 & 0 & \frac{x_2^{3/2}}{2}S_1(\epsilon_2) & -\frac{x_2^{3/2}}{2}S_2(\epsilon_2) & \frac{x_2^{3/2}}{2}S_3(\epsilon_2) & -\frac{x_2^{3/2}}{2}S_4(\epsilon_2) & -1 & 0 & 0 \\
-48(1-\nu_h^2) & 0 & 0 & 0 & E_h\alpha^3 x_1^{1/2}S_5(\epsilon_1) & -E_h\alpha^3 x_1^{1/2}S_6(\epsilon_1) & E_h\alpha^3 x_1^{1/2}S_7(\epsilon_1) & -E_h\alpha^3 x_1^{1/2}S_8(\epsilon_1) & 0 & 0 & 0 \\
0 & \frac{24(1-\nu_h^2)}{E_h\alpha^3\rho^2 x_1^{1/2}} & 0 & 0 & S_2(\epsilon_1) & S_1(\epsilon_1) & S_4(\epsilon_1) & S_3(\epsilon_1) & 0 & 0 & 0 \\
0 & 0 & -48(1-\nu_h^2) & 0 & E_h\alpha^3 x_2^{1/2}S_5(\epsilon_2) & -E_h\alpha^3 x_2^{1/2}S_6(\epsilon_2) & E_h\alpha^3 x_2^{1/2}S_7(\epsilon_2) & -E_h\alpha^3 x_2^{1/2}S_8(\epsilon_2) & 0 & 0 & 0 \\
0 & 0 & 0 & \frac{24(1-\nu_h^2)}{E_h\alpha^3\rho^2 x_2^{1/2}} & S_2(\epsilon_2) & S_1(\epsilon_2) & S_4(\epsilon_2) & S_3(\epsilon_2) & 0 & 0 & 0 \\
0 & 0 & 0 & \frac{G\eta_f}{4E_f t_f} & 0 & 0 & 0 & 0 & \frac{t_f}{4} & -\frac{\eta_f}{4\pi E_f t_f}+\frac{\eta_g}{\pi E_g t_g}-\frac{\eta_p}{\pi E_p t_p} & \frac{\nu_g}{2\pi E_g l_g} \\
0 & 0 & 0 & 0 & 0 & 0 & 0 & 0 & \frac{C-G}{2} & 0 & \frac{1}{K_g}+\frac{1}{K_b}+\frac{1}{K_p'}-\frac{1}{K_p''}
\end{bmatrix}
$$

APPENDIX III

"POLYFLG" program flow charts

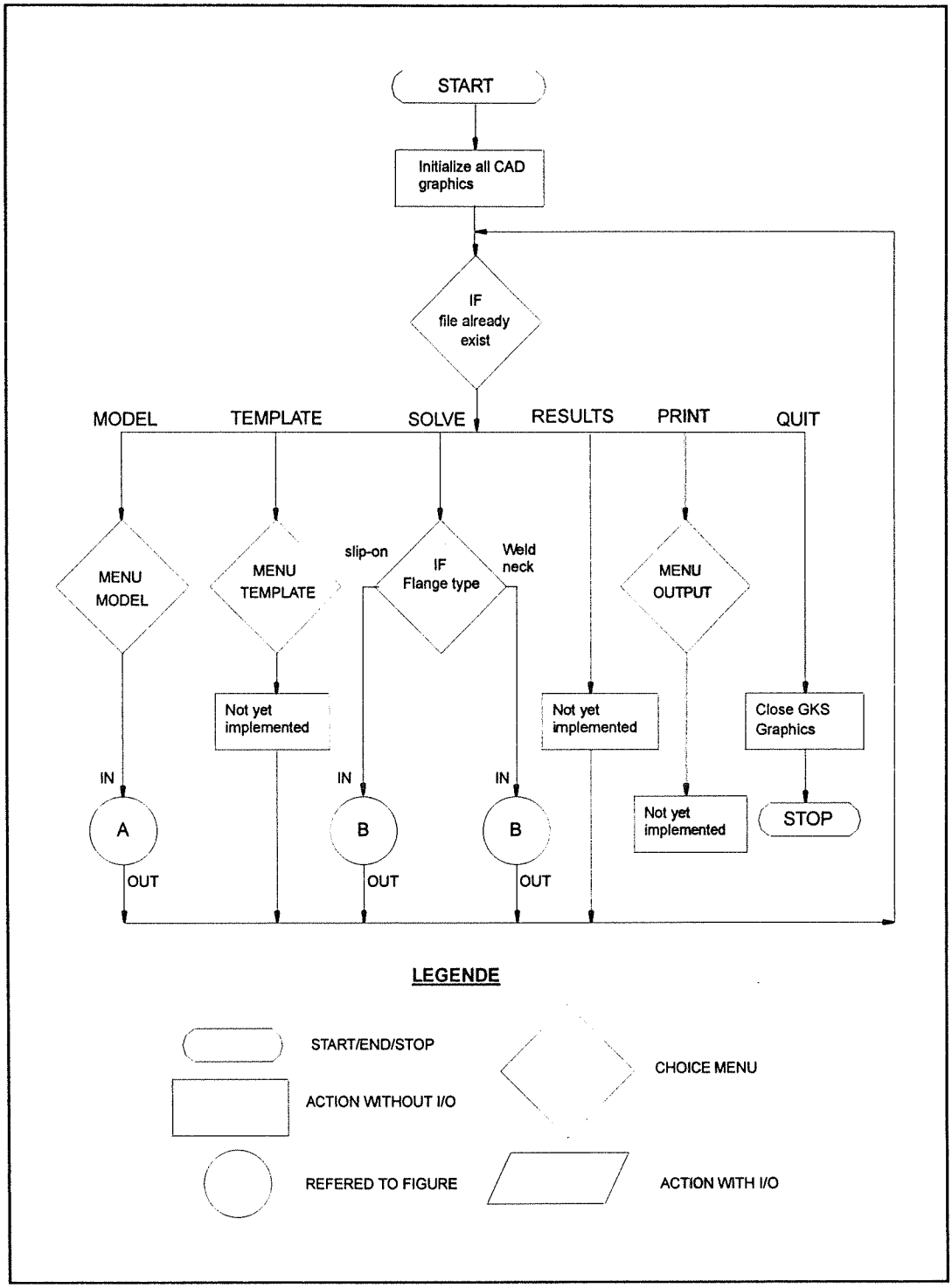

Figure III.1 "POLYFLG" main program

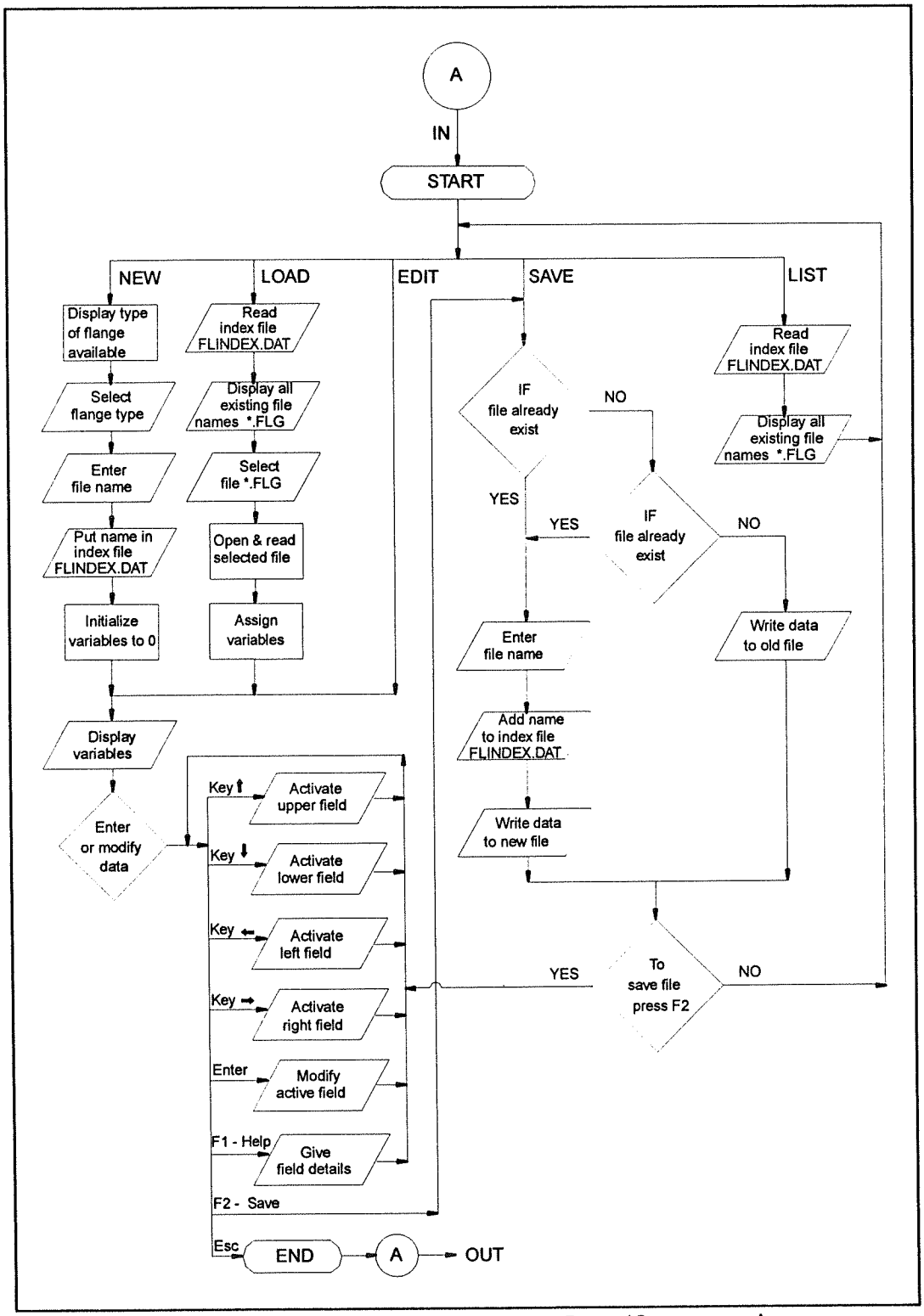

Figure III.2 "POLYFLG" Program Input/Output section

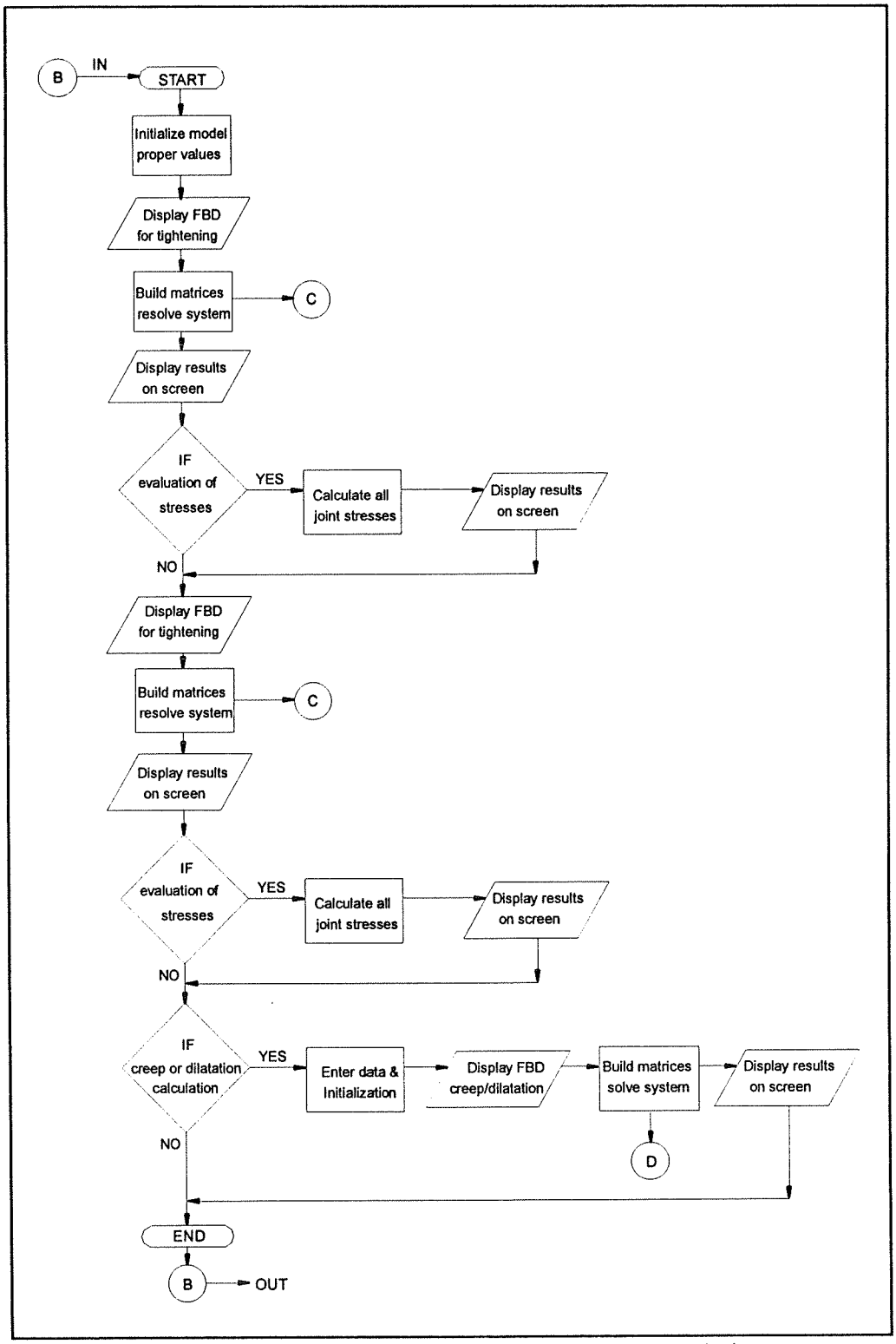

Figure III.3 "POLYFLG" main performed calculations

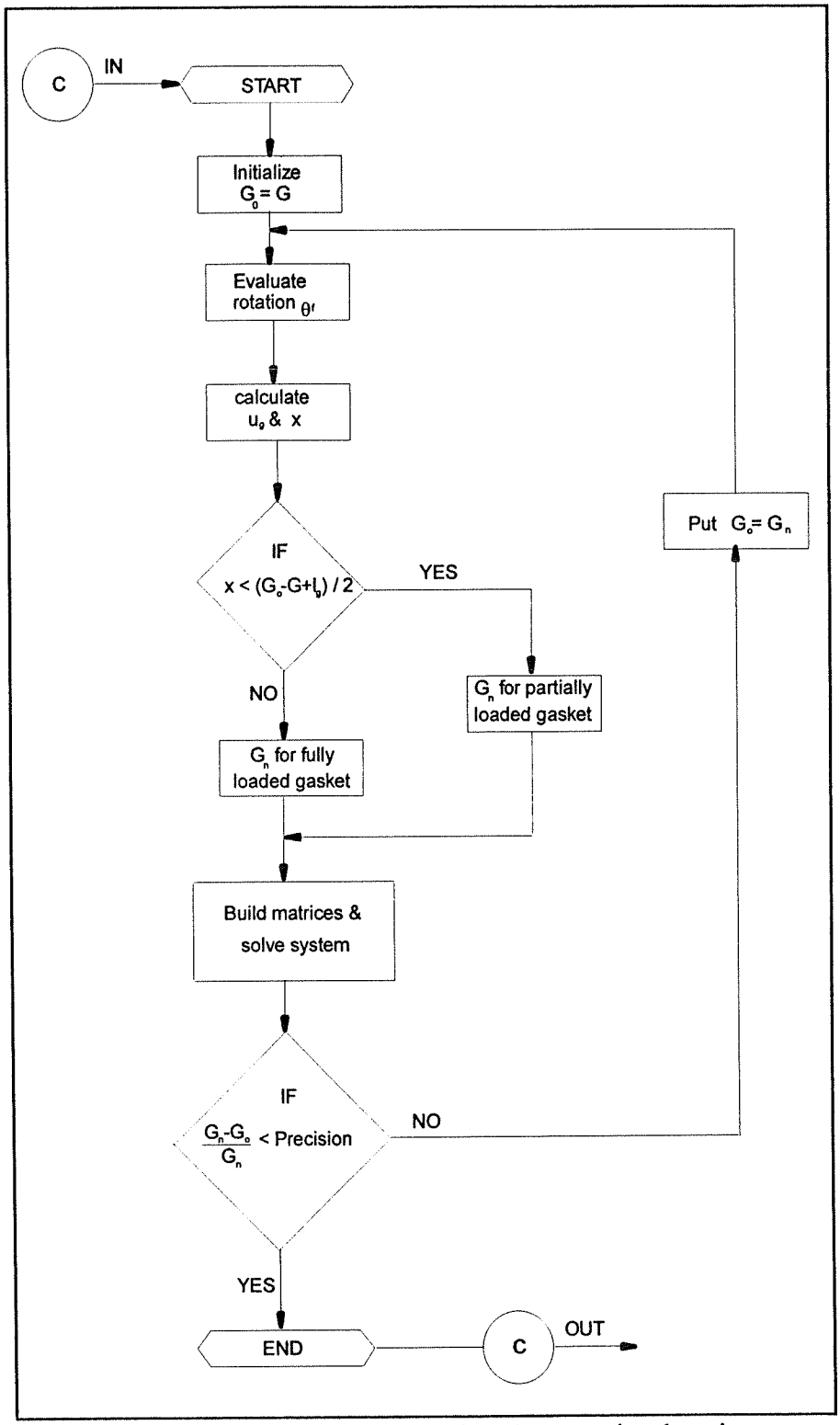

Figure III.4 Readjustment of gasket reaction location

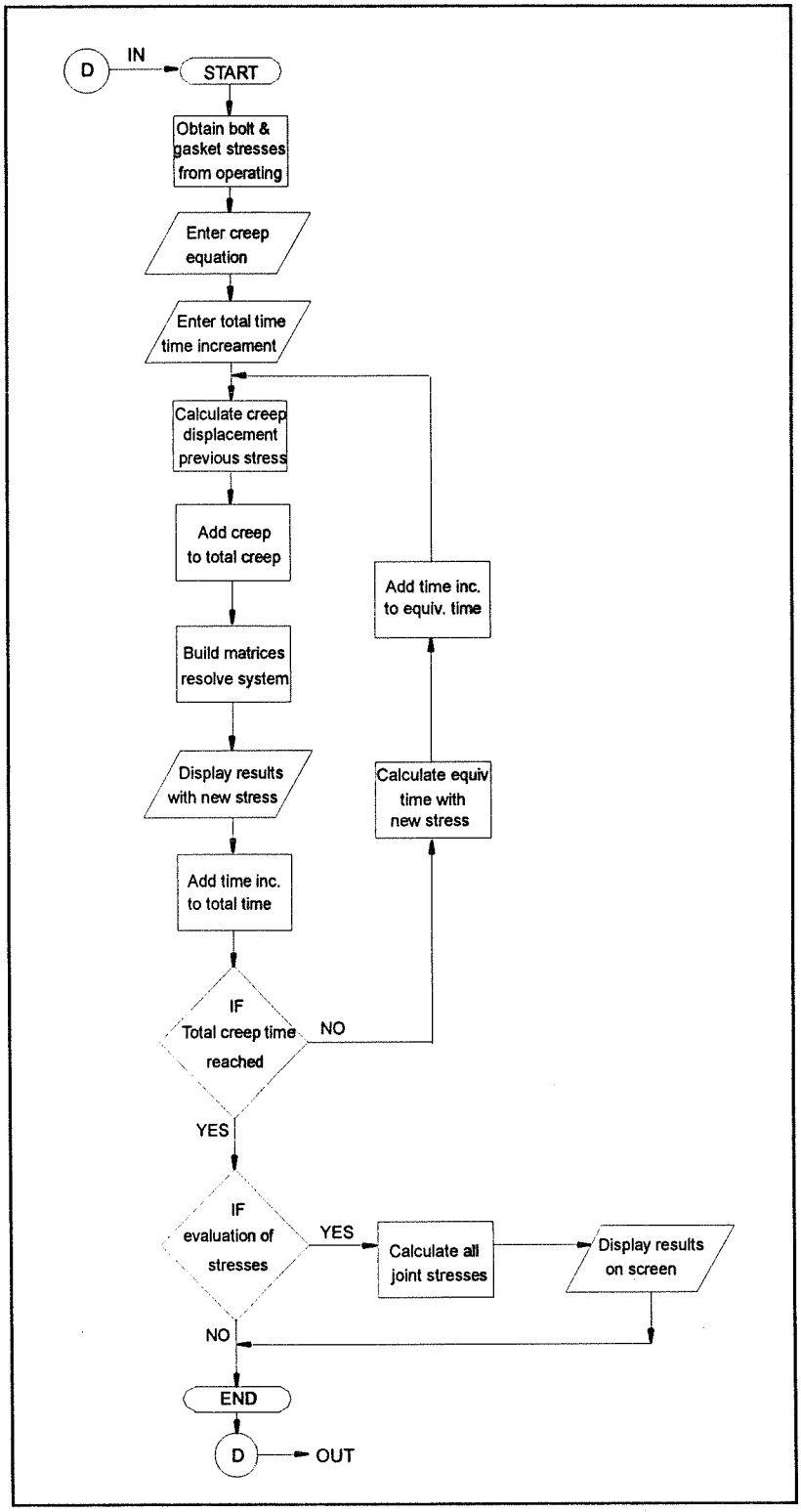

Figure III.5 Creep relaxation flow chart